APPLICATIONS OF HIGH RESOLUTION SOLID STATE CARBON-13 NMR TO THE STUDY OF MULTICOMPONENT POLYMER SYSTEMS

by

Tso-Shen Lin

Dissertation submitted to the Graduate Faculty of the
Virginia Polytechnic Institute and State University
in partial fullfillment of the requirements for the degree of

DOCTOR OF PHILOSOPHY

in

Chemistry

APPROVED:

Thomas C. Ward, Chairman

James E. McGrath

Garth L. Wilkes

James P. Wightman

Harry C. Dorn

August, 1983

Blacksburg, Virginia

To My Parents

ACKNOWLEDGEMENTS

The author is pleased to express his appreciation to Dr. Thomas C. Ward for his guidance and support of this work. Appreciation is extended to Drs. James E. McGrath, Garth L. Wilkes, James P. Wightman, Harry C. Dorn for their willingness to serve on the graduate committee. He also wishes to thank Drs. Harold M. Bell and Brian E. Hanson for serving on the examining committee and their time in going over the dissertation.

The author would also like to thank many people in the PMIL and Chemistry Department at VPI and SU. Especially, Mr. Tom Glass for his assistance in starting the "magic angle" solid state NMR experiments, Dr. Daniel P. Sheehy, Dr. Dillip K. Mohanty and Mr. Pradip K. Das for their helpful discussions. Finally, he wishes to thank Mrs. Debbie Farmer and Mrs. Diann Johnson for typing this dissertation.

Table of Contents

List of Figures

List of Tables

Chapter I

INTRODUCTION AND LITERATURE SURVEY

I. INTRODUCTION

Growth of the ability to control and design the physical and chemical properties of polymeric materials is one of the main reasons that polymers have been making a profound impact on modern technology and way of life. Many of the successes have been achieved through applications of multicomponent polymer systems including copolymers, polyblends and composites (1-6). Further advancement in polymer science and technology depends in part on understanding the molecular origins of macroscopic behavior. In this regard, techniques of nuclear magnetic resonance (NMR) have made notable contributions, especially through the high resolution spectra in the liquid state (7-10).

For years after the first successful detection of nuclear magnetic signals late in 1945 (11,12), high resolution NMR was almost a synonym for proton magnetic resonance in the liquid state. With the advent of commercial pulse Fourier transform NMR in the early 1970's (13-15) and subsequent developments in instrumentation, the NMR experiments became accessible for essentially the entire periodic table (16). Carbon-13 NMR in solution (17-21), in particular, has been extensively employed to investigate polymers (22-23). A high degree of resolution in carbon-13 spectra allows studies which are usually unachievable in proton NMR experiments, such as the quantitative data on stereochemical configuration and copolymer sequence distribution, to be determined (24). It also makes possible to obtain data on sidechain and backbone

reorientational motion through the measurement of spin-lattice, spin-spin and nuclear Overhauser relaxation parameters for each carbon (25,26).

In spite of the success of solution C-13 NMR, many interesting properties of bulk polymers disappear if the samples are put into solution. These are properties such as the degree of crystallinity, chain axis orientation, and primary and secondary molecular relaxations. Even aging processes as a function of chain scission and crosslinking have been studied by pulsed solid state (proton and fluorine-19) NMR through the measurements of second moments and other relaxation parameters. The spectrum of a solid polymer in these cases usually consists of a single broad resonance line having a full-width at half height of tens of KHz, and is known as a broad-line NMR spectrum (8, 27-31).

It might be assumed that if a high resolution NMR spectrum of a solid could be obtained, new details concerning the nature of the solid state of polymers might be uncovered. Recent advances in the techniques of multiple-pulse experiments and high speed magic angle spinning of samples have now made possible the partial realizaion of this goal (32-36). Commercial instruments for high resolution solid state NMR of some nuclei of either low natural abundance or of small magnetic moment became available in the late 1970's (37). Among them high resolution C-13 NMR achieved by employing the techniques of magic angle spinning and high power ^{13}C-^{1}H dipolar decoupling and cross polarization (the CPMAS method) (36) has drawn the most attention in the characterization

of organic solid polymers. The resolution of signals for individual carbons having bandwidths in the range of 10-100 Hz for polymeric solids not only made CPMAS attractive as an analytical technique for insoluble and crosslinked polymers but also provided a method for obtaining new information about solid state structure and dynamics at the atomic level (23,30, 38-41).

The work reported in this dissertation concerned application of the techniques of high resolution solid state C-13 NMR to a number of multicomponent polymer systems. Specifically, of major concern were: (1) the domain sturcture and molecular motion of two thermoplastic elastomer systems, including a series of styrene-isoprene-styrene linear triblock copolymers of various compositions, molecular weights and sample histories, and a poly(ester)urethane based on polybutylene adipate and 4,4'-diphenylmethane diisocyanate, (2) the compatibility of polymer blends containing poly(vinylidene fluoride), including its solution and mechanical blends with poly(methyl methacrylate), poly(vinyl acetate) and poly(vinyl methyl ether).

II. HIGH RESOLUTION SOLID STATE NMR

A. Fundamentals of Nuclear Magnetic Resonance (13-16,42-46)

1. The NMR Phenomenon

Basic Theory

A nuclear magnetic moment placed in a magnetic field has an interaction described by the Zeeman spin Hamiltonian,

$$H = -\bar{\mu} \cdot \bar{H} = -\gamma \bar{P} \cdot \bar{H} = -\gamma \hbar I_z H_0 \qquad (1)$$

where μ is the nuclear magnetic moment, P is the spin angular momentum of the nucleus, $\hbar$ is the Planck's constant divided by 2π, and H_0 is the static magnetic field which was chosen to be along the z-axis. I is the spin quantum number and its value depends on the type of nucleus and determines the maximum observable component of the nuclear angular momentum:

$$P_{max} = \hbar I \qquad (2)$$

Thus, $\hbar I_z$ is the component of the angular momentum along the z-axis. The magnetogyric ratio γ is:

$$\gamma = \frac{\bar{\mu}}{\bar{P}} \qquad (3)$$

and is a characteristic of the nucleus.

The eigenvalues of this system are:

$$E = -\gamma \hbar H_{0m} \qquad (4)$$

where m ranges from -I to +I, while the energy separation between adjacent levels is

$$\Delta E = \gamma \hbar H_0 = h\nu_0 \qquad (5)$$

where

$$\nu_0 = \frac{\omega_0}{2\pi} = \frac{\gamma}{2\pi} H_0 \tag{6}$$

is called the Larmor precession frequency as described by the equation of motion of the magnetic moment

$$\frac{d\bar{\mu}}{dt} = \gamma\bar{\mu} \times \bar{H}_0 = (-\gamma\bar{H}_0) \times \bar{\mu} = \bar{\omega}_0 \times \bar{\mu} \tag{7}$$

At equilibrium, the nuclei are populated among the energy levels according to a Boltzman distribution resulting in a net macroscopic magnetization along the z-axis:

$$M_z = M_0 = \frac{N_0\mu^2(I+1)}{3k_BTI} H_0 \tag{8}$$

where N_0 is the number of nuclei per unit volume, T is the absolute temperature and k_B is the Boltzmann constant.

The Resonance Phenomenon

The equilibrium state of the magnetic nuclei in $\bar{H}_0$ can be disturbed when a small magnetic field $\bar{H}_1$ is applied (In practice $\bar{H}_1$ is a linear radio frequency (RF) field oscillating in the x or y Cartesian coordinates), perpendicular to $\bar{H}_0$ and rotating about $\bar{H}_0$ in the same direction as $\bar{\mu}$ at frequency ν. Resonance is attained when the frequency of $\bar{H}_1$ exactly equals ν_0:

$$\nu = \nu_0 = \frac{\gamma}{2\pi} H_0 \tag{9}$$

At resonance, the net macroscopic magnetic moment tips away from the z-axis, according to the equation:

$$\frac{d\overline{M}}{dt} = \gamma \overline{M} \times \overline{H}_1 \qquad (10)$$

but the precession frequency remains constant.

In energy terms, it may also be stated that a field $\overline{H}_1$ of frequency ν induces transitions between the nuclear spin levels when its energy, $h\nu$, equals the energy difference $\Delta E = \gamma \hbar H_0$ between two adjacent energy levels, that is, when the condition of Equation (9) is fulfilled.

Rotating Frame of Reference

A better insight into the resonance phenomenon may be achieved by studying the motion in a frame of reference x'y'z' (S'), which is visualized as rotating about $\overline{H}_0$ in the same direction and with the same frequency as $\overline{H}_1$. For an observer in this system $\overline{H}_1$ appears fixed, for example, along the x' axis. In the absence of $\overline{H}_1$, the individual magnetic moments would be seen as motionless in the rotating frame.

It can be shown (47,48) that, when expressed in this new coordinate system, the equation of motion for the magnetization vector $\overline{M}$, is exactly the same as Equation (10)

$$\left(\frac{d\overline{M}}{dt}\right)_{rot} = \gamma \overline{M} \times \overline{H}_{eff} \qquad (11)$$

where the effective field $\overline{H}_{eff}$ is the resultant of $\overline{H}_0$, $\overline{H}_1$ and a fictitious field, $\overline{\omega}/\gamma$, which accounts for the rotation of the S' frame

about the z-axis at the angular velocity $\omega = 2\pi\nu$:

$$\overline{H}_{eff} = \overline{H}_0 + \overline{H}_1 + \frac{\overline{\omega}}{\gamma} \tag{12}$$

As represented in Figure 1, $\overline{H}_{eff}$ is fixed in the rotating frame of reference S' and Equation (12) once again characterizes a precession of of $\overline{M}$ about $\overline{H}_{eff}$ at an angular velocity $\overline{\Omega}$ defined by

$$\overline{\Omega} = -\gamma\overline{H}_{eff} \tag{13}$$

The magnitude of $\overline{H}_{eff}$ and $\overline{\Omega}$ can be further expressed as:

$$|H_{eff}| = [(H_0-\omega/\gamma)^2 + H_1^2]^{1/2} = 1/2[(\omega_0-\omega)^2 + (\gamma H_1)^2]^{1/2} \tag{14}$$

and

$$\Omega = [(\omega_0-\omega)^2 + (\gamma H_1)^2]^{1/2} \tag{15}$$

In the far-off-resonance condition, $H_{eff} \simeq 1/\gamma(\omega_0-\omega)$, $\overline{H}_{eff} \simeq \overline{H}_0 + \overline{\omega}/\gamma$, and $\overline{M}$ lies along and precesses about the z'-axis. As the resonance condition is approached, the component of $\overline{H}_{eff}$ along the z'-axis in Figure 1 decreases, and $\overline{H}_{eff}$ tips away from the z'-axis. If the rate at which $\overline{H}_{eff}$ tips is slow enough, $\overline{M}$ will follow and remain continuously aligned with $\overline{H}_{eff}$ (adiabatic passage). At resonance $\omega_0=\omega$, thus

$$\overline{H}_{eff} = \overline{H}_1 \text{ and } \overline{\Omega} = -\gamma\overline{H}_1 \tag{16}$$

In the rotating frame, the magnetization vector rotates about the direction of $\overline{H}_1$ at a frequency of $\gamma H_1/2\pi$.

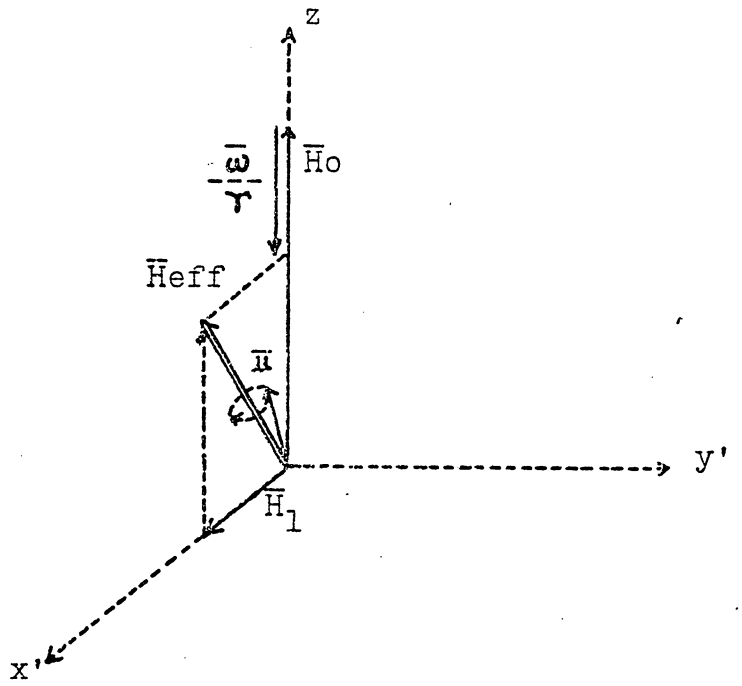

Figure 1. Motion of Magnetic Moment in the Rotating Frame of Reference.

2. Fourier Transform NMR

NMR experiments can be carried out either by sweeping the radio frequency (RF) applied to a sample in a fixed magnetic field or, alternatively, slowly sweeping the field with a fixed RF. Both techniques are referred to as continuous wave (CW) NMR.

Another method of observation, based on pulsed NMR, suggested by Bloch et al. (49,50) and put into practice initially by Hahn (51), makes use of short bursts, or pulses, of RF power at a descrete frequency known as the carrier frequency F. A short pulse of RF irradiation of t seconds duration is equivalent to the simultaneous excitation of all the frequencies in the range $F \pm t^{-1}$. Hence, by using a very short pulse, it is possible to excite all the magnetic nuclei of a given isotopic type in a molecule simultaneously.

In the pulsed NMR experiment, a RF pulse tips the magnetization away from the z-axis; the magnitude of M_{xy}, known as the free induction signal, starts to decay after the removal of the short pulse and is monitored along a fixed axis in the rotating frame (the y'-axis). The monitored signal as a function of time is known as the free induction decay (FID) or the time domain spectrum. The FID can be interconverted with the frequency domain spectra (those obtained in the CW NMR experiments) by means of the mathematical process of Fourier transformation.

The relationship between the time and frequency domains can be expressed in the form

$$F(\omega) = \int_{-\infty}^{+\infty} f(t) \exp(-i\omega t)dt \qquad (17)$$

and the inverse relationship

$$f(t) = \int_{-\infty}^{+\infty} F(\omega) \exp(i\omega t)d\omega \qquad (18)$$

where $F(\omega)$ is a function of frequency and $f(t)$ is the corresponding function of time. Thus pulse NMR with Fourier transformation is referred to as Fourier transform (FT) NMR.

Since the sweeping rates of the CW NMR are limited due to relaxation processes (section II.A.3), the total experimental time of FT NMR, which simultaneously excites all the nuclei of interest, can be substantially shortened in comparison. Therefore, FT technique enables NMR studies of systems of inherently poor sensitivity, many repeated pulses being applied.

A few of the techniques and terminologies of the pulsed FT NMR which will be referred to in this dissertation are discussed in the following.

Accumulation of Spectra

One of the simplest ways of overcoming sensitivity problems in spectroscopy is to record several spectra from a sample and then simply add them together. NMR signals will add coherently, whereas the noise, being random, will only add as the square root of the number of spectra accumulated. This leads to an overall improvement in signal-to-noise

ratio (S/N) by the square root of the number of spectra accumulated. For example, adding 100 spectra will lead to an increase in signal-to-noise ratio of 10:1. The principal drawback of this technique arises from the time taken to obtain an individual spectrum or scan. It is here that FT NMR makes a great contribution.

Pulse Duration and Flip Angle

As discussed in section II.A.1, in the rotating frame, at resonance, the magnetization vector rotates about the RF $\overline{H}_1$ at a frequency of $\gamma H_1/2\pi$ (Equation (16)). If $\overline{H}_1$ is chosen to be along the x'-axis, then a RF pulse of duration of t_p will flip the magnetization (in the y'z plane) away from the z-axis by an angle, the flip angle,

$$\Theta = \gamma H_1 t_p \text{ (rad)} \qquad (19)$$

For example, a pulse duration of $\pi/2\gamma H_1$ will flip the magnetization by 90° and align it along the y'-axis. The pulse is referred to as a 90° pulse.

Spin Locking

Immediately after a 90° pulse (along the x'-axis), the RF pulse may be phase shifted by 90° and applied along the y'-axis. In the rotating frame, the magnetization is then aligned along and precessing about the $\overline{H}_{eff}$ ($\overline{H}_{eff} = \overline{H}_1$) at a frequency of $\gamma H_1/2\pi$. This keeps the magnetization vector from dephasing due to magnetic field inhomogeneity and the process is referred to as spin locking.

Digital Resolution and Acquisition Time

In carrying out the Fourier transformation, half of the available data points are lost since the Fourier transform contains both real and imaginary components and only the real component is used to generate the spectrum (Equation (17)). Hence, if the original FID were accumulated with N data points, the transformed frequency domain spectrum will contain 0.5N data points. If the recorded spectral width in Hz is Δ, then the digital resolution or accuracy of the spectrum in Hz will be

$$R = \frac{2\Delta}{N} \tag{20}$$

Also, from the sampling theorem (Nyquist theorem), acquisition of a frequency spectrum Δ in width requires a minimum sampling rate of 2Δ points per second. Thus the free induction decay has to be acquired in a time A_t (data acquisition time) which fulfills the condition

$$2\Delta A_t = N \tag{21}$$

Combining Equations (20) and (21), one obtains an accuracy in Hz of

$$R = \frac{2\Delta}{N} = \frac{1}{A_t} \tag{22}$$

i.e., the more the data points of the FID or the longer the acquisition time, the better defined is the spectrum and the higher is the resolution.

Signal Weighting, Digital Filtering and Zero Filling

It is possible to alter the FID signals mathematically to improve either the resolution or the sensitivity (S/N) in the transformed spectrum. For example, multiplication of the FID by a simple exponential can reduce noise at the expense of some artificial broadening of the lines (resolution). The signal weighting process which reduces noise and improves S/N is referred to as digital filtering.

Another way to beneficially alter the FID signals is to supply additional zeros to the digitized FID signal to create apparently longer signals. The process, known as the zero filling, does not improve the resolution but it does improve spectral appearance and definition.

The Digitization Process and Dynamic Range

In FT NMR, every data point of the FID is digitized by an analog-to-digital converter (ADC) before being stored in a computer memory. If the largest signal, of intensity H_S, is adjusted so as to fill the whole conversion range, then for an ADC of d bits, the limit of the relative converter accuracy will be $H_S/2^d$. This limit characterizes the so-called "resolution of the converter" or the "numerical resolution". The smallest signal which can be recorded will have an intensity H_W such that

$$H_S/H_W = 2^d \tag{23}$$

This ratio is called the dynamic range of the spectrum.

The data accumulation in a FT NMR is carried out by repeating the sampling and conversion of each successive FID and then transferring to the computer memory in the addition mode for each data point. Complete filling of the memory without overflow is a key point which should be observed to avoid deterioration of the accumulation efficiency. For a computer of b-bits word and d-bits ADC, in an ideal spectrum composed of a single line, the maximum number of scans possible under this condition can be calculated by the following formula (52):

$$(n_s)_{max} = \left[\frac{-1+[1+4(S/N)[(S/N)+1]x2b-d]1/2}{2(S/N)}\right]^2 \qquad (24)$$

where (S/N) denotes the signal-to-noise ratio for a single scan. When (S/N) is large (>~10), Equation (24) becomes obviously

$$(n_s)_{max} = 2^{b-d} \qquad (25)$$

and the final signal-to-noise ratio is

$$(S/N)_f = (S/N)\ (n_s)1/2 \qquad (26)$$

Several methods have been used to overcome the problem of memory overflow. Double Precision, which increases $(n_s)_{max}$ by 2^b, uses two words for each data point. Frequency domain accumulation successively transforms the FID at a relatively small number of scans, then stores the transformed frequency domain spectra to the memory in the addition mode. Both methods require that one double the capacity of the computer memory. Another method, which does not require extra memory,

progressively reduces the ADC bits at the expense of dynamic range.

3. Relaxation Processes

T_1, T_2 and Lineshapes

Following any perturbation which disturbs the magnetic equilibrium of a spin system, for example, a 90° pulse which leaves $M_y'=M_0$ and $M_x'=M_z=0$, the system returns to equilibrium via at least two relaxation processes. The characteristic times T_1 and T_2 were initially used by Block to describe these with the decay of magnetization assumed to be a first-order process in each case (49,50). (This assumption turns out to be true for liquids but not for solids, at least as far as T_2 is concerned (53)). The longitudinal or spin-lattice relaxation time T_1, describes the repolarization of the magnetization along the z-axis as it comes to equilibrium through energy change with its surroundings ("the lattice"). The transverse or spin-spin relaxation time T_2, describes the dephasing of the mangetization in the xy plane without change of the total energy of the spin system. The Bloch equations can be written in the rotating frame as (47):

$$\frac{dM_x'}{dt} = -(\omega-\omega_0)M_y' - \frac{M_x'}{T_2} \tag{27}$$

$$\frac{dM_y'}{dt} = (\omega-\omega_0)M_x' + \gamma H_1 M_z - \frac{M_y'}{T_2} \tag{28}$$

$$\frac{dM_z'}{dt} = -\gamma H_1 M_y' + \frac{M_0-M_z'}{T_1} \tag{29}$$

After the removal of the RF pulse (which was chosen to be along the x'-axis), the system returns to equilibrium according to the following formulae:

$$\frac{dM_x'}{dt} = -\frac{M_x'}{T2} \tag{30}$$

$$\frac{dM_y'}{dt} = -\frac{M_y'}{T_2} \tag{31}$$

$$\frac{dM_z'}{dt} = -\frac{(M_z'-M_o)}{T_1} \tag{32}$$

The solutions of the Block equations give a Lorentzian line, centered at ν_o, with bandwidth at half intensity given by

$$\nu_{1/2} = \frac{1}{\pi T_2} \tag{33}$$

The observed bandwidth usually includes a contribution due to field inhomogeneity ΔH_o

$$\nu_{1/2}\ (obs) = \frac{1}{\pi T_2} + \frac{\gamma \Delta H_o}{2\pi} \tag{34}$$

or

$$\nu_{1/2}\ (obs) = \frac{1}{\pi T_2^*} \tag{35}$$

where T_2^* is defined as

$$\frac{1}{T_2^*} = \frac{1}{T_2} + \frac{\gamma \Delta H_0}{2} \qquad (36)$$

The Lorentzian lineshape and Equations 33-36 are indeed observed for the non-viscous liquids. Most rigid solids, however, exhibit more complex Gaussian lineshapes, where the transverse magnetization decays exponentially as t^2 (53).

Relaxation Mechanisms

In NMR (the probability of spontaneous emission being negligible) restoration of the equilibrium populations following a perturbation occurs relatively slowly and through stimulated emission. In general, any mechanism which gives rise to fluctuating magnetic fields at a nucleus is a possible relaxation mechanism. In this regard, a number of interactions have been found to be important. These mechanisms are:

1. Magnetic dipole-dipole interaction.
2. Electric quadrupolar interaction.
3. Chemical shift anisotropy interaction.
4. Scalar-coupling interaction.
5. Spin-rotation interaction.
6. Paramagnetic interaction, which includes both a dipole-dipole and a scalar-coupling interactions between an unpaired electron and a nucleus.

In fact, one or several of the mechanisms may be encountered in a sample. An experimental relaxation rate is usually considered as a summation of the specific rates of all the relevant mechanisms, m,

involved.

$$R_i = \frac{1}{T_{i(obs)}} = \sum_m \frac{1}{T_{im}} \qquad (i=1,2) \quad (37)$$

Correlation Time (τ_c) and its Relationships to the Relaxation Times

Since in a rotating frame, the magnetization $\overline{M}$ appears to be stationary, obviously only the fluctuating magnetic fields which are fixed in the rotating frame can perturb $\overline{M}$ and contribute to the relaxations. Therefore, all the possible relaxation mechanisms may be affected by molecular motion (or other equivalent processes, such as chemical exchange). In addition, the strength of any particular interaction along with the magnitude and frequency of the molecular motion, determines the relaxation rates.

The relaxation rates of each mechanism can be written as (13):

$$R_{im} = \frac{1}{T_{im}} = E_c^2 f_{im}(\tau_c) \qquad (38)$$

where E_c represents the strength of the specific relaxation interaction and $f_{im}(\tau_c)$ is determined by the molecular motion. An example of $f_{im}(\tau_c)$ or the effect of molecular motion on the relaxation rates may be obtained by comparing T_1 and T_2.

Spin-lattice relaxation processes which tend to bring the magnetization vector back toward its equilibrium state aligning along the z-axis are, inevitably, accompanied by a decrease in M_x and M_y and so also contribute to T_2. However, T_2 is always found to be equal to or smaller than T_1, i.e., additional processes exist which can dephase the

spins without exchanging energy with the lattice. In fact, T_1 and T_2 are governed by the same mechanisms and E_c for both T_1 and T_2 of any relaxation mechanism is the same. Thus, it is the function $f_{im}(\tau_c)$, or the effect of molecular motion, which differentiates the two relaxation times. It can be shown (13) that for a microscopic fluctuating field $\overline{h}$, h_x' and h_y' are effective in both T_1 and T_2 relaxation processes, while h_z' interacts effectively only with M_x' and M_y', i.e., it is only effective for the T_2 relaxation processes. Since a static component of $\overline{h}$ in the z' direction of the rotating frame is equivalent to a static component in the z direction of the laboratory frame, slow and low frequency processes affect only T_2. On the other hand, high frequency processes (at resonance frequency or higher) affect both T_1 and T_2. Thus, in non-viscous liquids, in which high frequency processes dominate, one usually finds that $T_1=T_2$, while in rigid solids, in which high frequency processes are extremely limited, $T_2<<T_1$ is the case.

In the function $f_{im}(\tau_c)$, τ_c is the molecular correlation time, which denotes the "average" time for a molecule in a state of motion or in other words, it characterizes the rate at which the local fluctuating field $\overline{h}$ loses memory of a previous value. For example, it can be expressed as the average time between molecular collisions for a small molecule in a liquid, or the average time required to effect a rotation of 1 radian for large molecules.

In the simplest case of a single correlation time, the correlation function can be written as

$$K(\tau) = C \cdot \exp(-|\tau|\tau_c) \qquad (39)$$

where C is a constant. (By definition, $K(\tau) = |Y(t) \cdot Y^*(t+\tau)|$, where Y^* is the complex conjugate of Y, and Y can describe a fluctuating field or be an equation of motion).

Furthermore, a correlation time can be Fourier transformed into a spectra density function

$$J(\omega) = \int_{-\infty}^{+\infty} k(\tau)\exp(i\omega t)d\tau \qquad (40)$$

For example, if a molecule persists in some state of motion for a time of 10^{-12} sec. (τ_c), then according to Equations (39) and (40), its motion will have frequency components from 0 to 10^{12} Hz.

The spectra density function $J(\omega)$ gives the intensity or probability of the molecular motions at any specific frequency. Thus, $J(o)$ which is related to T_2, and $J(\omega_o)$ as well as $J(2\omega_o)$ which is related to T_1 and T_2 may be obtained from the molecular correlation time τ_c, or vice versa. The value of τ_c and molecular dynamic information can be estimated from T_1 and T_2 (54-56) and other relaxation parameters. (The contribution to T_1 and T_2 from $J(2\omega_o)$ arises from a sort of molecular Doppler effect (13).)

In many organic systems, including the samples studied in this dissertation, the nuclear dipole-dipole interaction is the dominant relaxation mechanism. (Barring the presence of paramagnetic impurities, since the electron magnetic moment is much larger than the nuclear moments, the dipole-dipole effect results in T_1 (observed) $\simeq$ T_1 (paramagnetic)). An example of T_{1DD} and T_{2DD} as a function of the correlation time between two identical spin 1/2 muclei undergoing isotropic reorientation at various H_o is given in Figure 2 (57).

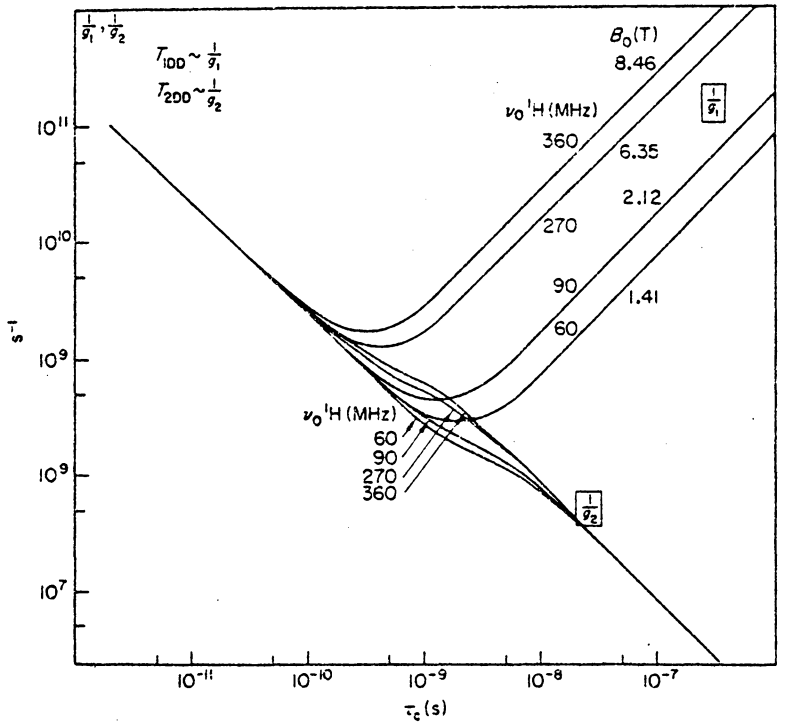

Figure 2. Behaviour of the Dipolar Spin-Lattice T_1 DD and Spin-Spin T_2 DD Relaxation Times as a Function of the Correlation Times τ_c for Interaction Between two Identical Spin 1/2 Nuclei Undergoing Isotropic Reorientation. The functions g_1 and g_2 represent the parts of the relaxation rates T_1-1 and T_2-1 which reflect the dependency on τ_c and are independent of the distance separating the nuclei. (57)

$$\frac{1}{T_{1\ DD}} = k g_1 \text{ with } g_1 = \frac{\tau_c}{1+\omega^2\tau_c^2} + \frac{4\tau_c}{1+4\omega^2\tau_c^2} \qquad (41)$$

$$\frac{1}{T_{2\ DD}} = k g_2 \text{ with } g_2 = \frac{1}{2}\left(3\tau_c + \frac{5\tau_c}{1+\omega^2\tau_c^2} + \frac{2\tau_c}{1+4\omega^2\tau_c^2}\right) \qquad (42)$$

where

$$k = \frac{3\mu_0^2}{160\pi^2}\frac{\hbar^2\gamma^4}{r_{IS}^6} \text{ (SI)} \quad \text{or} \quad k = \frac{3}{10}\frac{\hbar^2\gamma^4}{r_{IS}^6} \text{ (CGS)}$$

From Figure 2, it can be seen that the spin-lattice relaxation is the most effective when the molecular correlation frequency ($1/\tau_c$) is equal to the nuclear precession frequency (ν_o), and the spin-spin relaxation is the most effective when τ_c is the longest. Also, from Equations (41) and (42), it is obvious that in the case of a short τ_c (i.e., $\omega\tau_c<<1$),

$$T_{1DD} = T_{2DD} = \frac{1}{k(5\tau_c)} \tag{43}$$

4. Relaxation Time Measurements (13,15,45)

The basic versions of the most used methods for relaxation time measurements employing pulsed FT NMR are reviewed below:

T_1 Measurements

(1) Inversion Recovery Method

This method uses the following sequence: $(180°\text{-}\tau\text{-}90°\text{-}A_{t}\text{-}t)_n$ where τ is a variable delay, A_t is a data acquisition time and t is a recovery time (or pulse delay time) chosen as $(A_t+t)\geq 5T_1$. In this method, line intensity from the solution of the Block equation (Equation (32)) is expressed as

$$M(\tau) = M_o[1-2\exp(-\tau/T_1)] \tag{44}$$

where M_o practically can be achieved when $\tau=5T_1$. When an estimate of the T_1 value can be made, a ca. 10τ experiment spanning a range between 0.3 T_1 and $2T_1$ as well as a long $\tau(> 5T_1)$ is carried out and the value

of T_1 is obtained from the slope of the plot of $\ln(M_0-M(\tau)/2M_0)$ versus τ.

This method is considered to be the most reliable. However, a recovery time of $5T_1$ makes this method time consuming and infeasible for the systems with long T_1 values.

(2) Saturation Recovery Method

The sequence for this method is $(90°\text{-HSP-}\tau\text{-}90°\text{-}A_t\text{-HSP})_n$. Immediately after the first 90° pulse, $M_Z=0$, a homospoil pulse (HSP) further destroys the transverse magnetization. Following a variable delay time of τ, $M(\tau)=M_Z(\tau)$, is sampled by means of a second 90° pulse. The corresponding line intensity for this method is expressed as

$$M(\tau) = M_0[1-\exp(-\tau/T_1)] \qquad (45)$$

T_1 is obtained from the slope of the plot of $\ln(M_0-M(\tau)/M_0)$ versus τ.

(3) Progressive Saturation Method

This method is a modified version of the saturation recovery method and is limited to the case $T_1>>T_2$ (or $T_1>>T_2^*$). The sequence for this method is: $(90°\text{-}A_{t-\tau})_n$. The first five to ten scans are deleted to reach a spin-system steady state. The corresponding line intensity for this method is

$$M(\tau) = M_0[1-\exp(-(A_{t+\tau})/T_1)] \qquad (46)$$

Again, T_1 is obtained from the slope of the plot of $\ln(M_0-M(\tau)/M_0)$ versus τ (or $A_{t+\tau}$).

T_2 Measurements

T_2 measurements are much more demanding than T_1 experiments, especially in the case of short T_2 (i.e., rigid solids). Methods of accurate T_2 measurements have been achieved based on echo formation, such as the Carr-Purcell method and the Meiboom-Gill modification of the Carr-Purcell method (CPMG sequence).

No T_2 experiment was carried out in the present study, however, T_2*'s were estimated from lineshapes and FIDs. Thus, no further discussion will be provided on this topic.

$T_{1\rho}$ Measurement

As stated earlier, immediately after the onset of the process of spin locking $\overline{H}_{eff}=\overline{H}_1$, and a net magnetization of $M_0=C\cdot H_0$ is aligned along and precessing about $\overline{H}_1$ at a frequency of $H_1/2\pi$. In general, $H_0>>H_1$, therefore the magnetization will decay from M_0 to its new equilibrium state of $M_0'=C\cdot H_1=M_0(H_1/H_0)$, according to a first order relaxation mechanism. In fact, this relaxation can be described by the Block equation for spin-lattice relaxation. Its time constant, $T_{1\rho}$, is called the spin-lattice relaxation time in the rotating frame.

$T_{1\rho}$ can be measured by varying the duration of the applied locking field $(H_1)_{y'}$ by the sequence $(90°x'-(H1)y'\tau-At-t)n$, where, like the T_1 measurement, t is a recovery time and A_{t+t} should be longer than $5T_1$. The corresponding line intensity following this sequence is

$$M(\tau) = M_0 \exp(-\tau/T_{1\rho}) \qquad (47)$$

and the value of $T_{1\rho}$ is obtained from the slope of the plot of $\ln(M(\tau)/M_0)$ versus τ.

The $T_{1\rho}$ process is most effective when the molecular correlation frequency is equal to $\gamma H_1/2\pi$ (1-100KHz). Thus, the $T_{1\rho}$ experiment is a powerful tool for probing the low frequency processes in this range.

5. The NMR Parameters

Besides T_1, T_2, lineshapes and $T_{1\rho}$, four NMR parameters, which are important in the study of molecular structure and dynamics are discussed below.

Chemical Shift, δ

Deriving from the magnetic effect of the surrounding electrons, a nucleus "i" experiences a field $\overline{H}i = \overline{H}_0 - \overset{\Lambda}{\sigma i}\overline{H}_0$, where $\overset{\Lambda}{\sigma i}$ is the shielding tensor (of second rank) which characterizes the spatial electronic distribution around the nucleus.

In general, the electronic shielding is anisotropic. However, due to the existence of fast and isotropic molecular motion, an averaged isotropic value, σ_i, is detected by NMR experiments on liquids. This value represents the mean of the three principal components of the tensor $((1/3)tr\overset{\Lambda}{\sigma_i})$ and is called the shielding (or screening) constant.

The resonance frequency of the nucleus "i" is, according to Equation (6):

$$\nu_i = \frac{\gamma}{2\pi}(H_0 - \sigma_i H_0) = \frac{\gamma}{2\pi}(1-\sigma_i)H_0 \qquad (48)$$

The positions of the various signals are usually compared with the resonance of a standard substance (Tetramethyl Silane for ^{13}C and ^{1}H), and the chemical shift is defined as

$$\delta_i = \sigma_{ref} - \sigma_i = \frac{H_i - H_{ref}}{H_0} = \frac{\nu_i - \nu_{ref}}{\nu_0} \qquad (49)$$

δ_i is a dimensionless parameter which does not depend on the strength of H_0 (or ν_0) and is expressed in units of 10^{-6} (ppm).

Spin-Spin Coupling Constants

In addition to the electronic diamagnetic effect, a nucleus "i" may experience the fields associated with the presence of neighboring spins. Theoretically, two mechanisms of interaction between the nuclear magnetic dipoles are liable to intervene: a direct through-space interaction depending on the internuclear distances, and an indirect one transmitted through the bonding electrons. Both interactions are independent of the strength of H_0.

(1) Direct (Dipolar) Coupling Constant, D

The direct spin-spin coupling interaction is described by a traceless second rank tensor $\overleftrightarrow{D}$. In the case of two isolated spin 1/2 nuclei "i" and "j", the direct coupling constant is given by

$$D_{ij} = -\frac{h}{4\pi}\gamma_i\gamma_j\frac{(3\cos^2\theta_{ij}-1)}{r_{ij}^3} \quad \text{(in } H_z\text{)} \quad (50)$$

where θ_{ij} is the angle between the applied field $\bar{H}_0$ and the internuclear distance $\bar{r}_{ij}$. Doublet resonance lines centered at $\gamma_i H_0/2\pi$ (or $\gamma_j H_0/2\pi$) separated by $|2D_{ij}|$ are expected for the spectrum of nucleus i (or j).

In an ensemble, Equation (50) can be written as

$$D_{ij} = -\frac{-h}{4\pi}\gamma_i\gamma_j\frac{\langle 3\cos^2\theta-1\rangle}{r_{ij}^3} \quad (51)$$

where < > denotes a value averaged over all magnetic (i,j) dipoles. The magnitude of D_{ij} (for ^{13}C-^1H or ^1H-^1H) is in the order of 10^4-10^5 Hz. Therefore:

(i) In liquids, $\tau_c \ll 1/2\ D_{ij}$, isotropic motions result in $\langle 3\cos^2\theta-1\rangle=0$ and Dij is nullified.

(ii) In solids, $\tau_c > 1/2\ D_{ij}$, the orientation term of Equation (51) can not be averaged to a single value, and numerous dipolar couplings produce the very broad lines observed.

(iii) In highly oriented mesophases, D_{ij}'s have been successfully measured and form the basis for molecular geometry studies (58).

(2) Indirect (Spin) Coupling Constant, J

The indirect spin-spin coupling interaction is also described by a second rank tensor $\overset{\Lambda}{J}$. The interaction of the J-coupling is much weaker than the D-coupling (for ^{13}C and ^1H, by ca. 2-4 powers of ten). Thus in

solids, the J-coupling is obscured by the direct D-couplings. In liquids, due to the existence of fast and isotropic motions, $\overset{\Lambda}{J}$ is reduced to a constant, $(1/3)tr\overset{\Lambda}{J}$, whose magnitude is the mean of the three principal components of the $\overset{\Lambda}{J}$ tensor.

For two spin 1/2 nuclei, i and j, the indirect coupling is given by

$$J_{ij} = \frac{\hbar}{2\pi} \gamma_i\gamma_j \left(\frac{1}{3}tr\overset{\Lambda}{J}_{ij}\right) \tag{52}$$

Resonance lines of both i and j are split to form a doublet, separated by $|J_{ij}|$.

The signal multiplicity arising from the J-couplings facilitates the elucidation of the NMR spectra.

Resonance Line Intensity

Integrated areas under each NMR signal for the spectra obtained under certain appropriate conditions can be directly proportional to the number of nuclei in a particular environment. This provides for a quantitative analysis of the NMR spectra.

Nuclear Overhauser Factor, η

As stated earlier, two nuclei, i and j, when close enough, can interact through space in a dipole-dipole mechanism. When one of these nuclei (j) is irradiated (i.e., saturated by means of a complementary RF field H_2, or decoupled), it can lead to a modification of the energy level populations of the second (i) and results in a modification of the intensity of the resonance line of the nucleus i. This phenomenon,

known as the nuclear Overhauser effect (NOE), like T_1 and T_2, depends on the strength of H_o and on molecular mobility.

The NOE is characterized by an enhancement factor

$$\eta = \frac{I_i - I_{io}}{I_{io}} \tag{53}$$

where I_i and I_{io} are the resonance line intensities of nucleus i obtained with and without irradiating the nucleus j.

Besides the advantage of sensitivity enhancement by NOE in many cases (when $\eta > o$), the nuclear Overhauser factor, η, can also be used to determine the contribution of the dipole-dipole interactions to the total relaxation process and to probe the molecular mobility when τ_c is in the neighborhood of $1/\nu_o$ (i.e., viscous liquids or non-rigid solids) (59).

B. Introduction to Solid State NMR

As discussed briefly in the introduction and the last section, the anisotropic nature of most solid samples results in broadline NMR spectra. However, with recent advancements in NMR technology, namely the high speed magic angle spinning and multiple pulse decoupling techniques, high resolution "liquidlike" spectra of solid samples are attainable for all 118 NMR-active isotopes in the periodic table (60). Nonetheless, the most easily achieved and well developed experiments have been among those spin 1/2 nuclei which have weak (homonuclear) mutual coupling either by virtue of low natural abundance or small magnetic moments (e.g., ^{13}C, ^{31}P, ^{29}Si, ^{15}N, ^{195}Pt, ^{199}Hg). Therefore,

besides the resolution problem, sensitivity is another obstacle for the studies of those nuclei. The sensitivity problem arises not only from the weak macroscopic magnetic moments, but also from long spin-lattice relaxation times in solids, concomitant with the weak homonuclear dipolar interactions and aggravated by the lack of high frequency molecular reorientations in rigid solids.

The following two sections will review the resolution and sensitivity problems of solid state NMR and their solutions. A general treatment will be given, although the focus will be on ^{13}C and other spin 1/2 nuclei having weak mutual coupling.

C. The Resolution Problem: Sources of Line-Broadening and Methods for their Removal

In addition to electron shielding, direct dipolar interaction and indirect electron-coupled interaction as discussed in the previous section, another main source of line-broadening in solid state NMR spectra is electric quadrupolar interaction. The electric quadrupolar interaction has already been mentioned as a possible relaxation mechanism and is frequently encountered in heteronuclei NMR because at least 87 of the NMR active isotopes possess a spin value $I>1/2$ and, thus, have a quadrupole moment Q.

These four interactions just mentioned along with the natural lineshape (or lifetime-broadening, which may be regarded as an effect of the uncertainty principle, i.e., $\Delta E \cdot \Delta t = (h\nu_{1/2})\Delta t \geq h$ and $\nu_{1/2} = 1/\pi T_2$) determine the pattern of a solid state NMR spectrum, as shown in Figure 3 (60).

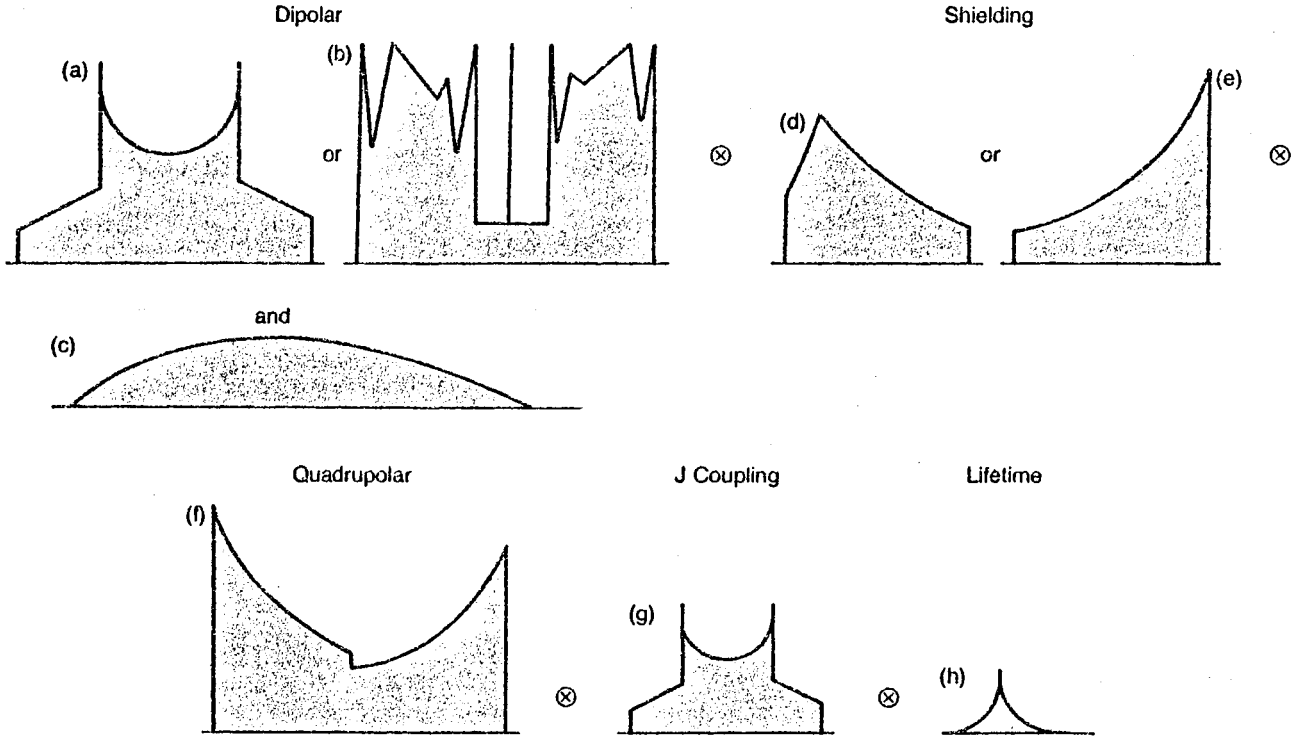

Figure 3. NMR Powder Patterns of Nuclei. The following interactions are present: 1) dipolar coupling between two isolated spins (a), dipolar coupling between three isolated spins (b), and dipolar coupling among many spins (c); 2) shielding anisotropy, nonsymmetric (d) and axially symmetric (e) patterns; 3) quadrupolar splitting, the central 1/2-1/2 transition for a spin 3/2 system (f); 4) J coupling, same form as two-spin dipolar pattern (g); and 5) lifetime broadening (h). The total spectrum of nuclei experiencing all of the above interactions will be a convolution ( ) of all of the above spectra. (60)

More precisely, the NMR spectrum of a nucleus may be described by a series of interaction Hamiltonians, including nuclear spin interactions with both the external fields (H_0, H_1) and internal fields,

$$H = H_{ext} + H_{int} \tag{54}$$

where

$$H_{ext} = H_0 + H_1 \tag{55}$$

H_0 and H_1 are the Zeeman interactions with the external fields $\bar{H}_0$ and $\bar{H}_1$, respectively. H_{int} consists of the four interactions which were referred to as the main sources of line-broadening observed in the solid state NMR spectra.

$$H_{int} = H_s + H_d + H_j + H_q \tag{56}$$

The various interactions may be written as:

electron shielding $$H_s = \hbar \sum_i \bar{I_i} \cdot \overset{\Lambda}{\sigma_i} \cdot \bar{H_0} \tag{57}$$

direct dipolar interaction $$H_d = \sum_{i<j} \bar{I_i} \cdot \overset{\Lambda}{D_{ij}} \cdot \bar{I_j} \tag{58}$$

indirect electron-coupled interaction $$H_j = h \sum_{i<J} \bar{I_i} \cdot \overset{\Lambda}{J_{ij}} \cdot \bar{I_j} \tag{59}$$

electric quadrupolar interaction $$H_q = \sum_i \frac{eQ_i}{6I_i(2I_i-1)} \bar{I_i} \cdot \overset{\Lambda}{V_i} \cdot \bar{I_i} \tag{60}$$

In Equation (60), $\overset{\Lambda}{V_i}$ is the electric field gradient tensor at nucleus i.

In Equations (57-60), among the four interaction tensors, $\overset{\Lambda}{D}$ and $\overset{\Lambda}{V}$ are traceless, while $\overset{\Lambda}{\sigma}$ and $\overset{\Lambda}{J}$ are not restricted. However, two traceless tensors, $\overset{\Lambda}{\sigma}^*$ and $\overset{\Lambda}{J}^*$ can be obtained by subtracting the constant isotropic trace from $\overset{\Lambda}{\sigma}$ and $\overset{\Lambda}{J}$.

$$\overset{\Lambda}{\sigma}^* = \overset{\Lambda}{\sigma} - \sigma\overset{\Lambda}{1} \text{ where } \sigma = (1/3)tr\overset{\Lambda}{\sigma} \tag{61}$$

$$\overset{\Lambda}{J}^* = \overset{\Lambda}{J} - J\overset{\Lambda}{1} \text{ where } J = (1/3)tr\overset{\Lambda}{J} \tag{62}$$

and $\overset{\Lambda}{1}$ is the unit tensor.

Equations (57) and (59) can be rewritten as:

$$H_S = \hbar\sum_i \overline{I}_i \cdot \overset{\Lambda}{\sigma}_i^* \cdot \overline{H}_0 + \hbar\sum_i \overline{I}_i \cdot \sigma_i \cdot \overline{H}_0 \tag{63}$$

$$H_j = \hbar\sum_{i<j} \overline{I}_i \cdot \overset{\Lambda}{J}_{ij}^* \cdot \overline{I}_j + \hbar\sum_{i<j} \overline{I}_i \cdot J_{ij} \cdot \overline{I}_j \tag{64}$$

In the instance of fast and isotropic molecular reorientations, the time-averaged Hamiltonians due to the four traceless interaction tensors drop out of the model. Thus,

$$H_S = \hbar\sum_i \overline{I}_i \cdot \sigma_i \cdot \overline{H}_0 \tag{65}$$

$$H_d = 0 \tag{66}$$

$$H_j = \hbar\sum_{i<j} \overline{I}_i \cdot J_{ij} \cdot \overline{I}_j \tag{67}$$

$$H_q = 0 \tag{68}$$

These terms then represent what is observed in the NMR spectra of non-viscous liquids.

Theoretically, for solid samples, one can see how an alternative approach would eliminate all the anisotropic interactions due to the internal fields (61,62); this becomes possible through magic angle spinning (MAS), an angle of about 54.7°. Because of experimental reasons, the direct dipolar interaction (H_d) is usually removed by the technique of decoupling, which also removes both the isotropic and anisotropic parts of the other interaction involving two nuclear magnetic dipoles (i.e. H_j). Both methods are discussed below in more details.

1. Magic Angle Spinning

The magic angle is 54° 44' 8" = arc cos $(1/3)^{1/2}$, and magic angle spinning is the technique of rotating the whole solid specimen (within a rotor) uniformly about an axis inclined to $\overline{H}_0$ at the magic angle. The power of the MAS can be partially realized by inspection of Equation (50) for the direct coupling constant. Either the isotropic average $\langle\cos^2\theta_{ij}\rangle=1/3$ or the magic angle $\cos\theta_{ij} = (1/3)^{1/2}$ can lead to $\langle 3\cos^2\theta_{ij}-1\rangle=0$ and, thus, $D_{ij}=0$. In fact, it is the angle β, between the mechanical spinning axis and $\overline{H}_0$ adjusted to be equal to the magic angle, irrespective of the θ_{ij}'s. Nonetheless, under spinning conditions, the time-independent term of the time-averaged θ_{ij} (the time-dependent terms generate spinning sidebands) will go to zero because, in spite of its initial value, it contains a multiplier $(3\cos^2\beta-1)$.

Spinning Rate

In order to remove the anisotropic interactions effectively by MAS, it is necessary that the rotation period for the sample be short compared to the spin-spin relaxation time or dephasing time, T_2, of the individual spins. In other words, the spinning rate (Hz) has to be large compared to the linewidths (Hz) associated with the spins (39).

The ultimate spinning rate of a gas-driven rotor is governed by the linear velocity of its periphery. It can not exceed the speed of sound (63). For example, a 1 cm diameter rotor has a maximum theoretical rotation rate of 10.5KH_Z in dry air. Although, using a selective driver gas, helium, for example, in which the speed of sound is 2.7 times greater than in air, one might achieve a maximum theoretical spinning rate which would be 2.7 times faster. However, this upper limit is usually impractical as most materials used to confine samples disintegrate due to centrifugal forces at such velocities (39).

In general, MAS is carried out at a rate in the range of 3-5 KHz. This is not fast enough to remove the proton-proton and carbon-proton dipolar interactions (in the range of 10-40 KHz), although it has been, indeed, successful in removing the dipolar interactions of some nuclei of small magnetogyric ratio (61,62,64). MAS is also able to remove the anisotropic part of the indirect electron-coupled interaction (65,66) as well as the (first order) electric quadrupolar interaction (67). However, since in solid state carbon-13 NMR, MAS is aimed at removing the chemical shift anisotropy (CSA) (ca. 1.8-3 KH_Z, for aromatic and carbonyl carbons at an external field H_0 of 1.4 Tesla), only the effects

of MAS on the CSA interaction are reviewed below.

Removal of the Chemical Shift Anisotropy by Magic Angle Spinning

Since any antisymmetric components of the shielding tensor $\overset{\Lambda}{\sigma}$, have negligible effects on the spectrum (68), the chemical shift of a nucleus i with principal shielding elements σ_{i1}, σ_{i2}, σ_{i3} and with direction cosines between the principal axes of $\overset{\Lambda}{\sigma}_i$ and $\overset{\Lambda}{H}_0$, λ_{i1}, λ_{i2}, λ_{i3} is given by (61,62)

$$\sigma_{izz} = \lambda_{i1}^2 \sigma_{i1} + \lambda_{i2}^2 \sigma_{i2} + \lambda_{i3}^2 \sigma_{i3} \tag{69}$$

If the solid sample in which i is resident, is rotated at angular velocity ω_r about an axis inclined to $\overline{H}_0$ at an angle β and at angles Φ_{i1}, Φ_{i2}, Φ_{i3} to the principal axes of $\overset{\Lambda}{\sigma}$, the direction cosines become (K=1,2,3)

$$\lambda_{ik} = \cos\beta \cos\Phi_{ik} + \sin\beta \sin\Phi_{ik} \cos(\omega_r t + \chi_{ik}) \tag{70}$$

where χ_{ik} is the azimuthal angle of the Kth principal axis (w.r.t. $\overline{H}_0$) at t = 0. From equation (70), one obtains:

$$\begin{aligned}\lambda_{ik}^2 = {} & 1/2[\sin^2\beta + (3\cos^2\beta - 1)\cos^2\Phi_{ik}] \\ & + 1/2[\sin^2\beta \sin^2\Phi_{ik} \cos(\omega_r t + \chi_{ik}) + \\ & \sin 2\beta \sin^2\Phi_{ik} \cos 2(\omega_r t + \chi_{ik})]\end{aligned} \tag{71}$$

where λ_{ik}^2 consists of a time-independent term $(\lambda_{ik}^2)_0$ and a time-dependent term $(\lambda_{ik}^2)_t$, which is periodic with zero mean value and will generate spinning sidebands if the spinning rate is insufficient.

$$\lambda_{ik}^2 = (\lambda_{ik}^2)_o + (\lambda_{ik}^2)_t \tag{72}$$

Substituting Equation (72) into Equation (69) one obtains:

$$\sigma_{izz} = \sum_{k=1}^{3} (\lambda_{ik}^2)_o \sigma_{ik} + \sum_{k=1}^{3} (\lambda_{ik}^2)_t \sigma_{ik} \tag{73}$$

Equation (73) describes a spectrum of a resonance line according to $\sum_{k=1}^{3} (\lambda_{ik}^2)_o \sigma_{ik}$ with spinning sidebands at multiples of ω_r.

The intensity of the sidebands decreases as the spinning rate increases. At a sufficient speed ($\omega_r > T_{2m}^{-1}$), the time-averaged value of $\langle \sum_{k=1}^{3} (\lambda_{ik}^2)_t \sigma_{ik} \rangle$ approaches zero and the sidebands become negligible (69). Therefore, time-average yields the observed chemical shift, specifically

$$\langle \sigma_{izz} \rangle = \sum_{k=1}^{3} (\lambda_{ik}^2)_o \sigma_{ik} = 1/2 \sin^2 \beta (\sigma_{i1}+\sigma_{i2}+\sigma_{i3}) + 1/2(3\cos^2 \beta - 1) \sum_{k=1}^{3} \cos^2 \Phi_{ik} \sigma_{ik} \tag{74}$$

If β is the magic angle, Equation (74) reduces to

$$\langle \sigma_{izz} \rangle = 1/3(\sigma_{i1}+\sigma_{i2}+\sigma_{i3}) = (1/3) \mathrm{tr} \overset{\Lambda}{\sigma}_i = \sigma_i \tag{75}$$

regardless of the initial orientation of the principal axes of $\overset{\Lambda}{\sigma}_i$ with respect to H_o and to the spinning axis.

Besides yielding "liquid like" spectra by high speed MAS of solid samples, the method may also be modified. MAS at insufficient rates (69,70) as well as off-MAS (variable angle spinning) at high speed (39) have been used to extract components of the shielding tensor and to study molecular orientation.

2. Decoupling (32,68)

As stated above, any interaction between two nuclear magnetic dipoles, homonuclear or heteronuclear, can be eliminated by saturating the Zeeman splitting of one of the nuclei with a complementary RF field H_2.

Heteronuclear Dipolar Decoupling

Heteronuclear decoupling can be carried out by irradiating the entire chemical shift range of the nucleus selected for decoupling (broad-band decoupling). Heteronuclear proton broad-band decoupling has become standard for C-13 NMR of liquid samples in order to remove the isotropic (scalar) indirect spin-spin interactions (J-couplings). In solid state C-13 NMR, the same procedure can be used to eliminate both the direct and indirect (isotropic and anisotropic) spin-spin interactions. However, the RF power required to remove the 10-40 KH_z dipolar coupling is considerably greater than that for the 100-200 H_z scalar coupling. For this reason, removal of heteronuclear spin-spin interactions by high power broad-band RF irradiation is referred to as "Dipolar Decoupling" (DD) (38).

In the case of ^{13}C or other nuclei having low natural abundance

and/or a small magnetic moment, the homonuclear spin-spin interaction is a negligible source of line-broadening relative to the heteronuclear interactions with nuclei having high natural abundance and/or a large magnetic moment. Furthermore, high speed MAS usually removes the weak homonuclear interactions to a large extent. Therefore, combining dipolar decoupling with MAS, high resolution "liquid like" solid state NMR can be achieved for ^{13}C and some other nuclei having weak macroscopic magnetic moments.

Dipolar Decoupling by Spin Locking (71)

In solid state C-13 NMR, proton dipolar decoupling is actually achieved by a spin locking process. A spin-locked nucleus, where individual dipoles precesses about $\overline{H}_1$, resulting in an oscillatory component along the z-axis, is decoupled from other kinds of nuclei provided the precessing or oscillating frequency (depends on H_1) is greater than the dipolar interaction expressed in hertz.

Homonuclear Decoupling

Homonuclear decoupling experiments, where the observed and decoupled nuclei are of the same type, are more demanding. In solution NMR, a time-sharing procedure has been developed to carry out homonuclear scalar decoupling (72). In solid state NMR, homonuclear decoupling has been achieved by a number of multiple-pulse sequences (73-76), which alternately drive the nuclear magnetic dipoles along the three orthogonal axes. This results in a time-averaged value of $\langle\cos^2\theta\rangle=1/3$ without saturating either the observed or "decoupled"

nuclei. These methods can eliminate the anisotropic direct and indirect spin-spin couplings. (In fact, they can remove both the homonuclear and heteronuclear couplings as well as the electric quadrupolar interactions.) The indirect scalar couplings are preserved while the chemical shifts are modified without averaging out the anisotropy.

Combining MAS with multiple-pulse decoupling, high resolution "liquid like" solid state NMR can be achieved for proton and many other nuclei (35,77).

3. Factors Affecting Resolution in the High Resolution Solid State NMR

The Gaussian lineshapes observed in the broad-line solid state NMR are mainly due to the direct nuclear dipolar interactions (78). After the removal of these interactions and other sources of line-broadening, the lineshapes of the high resolution "liquidlike" solid state NMR are observed to be Lorentzian (79). However, the resolution of the "liquidlike" solid state NMR is generally not as good as in the liquid case. Furthermore, unlike solution NMR, increasing the magnetic field may not help because chemical shift anisotropy is proportional to the strength of the applied field H_0.

Besides T_2, which determines the natural bandwidth, major factors affecting the ultimate resolution of the (DD-MAS) solid state C-13 NMR both in terms of technical limitations and sample effects are reviewed below (36,80). These factors are, of course, among the major factors affecting the resolution of the high resolution solid state NMR of other nuclei as well (62).

Technical Limitations

(1) Imperfect Adjustment to the Magic Angle

Let us assume that a spinning axis was 0.5° off the magic angle. This results in a residual CSA of 1% of the static value (61). However, this can usually be reduced further by trial-and-error adjustment of the angle.

(2) Insufficient Spinning Rate

In certain cases, especially at high external field strengths, as discussed before, if the spinning rate is less than the CSA, a spectrum is broken up into a complex profile of sidebands centered around each isotropic shift. This leads to a loss in sensitivity, as well as confusion in spectral assignments. Methods have been introduced to overcome this problem and thus to enable spinning-sideband-free solid state NMR spectra to be obtained in high field super conducting magnets, either by recovering the isotropic shifts from the sidebands (81) or using a phase-adjusted technique (82).

(3) Other possible technical limitations include rotor instabilities, insufficient decoupling power and off-resonance proton irradiation (80).

Sample Effects

Even under ideal experimental conditions, static and/or dynamic effects can limit resolution in certain solid samples. These effects include:

(1) Solid State Effect

Some carbons having the same chemical shift in the liquid state are

discernable (split) in the solid state NMR, (e.g., the two non-substituted aromatic carbons of poly(phenylene oxide)) due to higher degrees of molecular orientation.

(2) Chemical Shift Distributions

The heterogeneous nature of amorphous materials, such as glassy polymers, may result in a distribution of isotropic chemical shifts for a single carbon. This can contribute several ppm of broadening (38).

(3) Dynamic Effects

Ironically, interference between coherent motion introduced by the line-narrowing techniques (e.g., spin locking and sample rotation) and molecular motion can combine to degrade the resolution gained by these techniques (38,77,80,83).

(4) Another effect is the residual dipolar interaction between ^{13}C and nuclei having a large quadrupole moment (e.g., ^{14}N, ^{35}Cl), which may broaden the C-13 spectra of solids when the interaction is too strong to be eliminated by MAS and when T_1's of the quadrupolar nuclei are too long to induce "self-decoupling" (84).

Although these effects complicate and broaden the high resolution solid state C-13 spectra, they can also lead to new structural and dynamic information of the sample studied.

D. The Sensitivity Problem and Its Solution

In this section, the sensitivity problem and approaches to its solution are reviewed for carbon-13, although the discussion applies equally well to other spin 1/2 nuclei having weak mutual coupling.

For convenience of the treatment, the conventional symbolism S and I are employed to express the nuclei of ^{13}C and ^{1}H respectively. The local magnetic field induced by the magnetic moment of a proton is expressed as:

$$h_z^{\ell} = \frac{\mu_z^H}{r^3} \langle 1-3\cos^2\theta \rangle \tag{76}$$

where r can be either the homonuclear or heteronuclear distance. The Zeeman splittings due to this local field on its neighboring nuclei are expressed as:

$$\Delta\nu_{HH} = 2\, D_{HH} = \frac{\gamma H}{\pi} |h_z^{\ell}| \tag{77}$$

$$\Delta\nu_{CH} = 2\, D_{CH} = \frac{\gamma C}{\pi} |h_z^{\ell}| \tag{78}$$

1. General Considerations and Definitions

The sensitivity problem of the solid state C-13 NMR can be considered in three categories.

(1) Low Natural Abundance (1.1%) and a Small Magnetic Moment ($\mu_{C\simeq 1/4\mu_H}$).

(2) Poor Resolution. As discussed in the last section, even with all of the line-narrowing techniques available, NMR resolution in solids is still not as good as in liquids. Therefore, in terms of peak height, one must require a substantially greater number of accumulations in order to achieve the same S/N for a solid sample compared to a liquid

sample having the same (integrated) resonance line intensity and the same number of scans.

(3) Long ^{13}C's Spin-Lattice Relaxation Times. Due to the two problems indicated above, in general, a great number of accumulations are needed to achieve a solid state C-13 spectrum with reasonable S/N. Thus, the experimental time becomes limited by the rate at which carbon magnetization can be reestablished along $\bar{H}_0$ by spin-lattice relaxation process (e.g., in a 90° pulse sequence, a pulse delay time of ca. $5T_1$ between two scans). This process for C-13 in solids is usually ineffecient due to the small magnetic moment, lack of high frequency molecular reorientations and inefficient spin diffusion.

The first problem listed above can be circumvented with isotope enrichment, while the second is anticipated to be ameliorable as line-narrowing techniques progress. However, cross polarization (CP) techniques (85) have overcome the third problem thus making C-13 NMR studies of natural abundance solids possible. Cross polarization is a particularly effective version of a double resonance experiment in the rotating frame (71,86); it uses the large proton magnetization to polarize the ^{13}C nuclei. The rest of this section will review the principles and effects of the CP technique.

2. Spin-Lattice Relaxation in the Solid State

Comparison of ^{1}H's and ^{13}C's T_1's

Since the CP process uses proton magnetization to polarize the ^{13}C nuclei, the proton's T_1's have to be shorter than ^{13}C's T_1's in order to make the process effective. Recalling Equation (38)

$$R_{im} = \frac{1}{T_{im}} = E_c^2 f_{im}(\tau_c)$$

where E_c for protons and ^{13}C nuclei are γ_I^2/r^3 and $\gamma_I\gamma_S/r^3$, respectively, if one assumes that ^1H-^1H and ^{13}C-^1H dipole-dipole interactions are the dominant spin-lattice relaxation mechanisms for protons and ^{13}C nuclei, respectively. As stated before, the spectra density of motions at ω_I and $2\omega_I$ are responsible for proton's T_1's; it can also be shown that motions at ω_S and $\omega_I \pm \omega_S$ (i.e. $\omega_I/4$, $3\omega_I/4$ and $5\omega_I/4$) are responsible for ^{13}C's T_1's (13,43). Therefore, molecular motion is not a significant factor in that proton's T_1's are shorter than ^{13}C's T_1's. Further if one assumes that in a hydrocarbon compound, in which every proton and every C-13 nucleus can be considered to have about the same number of protons of about the same proximity in its neighgorhood, (polyethylene is a good case), then the proton's T_1 is expected to be 16 times shorter than ^{13}C's T_1. However, in the crystalline region of semi-crystalline polyethylene, ^{13}C's T_1 has been found to be 200-1000 times longer than the proton's T_1 (39). It is the very effective mechanism of spin diffusion among protons which makes proton's T_1's usually much shorter than what would be expected according to Equation (38).

Spin Diffusion

Spin diffusion is a process of rapid simultaneous transitions ("flip-flop") of dipolar coupled nuclei having antiparallel moments, without physical movement of the nucleus, when the coupled nuclei have

the "same" precession frequency (43).

Spin diffusion does not involve energy exchange with the lattice. However, spin diffusion among protons does lead to all of the protons exchanging energy with the lattice through preferred relaxation sites. When the spin diffusion process becomes more effective than the most effective spin-lattice relaxation process (the diffusion rate is roughly equal to $\Delta\nu_{HH}$), all the proton's T_1's observed will be the same. Even in an inhomogeneous (microheterogeneous) material, spin diffusion usually enables the rigid regions to relax faster with the lattice than would be possible without the process; again, semi-crystalline polyethylene is an example (39).

The CP process, indeed, utilizes the concept of spin diffusion by employing a double resonance technique to enable the protons and ^{13}C nuclei to precess at the "same" frequency in the rotating frame.

Another effect of the spin diffusion among protons is that the fluctuating magnetic fields due to the "flip-flop" process reduce ^{13}C-^{1}H interaction from $\Delta\nu_{CH}$ to $\Delta\nu_{CH}(\Delta\nu_{CH}/\Delta\nu_{HH})$ (43).

3. Relaxation in the Rotating Frame

This subject has been discussed before in the section on relaxation time measurements. Since CP is a process of double resonance in the rotating frame, $T_{1\rho}$ of the protons will be a factor in obtaining reliable intensities in the CP spectra, as discussed later.

Another concept, the spin temperature, which might provide an insight into the relaxation in the rotating frame and other nuclear relaxation processes, as well as to the CP process, is reviewed below.

Spin Temperature in Solids (43,44)

Equation (8) describing the equilibrium macroscopic magnetization can be rewritten as

$$M_0 = \frac{CH_0}{kT_L} \tag{79}$$

where C is the Curie constant,

$$C = \frac{N_0\mu^2 (I+1)}{3I} = \frac{N_0\gamma^2h^2I(I+1)}{3} \tag{80}$$

and Equation (79) is known as the Curie's law. In Equation (79) T_L denotes the lattice temperature to distinguish it from the spin temperature T_S. Obviously, in the equilibrium state

$$T_S = T_L = \frac{CH_0}{kM_0} \tag{81}$$

As discussed earlier, when a spin system is perturbed, in the existence of effective spin diffusion, a thermal equilibrium inside the nuclear spin system characterized by a uniform spin temperature T_S can be achieved in a time much shorter than T_1 (i.e., when $T_1 >> T_2$, since $\Delta\nu HH\text{-}1 \sim T_{2DD}$). The spin temperature of such an "internal equilibrium" system is given by

$$T_S = \frac{CH_{eff}}{kM_0^*} \tag{82}$$

Where M_0^* is the internal equilibrium macroscopic magnetization.

Therefore, T_S can be significantly different from T_L in these spin systems before the completion of the spin-lattice relaxation process. On the other hand, the spin-lattice relaxation process of these systems can be regarded as a thermal process of cooling the spin systems to reach thermal equilibrium with the lattice.

In the rotating frame, at the beginning of the spin locking process, $H_{eff} = H_1$, $M_0^* = M_0$ and Equation (82) becomes

$$T_S = \frac{CH_1}{kM_0} = \frac{CH_0}{kM_0} \cdot \frac{H_1}{H_0} = T_L \frac{H_1}{H_0} \qquad (83)$$

Note that H_0 is usually much greater than H_1. Therefore, relaxation in the rotating frame is a "heating" process, which finally reaches $T_S = T_L$ with a much smaller macroscopic magnetization $M_0(H_1/H_0)$ in the rotating frame.

4. Cross Polarization (85)

Many CP schemes are possible (85), but only the commonly used single-contact spin lock version is reviewed in the following.

Hartmann-Hahn Condition (86)

The Hartmann-Hahn matching condition for nuclear double resonance in the rotating frame is the key to the success of the CP method. The condition is achieved by simultaneously applying two resonant alternating RF fields in the xy plane, $\overline{H}_{1I}$ and $\overline{H}_{1S}$, to the respective I and S spins such that

$$(\gamma_I/2\pi)H_{1I} = \nu_I = \nu_S = (\gamma_S/2\pi)H_{1S} \qquad (84)$$

Thus, in the rotating frame, I spins are precessing about $\overline{H}_{1I}$ and S spins are precessing about $\overline{H}_{1S}$ at the same frequency. Both spin systems generate oscillatory components along the z-axis at the same frequency regardless of the phase angle between $\overline{H}_{1I}$ and $\overline{H}_{1S}$. This enables a heteronuclear (IS) spin diffusion (39) between the I-spins and the S-spins. The two spin systems usually can reach thermal equilibrium such that $T_S^I = T_S^S$ in a time much shorter than T_{1I} and T_{1S}.

The period of time in which the $\overline{H}_{1I}$ and $\overline{H}_{1S}$ fields are simultaneously applied is referred to as the contact time (38).

Cross Polarization Procedure

One of the variety of experimental methods (85) for establishing contact of I and S spin systems and then observing the S-spin magnetization is represented by the following sequence:

(1) establish I-spin magnetization in $\overline{H}_0$ in a period of time of ca. $5T_{1I}$.

(2) spin-lock I-spins along $\overline{H}_{1I}$ and simulatneously apply $\overline{H}_{1S}$ to contact S and I spins with a Hartmann-Hahn match.

(3) turn-off H_{1S} and record S-spin FID. Keep H_{1I} on as a dipolar decoupler until the completion of S-spin data acquisition.

(4) repeat steps (1) - (3).

A modification of this sequence (87) shifts $\overline{H}_{1I}$ by 180° every other spin lock sequence. Thus the S-spin magnetization grows alternately parallel or antiparallel to $\overline{H}_{1S}$, even though the $\overline{H}_{1S}$ itself

retains the same phase. By alternately adding and subtracting the S-spin FID, RF transients are subtracted out, while the S-spin FIDs are coherently added. Therefore, artifacts, such as pulse breakthrough due to long receiver recovery times can be minimized or eliminated. The sequence and its modification described above are used as a standard procedure in all the CP spectra of this dissertation.

Sensitivity Enhancement (85)

As discussed before, establishing the Hartman-Hahn condition allows the I and S spin systems to reach an internal equilibrium in a time much shorter than T_{1I} and T_{1S}. Assuming that $(T_{1\rho}{}^I)^{-1}$ is neglible (i.e. $T_{1\rho}{}^I$ approaches infinity) relative to the cross relaxation rate (IS spin diffusion), the spin temperature of the internal equilibrium state will be:

$$T_S{}^I = T_S{}^S = (1+\varepsilon)\frac{H_{1I}}{H_o} T_L \qquad (85)$$

where $\varepsilon = C_S/C_I$ and C_S and C_I are the Curie constants for the S-spins and I-spins, respectively.

The cross-polarized S spin magnetization can be calculated by substituting Equation (84), (85) and $H_{eff}=H_{1S}$ for the S-spin into Equation (82).

$$Mo^*S = (1-\varepsilon)\frac{H_{1S}}{H_{1I}} M_oS = (1-\varepsilon)\frac{\gamma I}{\gamma S} M_oS \qquad (86)$$

Since $1-\varepsilon \sim 1.0$ in most organic compounds and $\gamma_H/\gamma_C \sim 4.0$, then $M_o{}^*C \sim 4M_o{}^C$.

Therefore, the CP method not only polarizes the carbons more quickly (by ~ T_{1H}/T_{1C} (longest)) but also, to a greater degree (by about four times) than is possible by natural relaxation processes. When compared to the conventional single 90° pulse sequence, the CP sequence can shorten the experimental time by a factor of $(4\ T_{1C}\ (\text{longest})/T_{1H})^2$ in an ideal case.

Spin Lock Cross Polarization Dynamics (88)

Sensitivity enhancement actually achieved by the CP process is usually smaller than that predicted from Equation (86). In fact, not only the I-spin magnetization relaxes in the rotating frame, so does the S-spin magnetization. Assuming both processes as well as the cross polarization (cross relaxation) to be first order mechanisms characterized by rate constants $T_{1\rho}{}^I$, $T_{1\rho}{}^S$ and T_{IS}, then the SL CP dynamics can be described by the equation:

$$\frac{dMS(t)}{dt} = \frac{M_0{}^*S\exp(-t/T_{1\rho}) - MS(t)}{T_{IS}} - \frac{MS(t)}{T_{1\rho}{}^S} \qquad (87)$$

where $MS(t)$ is the S-spin magnetization as a function of contact time t.

Since $MS(t=0)=0$, Equation (87) yields the solution

$$MS(t) = \frac{M_0{}^*S}{T_{IS}} \frac{\exp(-t/T_{1\rho}{}^I) - \exp[-t(1/T_{1\rho}{}^S + 1/T_{IS})]}{1/T_{1\rho}{}^S + 1/T_{IS} - 1/T_{1\rho}{}^I} \qquad (88)$$

When the CP process is very effective, i.e. $T_{1\rho}{}^I >> T_{IS}$ and $T_{1\rho}{}^S >> T_{IS}$, Equation (88) reduces to:

$$M^S(t) = M_0{}^*S\ [\exp(-t/T_{1\rho}{}^I) - \exp(-t/T_{IS})] \qquad (89)$$

Therefore, immediately after the contact ($T_{IS} >> t$)

$$M^S(t) = M_0{}^*S[1 - \exp(-t/T_{IS})] \qquad (90)$$

and when the contact time becomes longer ($t >> T_{IS}$)

$$M^S(t) = M_0{}^*S \exp(-t/T_{1\rho}{}^I) \qquad (91)$$

Indeed, when $T_{1\rho}{}^I >> T_{IS}$ (e.g., $T_{1\rho}{}^I > 200\ T_{IS}$), the optimum sensitivity enhancements predicted by Equation (86) can be practically achieved ($M^S > 0.95\ M_0{}^*S$), within a certain period of contact time ($0.05\ T_{1\rho}{}^I > t > 3T_{IS}$).

Furthermore, from the S-spin magnetization polarized as a function of contact time, the CP rate (T_{IS}) and the I-spin rotating frame relaxation time ($T_{1\rho}{}^I$) can be estimated according to Equations (90) and (91), respectively.

Relative Intensities in CP Spectra (36)

It is well known that in solution C-13 NMR T_1's of each individual carbon can be substantially different from one another. Therefore, quantitative work can be assured only if a spectrum is obtained under certain appropriate conditions.

In the C-13 CP spectra of solids, it has been calculated (85) that the CP rate at the matching condition to be:

$$T_{CH}{}^{-1} \sim \Delta\nu_{CH}^2/\Delta\nu_{HH} \qquad (92)$$

Thus, the CP rate depends on r_{CH}^{-6}, so that carbons which have no bonded protons will cross polarize significantly more slowly than will the protonated carbons. This disparity, like that of T_1's in the solution C-13 NMR, can be exploited in a variety of ways (38,89). Nonetheless, when quantitative works are carried out on a CP spectrum, appropriate experimental conditions have to be considered. (The condition of 0.05 $T_{1\rho}H$ > contact time > 3 T_{CH} (longest) in the C-13 spectra of solids, is equivalent to a pulse delay time greater than 3 T_{1C} (longest) in the solution C-13 NMR with a 90° pulse sequence).

5. Relaxation Time Measurements - The Cross Polarization Methods

The methods of the conventional relaxation time measurements described in the previous section are usually unsuitable, due to the sensitivity problem, for nuclei with long T_1's. Since the CP method enhances sensitivity of the rare spins, relaxation time (T_1 and $T_{1\rho}$) measurements using CP sequences have been introduced for the C-13 NMR of solids.

Two methods which use a single-contact spin lock CP sequence are reviewed in the following paragraphs.

$T_{1\rho}$ CP Method (38)

The pulse sequence of this method can be described in three parts.

(1) The first part is a matched Hartmann-Hahn CP preparation of carbon magnetization (Step 1 and 2, described in the CP procedure).

(2) The second part is the variable time, τ, that the carbon magnetization is held in $\overline{H}_{1C}$ without CP contact (H_{1H} turned off) and

relaxes, with a time constant $T_{1\rho}$.

(3) The third part is the observation of the carbon FID with proton dipolar decoupling (H_{1C} off, H_{1H} on).

The corresponding line intensity for this sequence is given by:

$$M(\tau) = M_0^* \exp(-\tau/T_{1\rho}) \tag{93}$$

T_1 CP Method (90)

The pulse sequence of this method may also be described in three parts. The first and third parts are the same as the $T_{1\rho}$ CP method. The second part consists of three steps.

(1) CP contact is broken by turning off H_{1H}. Simultaneously, $\overline{H}_{1C}$ is phase shifted by 90° and rotates the carbon magnetization from the xy plane to the z-axis, at which time H_{1C} is turned off.

(2) This step involves a variable time, τ, the carbon magnetization is held in $\overline{H}_0$ (=Heff) and relaxes from M_0^* (~ $4M_0$) to M_0, with a time constant T_1.

(3) A 90° H_{1C} pulse rotates the carbon magnetization back into the xy plane for observation.

The corresponding line intensity for this sequence is given by:

$$M(\tau) = (M_0^* - M_0) \exp(-\tau/T_1) + M_0 \tag{94}$$

T_1 values of carbon-13 nuclei determined by this CP method have been found to be in good agreement with those measured by the conventional inversion-recovery method.

MULTICOMPONENT POLYMER SYSTEMS

Multicomponent polymer systems, which combine two or more monomers or homopolymers to achieve optimum properties by various means, represent alternative approaches to improve the overall performance of polymeric materials. Such approaches are usually more versatile and feasible than those involving developing new monomers or homopolymers, even though synergistic combinations among the existing monomers or homopolymers are rare on a random basis. Furthermore, the multicomponent systems may achieve unique and novel properties which are unattainable in homopolymers.

The multicomponent polymer systems can be divided into three categories: copolymers, polyblends and polymer composites (which may and usually do contain non-polymer "foreign" materials). The scheme of classification will be briefly reviewed in the first part of this section. In the second part the concept of polymer-polymer miscibility will be discussed.

A. Classification (1-2)

1. Copolymers

In copolymers the components are linked by strong covalent bonds. According to their architectures, copolymers can be classified into five groups.

Random Copolymers

In random copolymerization, two or more monomers are present simultaneously in a reactor, the resulting copolymers are characterized by a statistical placement of the comonomers repeat units along the

backbone of the chain.

Alternating Copolymers

Alternating copolymerization is a special case of the random copolymerization, it requires pairs of monomers having highly specific copolymerization reactivity ratios and/or special reaction conditions.

Block Copolymers

In anionic block copolymerization, typically one monomer is polymerized and another monomer is polymerized onto the living ends of the polymeric chains. Depending on the synthetic methods, such block copolymers may have either a diblock, triblock or multiblock linear chain, or even a star-shaped radial type of subarchitecture.

Graft Copolymers

In graft copolymerization, one polymer is prepared, and one or more monomers are grafted onto this polymer. The final product consists of a polymeric backbone with one or more side chains.

Crosslinked Copolymers

Crosslinking one linear polymer with a second polymer can be achieved, among many other ways, by generating free-radical sites on a preformed polymer in the presence of another monomer. Grafting occurs on this site and combination by termination may result in crosslinking.

2. Polyblends

In contrast to copolymers, in polyblends the components adhere together only through secondary bond forces, either van der Waals forces, dipole interactions or hydrogen bonding. Polyblends generally consist of a polymeric matrix in which another polymer is imbedded. They

are made by a variety of methods including mechanical methods such as compounding on mill rolls, in extruders or in Banbury mixers and by solution casting methods. According to the properties of the matrix and the dispersed phase, polyblends can be classified into four groups (91) as given in Table 1.

3. Composites

In contrast to polyblends, polymer composites consist of a polymer matrix in which a foreign material is dispersed rather than dissolved. They also may be classified into four groups (91) as shown in Table 2.

In addition to those composites listed above, in which polymers are reinforced by fillers, inorganic materials can also be reinforced by polymers. For example, it has been found that monomers can be soaked into concrete and polymerized *in situ* to increase the strength by as much as four times that of untreated concrete (92).

B. Polymer-Polymer Miscibility (5,6,93-95)

A solution is defined, in general, as a random mixture of two or more components consituting a single phase. But the concept of a phase is very difficult to define, particularly in the case of polymers. As a matter of fact, a miscible polymer-polymer solution is a relative, rather than an absolute, state, with the uniformity requirements calling for a length scale and the reproducibility and stability requirements calling for a time and energy scale (96).

For practical purposes, a miscible polymer mixture is defined as a

Table 1

Polyblends (91)

	Matrix	Dispersed Phase	Improvement	Examples
1.	rigid	soft	tougher	impact PS, ABS, rigid PVC
2.	rigid	rigid	fast melt flow higher impact strength reduced shrinkage	PPO + impact PS PVC + ABS or MBS thermoplast in polyester
3.	soft	soft	lower wear	SBR + natural rubber SBR + cis-polybutadiene
4.	soft	rigid	increased strength reduced abrasion cut growth and flex cracking	SBR + PS

Table 2

Composites (91)

Matrix	Dispersed Phase Filler or Reinforcing Material
1. thermoplastics	short glass fibers, beads, hollow spheres, minerals
2. thermosets	wood flour, paper, asbestos, clay
3. vulcanized rubber	carbon black, calcium silicate
4. polyether, polyepoxides, structural resins	long glass fibers, mat or cloth; graphite fibers, boron whiskers

stable homogeneous combination which exhibits macroscopic properties expected of a single-phase material. Homogeneity is defined in terms of a domain whose dimension is similar to that responsible for macrosopic properties such as the glass transition and light transparency (95).

Thermodynamics of and methods for determining polymer-polymer miscibility will be reviewed in terms of polyblends. However, most of these with a few modifications are applicable to block copolymers, which generally differ from polyblends by only a few chemical bonds.

1. General Thermodynamics of Polymer-Solvent and Polymer-Polymer Systems

Based on solution thermodynamics of small molecules, using the lattice concept (93), and taking into account that a polymer segment must have at least two adjacent sites occupied by polymer segments, one may arrive at the Flory-Huggins expression for the entropy of mixing of polymer with solvent (with subscript 1 representing solvent and subscript 2 representing polymer).

$$\Delta SM = -k(N_1 \ln\phi 1 + N2 \ln\phi 2) \qquad (95)$$

where N_i and ϕi are the number of molecules and the volume fraction of component i, respectively.

With the same assumptions, the enthalpy of mixing can be expressed as:

$$\Delta HM = (N_1 + N_2 \frac{V_2}{V_1}) zw\phi 1\phi 2 = \frac{V}{V_1} zw\phi 1\phi 2 \qquad (96)$$

where $V = N_1V_1 + N_2V_2$ is the total volume of the system, z is a coordination number and w is an exchange energy,

$$w = 1/2\ \varepsilon_{11} + 1/2\ \varepsilon_{22} - \varepsilon_{12} \tag{97}$$

where ε_{ij} is the energy of a contact between components i and j.

Since the free energy of mixing is

$$\Delta G^M = \Delta H^M - T\Delta S^M \tag{98}$$

on substituting Equation (95) and (96) into Equation (98) the free energy of mixing on a volume basis is

$$\frac{\Delta G^M}{V} = kT\left[\frac{\Phi_1}{V_1}\ln\Phi_1 + \frac{\Phi_2}{V_2}\ln\Phi_2 + \left(\frac{zw}{kT}\right)\frac{\Phi_1\Phi_2}{V_1}\right] \tag{99}$$

where the quantity zw/kT is often called the Flory interaction parameter χ_{12}.

$$\chi_{12} = \frac{zw}{kT} \tag{100}$$

Equations (95-100) can also be applied to the polymer-polymer systems, with V_1 in the enthalpic term replaced by V_s. V_s is the interacting segment volume which is assumed to be the volume of the smallest polymer repeat unit. Thus, the free energy of mixing between two polymers on a volume basis is:

$$\frac{\Delta G^M}{V} = kT\left[\frac{\Phi_1}{V_1}\ln\Phi_1 + \frac{\Phi_2}{V_2}\ln\Phi_2 + \left(\frac{zw}{kT}\right)\frac{\Phi_1\Phi_2}{V_s}\right] \tag{101}$$

Because of the large polymer volume, in polymer-polymer systems the entropic contribution to the free energy of mixing is seen to be negligible.

2. Stability and Phase Separation Phenomena

Unlike most of solutions of small molecules, in polymer-polymer systems, a negative free energy of mixing is a necessary but not a sufficient condition for miscibility. For a homogeneous single-phase polymer blend, ΔG^M is negative. However, depending on the shape and location of the co-existence curve, the same blend could actually achieve an even lower free energy state by separating into two phases. Figure 4 (95) gives the free energy of mixing as a function of concentration in a binary liquid system. The concentration corresponding to the crest ($\phi_2'' < \phi_2 < \phi_2'$) of the free energy curve at T_2 fits the situation under consideration. The crest may reflect the heat of mixing but could equally well spring from a deviation of the entropy of mixing from mere combinatorial terms (95).

From the Gibbs-Duhem theory of thermodynamic stability (97), a stable or metastable state can be achieved if and only if

$$\Delta G < 0, \text{ and } (\partial^2 \Delta G/\partial \phi^2)_{T,P} > 0 \qquad (102)$$

From these criteria, the crest of the free energy curve for T_2 can be divided into two regions. In the region of compositions ranging from $\phi_{2,sp}'$ to $\phi_{2,sp}''$, $(\partial^2 \Delta G^M/\partial \phi^2) < 0$, any small perturbation of composition results in a lower free energy state of the system, thus a spontaneous

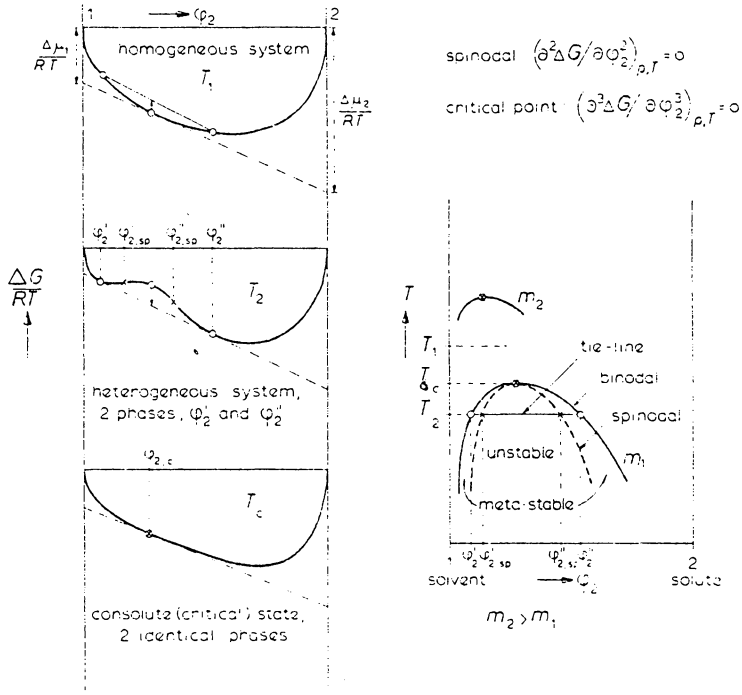

Figure 4. Gibbs Free Energy of Mixing as a Function of Concentration in a Binary Liquid System Showing Partial Miscibility. (95)

phase separation may occur, and this region is called the unstable state. In the region of compositions ranging from ϕ_2' to $\phi_{2,sp}'$ and from $\phi_{2,sp}''$ to ϕ_2'', the stability criteria, (Equation (102)) are satisfied. Any small perturbation of composition results in a higher free energy state of the system. But the state becomes unstable to some finite perturbation; e.g., if a nucleus of composition ϕ_2'' is formed, the composition in its immediate neighborhood will become ϕ_2'. Therefore, this region is called the metastable state.

In the free energy curves of Figure 4, the loci where the stable and metastable regions are divided are known as binodals (ϕ_2',ϕ_2'') and are defined by the equation:

$$(\partial \Delta G^M/\partial \Phi)_{T,P} = 0 \quad \text{or} \tag{103}$$

$$\Delta\mu_1 = \Delta\mu_1' \text{ and } \Delta\mu_2 = \Delta\mu_2' \tag{104}$$

where μ_i and μ_i' are the chemical potentials of polymer i in the two equilibrium phases. The locations where the metastable and the unstable regions are divided are known as the spinodals, ($\phi_{2,sp}'$,$\phi_{2,sp}''$), and are defined by the equation:

$$(\partial^2 \Delta G^M/\partial \Phi^2)_{T,P} = 0 \tag{105}$$

The critical point or consolute state is reached when

$$(\partial^3 \Delta G^M/\partial \Phi^3)_{T,P} = (\partial^2 \Delta G^M/\partial \Phi^2)_{T,P} = 0 \tag{106}$$

A spontaneous phase separation process in the unstable region is

referred to as spinodal decomposition. For polymer-polymer systems, this process usually results in co-continuous phases. Phase separation in the metastable region is usually via a nucleation and growth mechanism. For polymer-polymer systems, this process usually results in a finely dispersed two-phase structure whose final droplet size as well as inter-particle size depends on the time scale of the experiment and on the rate of diffusion.

3. Solubility Parameter Approach (98,99)

Early attempts at predicting the miscibility of polymer blend concentrated on the use of Hildebrand's (98) solubility parameter as popularized by Bohn (99) for polymer-polymer systems.

The solubility parameter is defined as the square root of cohesive energy density, i.e., the energy of vaporization per unit volume of material, and is given the symbol δ (98).

$$\delta = (\Delta Ev/V)1/2 \qquad (107)$$

Thus, δ is proportional to the cohesion of the material or the strength of attraction between the molecules making up the material.

The solubility parameter approach, which has the utility of characterizing a system using only component properties without any system parameters, enables a practitioner to pick compatible components without having to do any experiments. With a geometric mean assumption of the contact energies (98):

$$\varepsilon_{12} = (\varepsilon_{11} \cdot \varepsilon_{22})^{1/2} \qquad (108)$$

which relates them to the cohesive energy density by

$$\delta_i^2 = \frac{\Delta E_i^v}{V} = \frac{z\varepsilon_{ii}}{2V_s} \tag{109}$$

The free energy of mixing of a binary polyblend can be predicted from the solubility parameters and volume fractions of the two constituent polymers by the equation:

$$\frac{\Delta G_M}{V} \simeq \frac{\Delta H_M}{V} = (\delta_1 - \delta_2)^2 \Phi_1 \Phi_2 \tag{110}$$

In spite of the tremendous amount of work using this approach, there have been a great number of dismal failures in predicting miscibility of polymer blends. Further refinements have been attempted by a multidimensional approach, breaking the cohesive energy density into several terms corresponding to the various molecular forces (5).

4. Statistical Mechanical Approaches

A number of equilibrium statistical mechanical approaches have been developed for predicting the complex and peculiar phase behaviors of polymer-solvent and polymer-polymer systems. In principle, there are two distinct methods of formulating these theories. The first is the method of radial distribution functions (100). It generally attempts to specify the probability of finding polymer segments in particular conformations. The second method proceeds from an assumed structure which usually resembles the regular lattice structure of crystalline solids. The lattice method is considered from two points of view. The

first is the purely statistical approach generally referred to as the approach generally referred to as the Flory-Huggins lattice model, or the lattice model for short (101-104). The other is developed from the statistical mechanical partition function and, according to current literature convention, is referred to as the equation-of-state approach (105-106).

5. Thermodynamics of Block Copolymer Systems

Fundamental differences exist between the phase separations which occurs in a simple mixture of two polymers and that which occurs in block copolymers. In the former case, phase separation is macroscopic in nature. However, in the case of block copolymers, phase separation is microscopic; the separate phases, or domains, have well-defined sizes and shapes. Furthermore, the presence of covalent bonds in copolymers places some constraints on the number of possible arrangements, resulting in an appreciable loss in configurational entropy of mixing. Because of the entropy loss, the critical molecular weight required for "microphase separation" in copolymers is predicted to be considerably higher than in the analogous homopolymer mixtures.

In an analysis developed by Meier (107) for establishing the criteria for phase separation in AB diblock copolymers, a surface free energy contribution representing the interaction of A and B segments at the domain interface, as well as three contributions responsible for the entropy decrease of the block copolymer relative to that of a simple mixture of the components, were taken into account. The three entropic contributions were referred to as:

(1) placement entropy: due to the restriction of the AB covalent bonds between the domains,

(2) restricted volume entropy: due to the requirement that A segments remain in domain space A and that B segments remain in the B domain.

(3) elastic entropy: arising from the perturbation of chain dimensions in either domain system from their random flight values (93) which are assumed to hold when the chain is in a homogeneous system.

Using appropriate estimations, the analysis determined that the critical molecular weight for phase separation would be 2.5-5 times higher in a block copolymer than in the analogous homopolymer mixture.

The analysis has been extended (108) to estimate the most stable configuration as a function of block copolymer volume fraction. Assuming an interfacial tension of 15 dynes/cm, an unperturbed root-mean-square end-to-end chain dimension (93) to molecular weight ratio of 7.5×10^{-9} (c.g.s unit) and a temperature of 300°K, spherical domains are preferred below volume fractions of 0.20; cylindrical domains are preferred between 0.20 and 0.30 with lamellar structure existing above 0.30. The theoretical predictions are in qualitative accord with the experimental results on a styrene-butadiene system.

In Meier's extended analysis, the influence of casting solvent on domain morphology was also considered. Qualitatively, the effect of a preferential solvent is similar to an increase in the volume fraction of that component which interacts preferentially with the solvent.

Another treatment was developed by Krause (109,110). It is not

limited to a particular type of block copolymer; it is applicable to multiblock systems, as well as to mixtures of one or more of the copolymers with the constituent homopolymers. Phase separation resulting from a crystallizable constituent is also covered in this model. However, the model is concerned only with thermodynamic phase separation and not with the morphology of the domain structure.

The prior treatments due to Meier and Krause have all assumed a discrete interface with no intersegmental mixing. Another approach considering incorporation of a mixed region at the interface (which is assumed to exhibit single-phase behavior) has been developed by Leary and Williams (111-113) for ABA triblock copolymers and by Meier (114) for AB diblcok copolymers. The results are presumed to be applicable to ABA copolymers that could be represented by (A-B/2) diblock structures.

Although the extent of phase mixing at domain boundaries is still controversial, both approaches, nonetheless, actually predict the specific microstructure which is thermodynamically favored.

6. Methods for Determining Polymer-Polymer Miscibility (5)

As stated before, the homogeneity of a multicomponent polymer system is a relative term which can be defined by the technique used to measure the system. In fact, a compatibility number has been defined by Kaplan (115) as

$$N = \frac{\text{exp. probe size}}{\text{domain size}} \qquad (111)$$

The experimental probe size in a mechanical test, for example, would be

the segmental length associated with the glass transistion phenomenon. The domain size is the average length in which only one component exists. For a specific technique, obviously, the larger the compatibility number, the better the homogeneity of a multicomponent polymer system.

A number of methods having been employed to determine polymer-polymer miscibility are reviewed in the following. Among them, only the melting point depression method and NMR method, both of which were used in this study, are discussed in greater detail.

Glass Transition Temperature

The most commonly used method for determining polymer-polymer miscibility is through the measurement of the glass transition(s) in the blend versus those of the constituent components. A miscible polymer blend will exhibit a single glass transition between the T_g's of the components with a sharpness of the transition similar to that of the components. In the cases of limited miscibility, broadening of the transition or two separate transitions between those of the constituents may occur.

A variety of mechanical, dielectric, dilatometric, calorimetric and thermo-optical methods have been used to determine the glass transition(s). Despite a "universal" experimental probe size of 150Å as suggested by Kaplan (115), the level of molecular mixing associated with the glass transition method is still uncertain.

Microscopy

Direct visual studies by microscopy can determine not only the presence but also the connectivity or morphology of the phases. Electron microscopy, with 50Å resolution, has shown that heterogeneity exists even in polyblends having a single glass transition (116,117).

Melting Point Depression

Like the melting point depression phenomena of crystalline or semicrystalline polymers in the presence of low molecular weight soluble compounds, in miscible polyblends, in which one component is crystallizable, melting point depressions are also observed (118,119). The general equation for melting point depression of a binary polyblend is

$$\frac{1}{T_m} - \frac{1}{T_m^\circ} = -\frac{RV_2}{\Delta H_2 V_1}\left[\frac{\ln\Phi_2}{m_2} + \left(\frac{1}{m_2} - \frac{1}{m_1}\right)(1-\Phi_2) + \chi_{12}(1-\Phi_2)^2\right] \qquad (112)$$

where subscript 1 represents the amorphous polymer and subscript 2 represents the crystallizable polymer, χ_{12} is the Flory interaction parameter, T_m is the experimental melting point, T_m° is the equilibrium melting point of pure polymer 2, ΔH_2 the heat of fusion of 100% crystalline polymer per mole of repeat unit, V_1 and V_2 the molar volumes of repeat units, ϕ_2 the volume fraction, m_1 and m_2 the degree of polymerization.

For high molecular weight polyblends, m_1 and m_2 are very large, thus

$$\frac{1}{T_m} - \frac{1}{T_m^\circ} = -\frac{RV_2}{\Delta H_2 V_1} \chi_{12}(1-\Phi_2)^2 \qquad (113)$$

The equation indicates that a negative χ_{12} will yield a melting point depression, while a positive interaction parameter will result in a melting point elevation.

Solid State NMR

In NMR experiments, the magnitudes of T_1, T_2, $T_{1\rho}$ and other relaxation parameters are influenced by molecular motions. Therefore, comparison of the relaxation times of a polymer mixture or copolymer with its constituent components usually can reveal the degree of interaction between the components. Furthermore, in proton NMR, free induction decays (T_2 relaxations) as well as the T_1 and $T_{1\rho}$ relaxations can be analyzed in terms of the total proton content of each phase. The experimental probe size of solid state proton NMR is determined by the maximum spin diffusive path length, which may be given by the approximate formula (120):

$$L = (6D/k)1/2 \qquad (114)$$

where D is the diffusion coefficient and k is the relaxation rate of a particular relaxation mechanism.

Besides being used for studying the degree of microphase inhomogeneity and phase separation behavior of compatible polymer blends (120-125), broadline solid state proton NMR has been employed to investigate the dynamic and kinetic behaviors of domain structures of

block copolymers, including block copolymers of styrene and butadiene (126-128), as well as multiblock segmented polyurethane systems (128-132).

The recent advent of the CPMAS high resolution solid state carbon-13 NMR, in which relaxation parameters (T_1, T_2, $T_{1\rho}$, T_{CH}, η) usually can be resolved for each individual nuclei, has lead to several new qualitative conclusions regarding the microstructure and dynamics of compatible polymer blends (133-135) and microphase-separated copolymers (70,136). For example, T_1's and $T_{1\rho}$'s can be used to characterize individual main- and side-chain motions in the MHz-and KHz-frequency ranges, respectively.

Other Methods (5)

Other methods which are frequently used in determining polymer-polymer miscibility include scattering methods, ternary-solution methods, studies of rheological properties, volumes of mixing, and heats of mixing as well as infrared, ultraviolet and excimer fluorescence spectroscopic methods.

Chapter II

CHARACTERIZATION OF STYRENE-ISOPRENE-STYRENE TRIBLOCK COPOLYMERS AND POLYURETHANES

I. INTRODUCTION

Thermoplastic elastomers (138,139) form an example illustrating the fact that multicomponent polymer systems can achieve novel properties unattainable in homopolymers. They are a unique new class of polymers, in which the end use properties of vulcanized elastomers are combined with the processing advantages of thermoplastics.

In general, thermoplastic elastomers are ordered, tri-or multi-block copolymers of structure A-B-A or $(A-B)_n$, where A represents a polymer segment which is glassy or crystalline at service temperatures but fluid at higher temperatures, and B represents a polymer segment which is elastomeric at service temperature. Choice of segment type and length and the weight fractions of A and B are crucial in achieving elastomeric performance.

The unique properties of the thermoplastic elastomers result from microphase separation or domain formation. It is well known that the physical properties and mechanical behaviors of those copolymers are strongly dependent on the nature and degree of microphase separation (3,4,137).

Many methods have been used to investigate thermoplastic elastomer microphase separation. Since the distinction between domains is based on segmental mobility and this mobility plays a very important role in determining properties of a material. So nuclear magnetic resonance,

having well-established relationships between molecular motions and a variety of relaxation parameters, is particularly suited to study domain structure and dynamics of these copolymers.

Pulsed proton NMR has been extensively employed to investigate the structure and dynamics of solid block and segmented copolymers (126-132). The main limitations of solid-state proton NMR are poor resolution and also a very effective spin diffusion among the protons. On the other hand, solid state C-13 NMR can overcome those problems. With high power heteronuclear dipolar decoupling and magic angle spinning, chemically distinct carbons, in general, have separate C-13 NMR resonances. Furthermore, dipolar decoupling, magic angle spinning, and cross polarization can be used in various combinations to obtain more detailed information on these copolymers. In this regard, a series of styrene-isoprene-styrene triblock linear copolymers (SIS) with different composition and/or molecular weights and a poly(ester)urethane (PU) based on polybutylene adipate and 4,4'-diphenylmethane diisocyanate (MDI) were studied by solid state C-13 NMR and this work is presented in this chapter.

For the long block styrene-diene-styrene copolymers, it is believed that domain existence is independent of temperature over a wide range and the morphology of the domain structure depends primarily on the composition (128). However, there are disagreements in explaining certain thermal transitions and viscoelastic behaviors of the copolymers. Some phenomena can be interpreted by either a diffusive mixing interface model or a dynamic interaction model which neglects the

geometry of the interface between the two phases (107-114,127,140-145). In this study, the details of the domain boundaries as well as the molecular motions (in terms of frequency and orientation) as functions of composition, molecular weight, and selective casting solvents of the SIS samples were investigated through measurements and analysis of ^{13}C's T_1's, bandwidths of resonance peaks (both with and without magic angle spinning) of the isoprene segments and ^{13}C's $T_{1\rho}$'s of the styrene segments.

For the segmented polyurethane, the domain structure and morphology are more complicated and believed to be time and temperature dependent (128-130,146-147). In this study, the phase separation, domain boundaries, and molecular motions of a thermally stable polyurethane were investigated through the measurements and analysis of ^{13}C's T_1's, protons' $T_{1\rho}$'s (C-13 spectra resolved). The resonance intensities of spectra obtained at various experimental conditions were also compared.

II. EXPERIMENTAL

A. Samples

SIS Copolymers. Styrene-isoprene-styrene (SIS) linear triblock copolymers in styrene content ranging from 20 to 60 percent by weight were obtained from the Phillips Petroleum Company. Table 3 summarizes the sample series by styrene content and block number average molecular weight. The dispersity ratios were provided by Phillips as determined by gel permeation chromatography. No evidence of

Table 3

Composition of SIS Copolymers

Sample No.	Weight Percent Styrene	M_W/M_N (10^{-3})	S/I/S M_N (10^{-3})
10-80-10	20	264/239	24/191/24
20-60-20-H	40	261/238	48/142/48
20-60-20-L	40	114/109	22/65/22
30-40-30	60	81/77	23/31/23

homopolymer, diblock, or stabilizer additives could be seen in the chromatograms.

Samples as received and/or the solution-cast films of about 0.15 mm in thickness prepared at the ambient conditions from either methyl ethyl ketone (MEK) or hexane were used for the NMR experiments.

Polyurethane. The polyurethane sample used in this study was a segmented polyester-MDI system produced by BF Goodrich Company. The hard segment is a 1,4-butanediol extended MDI (4,4'-diphenylmethane diisocyanate) and the soft segment is based on polytetramethylene adipate of an average molecular weight of 1,000. The composition of the sample studied is 31% MDI and 69% soft segment polyol plus chain extender.

Hard Segment

$$-CO-NH-C_6H_4-CH_2-C_6H_4-NH-CO-(O(CH_2)_4O-CO-NH-C_6H_4-CH_2-C_6H4\_NH-CO-)_x$$

Soft Segment

$$-O(CH_2)_4O-(CO(CH_2)_4CO-O(CH_2)_4O-)_y$$

Films of the polyurethane sample of ca. 0.3 mm in thickness were compression molded with care being taken to minimize any thermal degradation. Films were then stored at the ambient conditions for at least one week before being punched into disks for the solid state NMR experiments.

B. NMR

The solid state carbon-13 NMR experiments were carried out at

15.0 HMz on a JEOL-60Q spectrometer at room temperature. Various experimental conditions were employed to obtain the spectra of the copolymers. These are outlined in the following.

SP-DD-MAS. Single pulse, dipolar decoupled, magic angle spinning NMR spectra were obtained using a (90°-t) pulse sequence. The 90° pulse was 7.6 μs in duration.

SP-DD-Static. Single pulse, dipolar decoupled, static NMR spectra were also obtained using the (90°-t) pulse sequence with the duration of the 90° pulse adjusted to 7.6 μs.

DD-MAS-CP. Dipolar decoupled, magic angle spinning, cross polarization NMR spectra were obtained at a matched spin-lock cross polarization transfers employing 'H_1's of 33 KH_Z with selected contact and pulse delay times.

The strength of the high power proton dipolar decoupling field was ca. 33 KHz (7.75 G). The magic angle spinning experiments were carried out using a Kel-F 'bullet' type rotor and ca. 2.0 KHz spinning rates. Polymer samples in the form of either rolled thin films or punched disks were packed into the Kel-F rotor. Each sample represents about 0.5 g of polymers.

The Hartmann-Hahn condition and the magic angle were adjusted using the aromatic signal from hexamethylbenzene; the rates of magic angle spinning were also calibrated using the sidebands of that signal. All the spectra were externally referenced to liquid tetramethyl silane (TMS), based on substitution of hexamethylbenzene (HMB) as the secondary

reference and assigning 132.3 and 16.9 ppm to the shifts of the aromatic and aliphatic carbons, respectively, of HMB relative to liquid TMS.

All the spectra were obtained from 1 K FT with zero filling to a total of 4 K points. A spectral width of 8000 Hz and an acquisition time of 64 ms were selected for all the spectra.

T_1 Measurements. T_1 values of the carbon-13 nuclei in the isoprene segments of the SIS copolymers and in the polyurethane were measured using a (180°-τ-90°-t) inversion recovery pulse sequence as described in Chapter I. All the spectra for the T_1 measurements were obtained with dipolar decoupling and magic angle spinning. The time between pulse sequence, t, was chosen to be ca. five times the longest T_1 of the nuclei of interest. Measurements were made for 6-10 values of τ which ranged from 0.001 s to t. Peak heights were used for the analysis of each T_1 data set and T_1 values were calculated with a built-in program in the spectrometer.

$T_{1\rho}$ (^{13}C) Measurements. T_1 values of the carbon-13 nuclei in the styrene segments of the SIS copolymers were measured using a cross polarization procedure as described in Chapter I. All the spectra for the ^{13}C $T_{1\rho}$ measurements in this study were obtained with dipolar decoupling and magic angle spinning. Six spectra were used for the calculation which was performed by a program in the spectrometer's computer.

III. RESULTS

A. SIS Copolymers

1. General Description of Spectra

The isoprene segments of the SIS copolymers are mobile enough to result in short T_1's for the C-13 nuclei in the order of one tenth of a second to one second. In contrast the C-13 nuclei in the styrene segments have long T_1's typical of rigid solids. Figure 5(b) shows a single pulse (90°-t)-DD-MAS spectrum of the SIS 20-60-20H sample. With a pulse delay time of three seconds, the resonance signals predominantly came from the isoprene components; nevertheless, weak resonance signals from the styrene components were detectable. On the other hand, since higher molecular mobility reduces or even eliminates the effect of nuclear dipole-dipole interactions, use of a ^{13}C-^{1}H cross polarization pulse sequence (DD-MAS-CP) for the SIS copolymers resulted in C-13 resonance signals almost exclusively from the styrene segments as shown in Figure 5(a).

Single pulse spectra obtained without spinning (SP-DD-Static) were still resolvable in terms of the resonance signals of the saturated and unsaturated carbons of the isoprene segments for all the SIS samples; some of these were resolvable between the two unsaturated carbons at half peak height as shown in Figure 7. The resonance signals of these static spectra were much sharper than those observed for the powder spectrum of polydienes studied at low temperature (39), although the bandwidths were still ca. five-fold broader than those in the spectra obtained with magic angle spinning.

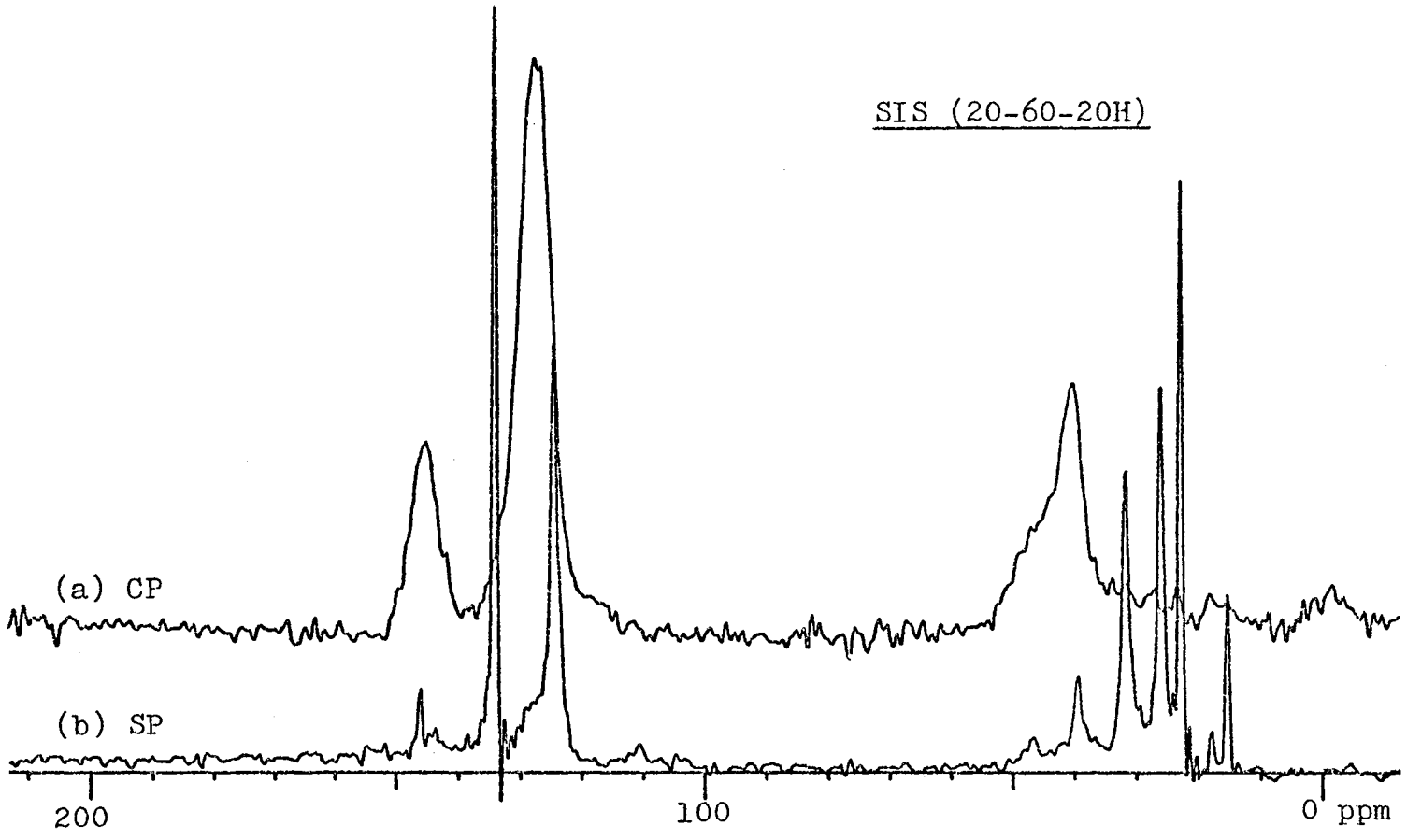

Figure 5. Proton Dipolar Decoupled, Magic Angle Spinning 15.0 MHz C-13 NMR Spectra of the SIS 20-60-20H Copolymer. Spectrum (a) was obtained from 4500 FID accumulations of a cross polarization pusle sequence with a contact time of 1.5 ms and a pulse delay time of 3.5 s. Spectrum (b) was obtained from 3,000 FID accumulations of a single pulse sequence with a 90° pulse of 7.6 μs and a pusle delay time of 3 s. Peak assignments are described in the text.

Various peaks in Figure 5 were assigned on the basis of the solution C-13 NMR spectra of polystyrene and polyisoprene available in the literature (148). For the styrene segment observed in the cross polarization spectrum (a), the peak at 145 ppm arises from the non-protonated aromatic carbon, the peak at 128 ppm is due to all the other five protonated aromatic carbons. The peak at 41 ppm arises primarily from the methylene carbon and the downfield shoulder of that peak is due to the methine carbon.

For the isoprene segment in the single pulse spectrum (b), assuming the nomenclature

cis-configuration

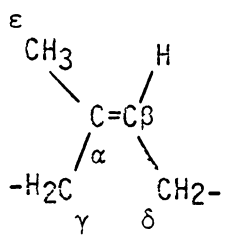

trans-configuration

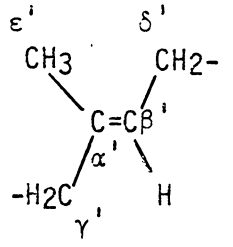

the peaks at 134.0, 124.7, 39.5, 31.7, 25.9, 22.8 and 15.3 ppm are assigned to carbons α & α', β & β', γ', γ, δ & δ', ε, ε', respectively. From the well resolved γ, γ' and ε, ε' carbon resonances, it was determined that the isoprene segments in this (20-60-20H) and other SIS samples were ca. 85% in the cis-configuration.

2. Mobile Domains

T_1 Measurements. The T_1 values for four SIS samples with different composition, molecular weights and morphologies (casting

solvents were different) are listed in Table 4. The T_1 values for the two samples with higher isoprene content were measured twice in order to show the reproducibility of the method. It appears that within the experimental errors of this study, the spin-lattice relaxation times in the mobile domains of the SIS copolymers are independent of the composition and morphology of the polymers.

Data analysis (149) also indicates that there is a one-component exponential behavior for the spin-lattice relaxations in the mobile domains of the SIS samples. Table 5 gives the results of this treatment of the T_1 measurements, where Y(X=0) is the calculated value of $\ln \frac{Mo-M(\tau)}{2Mo}$ at $\tau=0$, or the intercept of the linear regressed line: $\ln \frac{Mo-M(\tau)}{2Mo} = -\tau/T_1$ in a $\ln \frac{Mo-M(\tau)}{2Mo}$ vs. τ graph such as in Figure 6. In the ideal case of one component, first order relaxation with no experimental errors, Y(X=0)=0. The variance is defined as

$$\text{VARIANCE} = \frac{\Sigma\left[\left(\ln \frac{Mo-M(\tau)}{2Mo}\right)_{\text{observed}} - \left(\ln \frac{Mo-M(\tau)}{2Mo}\right)_{\text{calculated}}\right]^2}{N}$$

where N is the number of the observation points used in the calculation. Since a threshold parameter of 80% was used for all the T_1 calculations to limit error, (i.e., only when the observed magnetization $M(\tau)$ satisfied the condition of $\frac{Mo-M(\tau)}{2Mo} > 0.20$ were the data used), the number N could be different in different sets of data or between different carbons in an experiment. Again in the ideal case, VARIANCE = 0.

Table 4

^{13}C NMR T_1 Values for the Isoprene Segments of Four SIS Copolymers

Sample No.		10-80-10	20-60-20H	30-60-30	30-40-30
$(M_W/M_N)x10^{-3}$		264/239	261/238	81/77	81/77
Casting Solvents		---	---	Hexane	MEK
T_1 (ms)	α	546 618	618 541	469	546
	β	64 55	75 66	69	81
	γ	33 31	31 38	30	38
	δ	43 38	41 45	41	30
	ε	208 253	264 251	226	228

Table 5

Data Analysis of the T_1 Measurements of the Isoprene Segments in SIS Copolymers

Sample No. (casting solvents)	Carbons	T_1 (ms)	Y(X=0)	Variance	N
10-80-10	α	546	-0.0015	0.0003	9
	β	64	-0.0581	0.0001	6
	γ	33	-0.0414	0.0097	4
	δ	43	-0.0622	0.0011	5
	ε	208	-0.0070	0.0015	6
10-80-10	α	618	-0.0307	0.0001	7*
	β	55	+0.0083	0.0002	7
	γ	31	+0.0065	0.0013	6*
	δ	38	+0.0273	0.0017	6
	ε	253	-0.1022	0.0014	5
20-60-20H	α	618	-0.0344	0.0003	8
	β	75	-0.0821	0.0003	5
	γ	31	-0.0821	0.0014	3
	δ	41	-0.0727	0.0019	4
	ε	264	-0.0924	0.0003	6
20-60-20H	α	541	+0.0275	0.0003	7
	β	66	-0.0862	0.0002	8
	γ	38	-0.0757	0.0011	6
	δ	45	-0.0432	0.0006	6
	ε	251	-0.1107	0.0045	5
30-40-30 (Hexane)	α	469	+0.0232	0.0001	5
	β	69	-0.0375	0.0036	4
	γ	30	+0.1381	--	2
	δ	41	+0.0166	0.0006	3
	ε	226	+0.0384	0.0002	3
30-40-30 (MEK)	α	566	-0.0008	0.0000	5
	β	81	-0.1182	0.0026	4
	γ	38	-0.0639	0.0262	3
	δ	30	+0.1361	--	2
	ε	228	-0.0399	0.0002	4

* Data plotted in Figure 6.

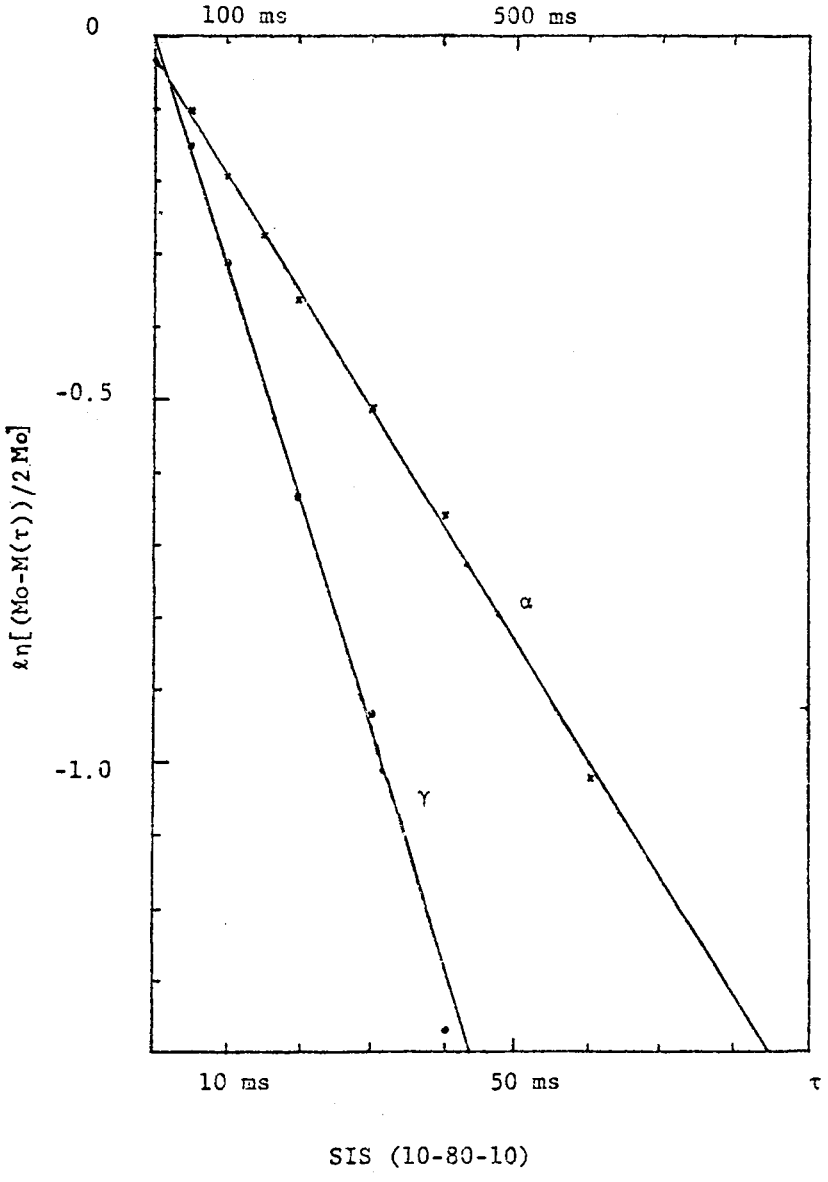

Figure 6. One Component, First Order Spin-Lattice Relaxation Behavior of the Isoprene Segments of the SIS 10-80-10 Copolymer.

Figure 6 contains a plot of the one-component, first order spin-lattice relaxations of the isoprene segments for two of the carbons of the SIS 10-80-10 sample.

Bandwidths With and Without Magic Angle Spinning. Table 6 lists the bandwidths of the single pulse, proton dipolar decoupled C-13 resonances obtained with magic angle spinning for five SIS samples. The results show that with magic angle spinning, the bandwidths of the isoprene carbons in the SIS copolymers are essentially independent of the composition, molecular weight and morphology (casting solvents) of the polymers.

Table 7 lists the bandwidths of the single pulse, proton dipolar decoupled C-13 resonance obtained without spinning the sample for the two unsaturated isoprene carbons (α and β) in seven SIS samples. The results show that higher styrene content and lower molecular weights tend to result in broader bandwidths for these two carbons, although the differences are probably not significant considering the experimental precision. (Two SIS 10-80-10 samples obtained from the same batch were studied independently and were found to have a 15% difference in bandwidths.) The significant difference in the bandwidths was observed in the case of the two samples cast from MEK. The resonance lines of the two unsaturated isoprene carbons in these two samples were much broader than the resonance lines of the other samples studied. They were overlapped to a large extent, and unlike those peaks in the other samples, spectra were unresolvable at half peak heights. Figure 7 shows static spectra of two SIS 20-60-20H samples: spectrum (a) was

Table 6

Bandwidths of the Isoprene Segments in SIS Copolymers (with MAS)

Sample No.		10-80-10	20-60-20H	20-60-20L	30-40-30	30-40-30
(Mw/Mn)x10-3		264/239	261/238	114/109	81/77	81/77
Casting Solvents		--	--	--	Hexane	MEK
$\nu_{1/2}$ ‡ (Hz)	Carbon*					
	α	15	16	14	15	14
	β	23	26	26	27	26
	γ	25	26	27	28	25
	δ	21	24	23	29	22
	ε	15	16	15	14	13

* $(CH_2\text{-}C\cdot CH_3 = CH\text{-}CH_2)$ $(\gamma\text{-}\alpha\cdot\varepsilon = \beta - \delta)$

‡ Digital resolution = 3.9 Hz

Table 7

Bandwidths of Isoprene Segments in SIS Copolymers (Static)

Sample No.	(Mw/Mn) x 10^{-3}	Casting Solvents	$\nu_{1/2}^{\ddagger}$ (Hz)	
			α	β
10-80-10	264/239	--	75 86	80 92
20-60-20H	261/238	--	88	100
20-60-20L	114/109	--	99	104
30-40-30	81/77	Hexane	100	110
20-60-20H	261/238	MEK	125*	155*
30-40-30	81/77	MEK	120*	175*

* Estimated from the overlapped peaks.

‡ Digital resolution = 3.9 Hz. A digital filtering which increased the bandwidths by 3.1 Hz was employed in the Fourier transformation for all the static nmr experiments.

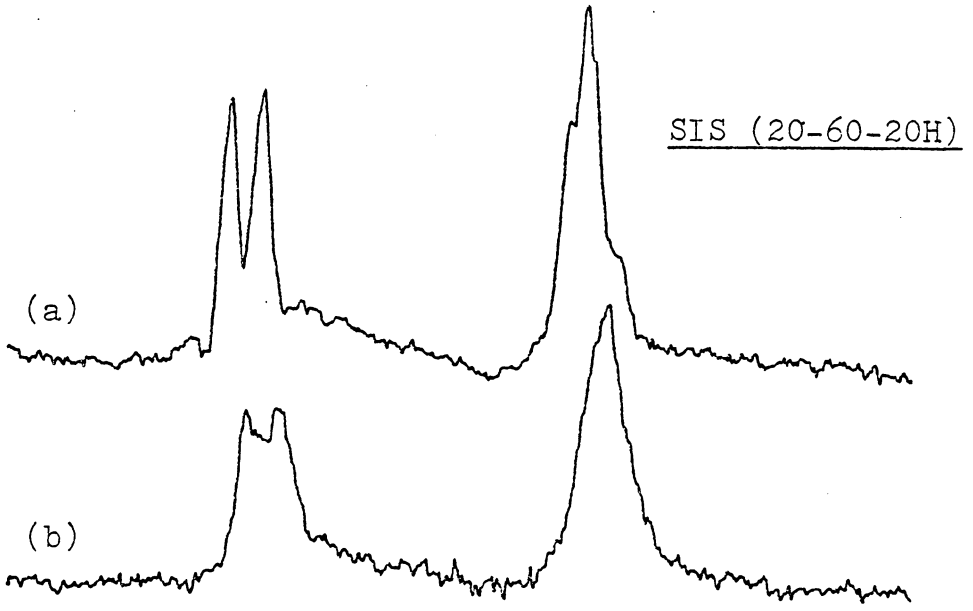

Figure 7. Static Spectra of the SIS 20-60-20H Copolymers. Single pulse proton dipolar decoupled, static C-13 NMR spectra of two SIS 20-60-20H samples. (a) is the spectrum of the sample as recieved, and (b) is the spectrum of the sample cast from MEK. A 90° pulse of 7.6 μs and a pulse delay time of 3 s were used for both spectra.

obtained from the sample as received, and spectrum (b) obtained from the MEK cast sample. Similar differences were also observed for the SIS 30-40-30 samples cast from hexane and MEK.

3. Rigid Domains

$T_{1\rho}$ (^{13}C) Measurements. Table 8 gives the ^{13}C NMR $T_{1\rho}$ values for two SIS 30-40-30 samples cast from two different solvents (hexane and MEK). Data analysis results are also listed in the table, where the definitions of Y(X=0), VARIANCE and N are the same as those described in the T_1 measurements for the mobile domains, except that $\ln(\frac{M(\tau)}{Mo})$ was used instead of $\ln(\frac{Mo-M(\tau)}{2Mo})$ in the analysis. The values of $T_{1\rho}$ were calculated from the peak intensities at 145,128 and 41 ppm, which corresponded to the non-protonated aromatic, protonated aromatic and predominant methine overlapped with methylene carbons, respectively. Within the experimental conditions (limited sensitivity, resolution and data points, as shown in Figure 8), no significant difference between ^{13}C $T_{1\rho}$ of these two samples could be distinguished.

B. Polyurethane

1. General Description of Spectra

Unlike the SIS copolymers investigations, with the single (SP-DD-MAS) and with the cross polarization (DD-MAS-CP) pusle sequences, C-13 NMR resonance signals were obtained from both the hard and the soft segments of the polyurethane. However, the relative intensities of the two segments depended on the experimental conditions. Figure 9 illustrates the solid state C-13 NMR spectra of the polyurethane

Table 8

^{13}C NMR $T_{1\rho}$ Values for the Styrene Segments in Two SIS 30-40-30 Samples Cast from Different Solvents

Casting Solvents	Carbons (ppm)	$T_{1\rho}$ (ms)	Data Analysis		
			Y(x=0)	Variance	N
Hexane	C_1 (145)	47.2	-0.0376	0.0020	3
	C_{2-5} (128)	12.1	-0.0528	0.0000	3
	CH (41)	9.3	-0.2178	0.0068	3
MEK	C_1 (145)	32.5	-0.0775	0.0017	4
	C_{2-5} (128)	14.8	-0.0792	0.0007	3
	CH (41)	10.5	-0.3048	0.0004	3

Numbering Scheme:

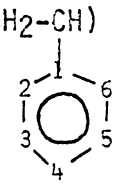

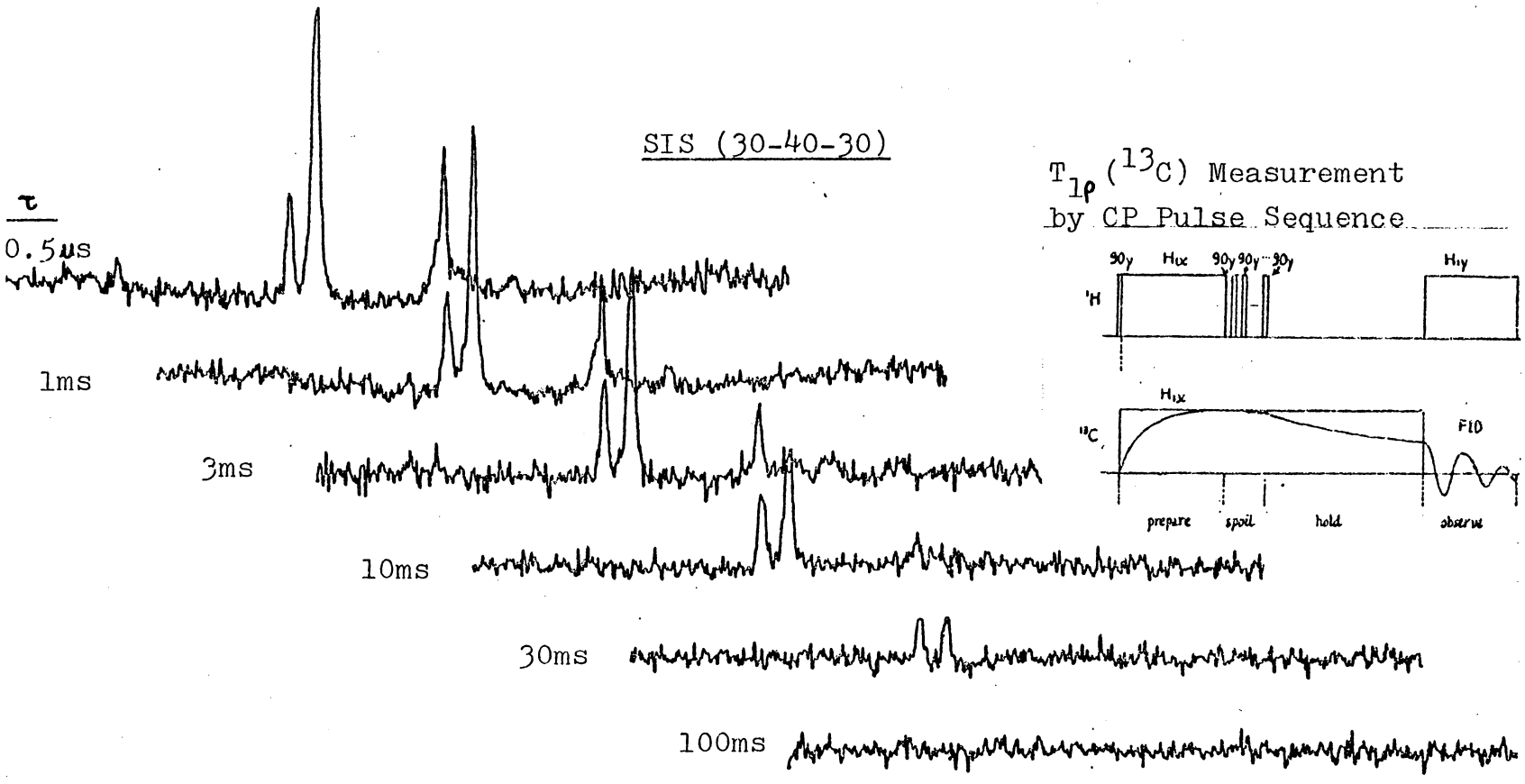

Figure 8. ^{13}C $T_{1\rho}$ Measurement for the Styrene Segments of the SIS 30-40-30 Samples Cast from Hexane. A contact time of 1.5 ms and a pulse delay time of 3.5 s were used. 600 scans were accumulated for each spectrum.

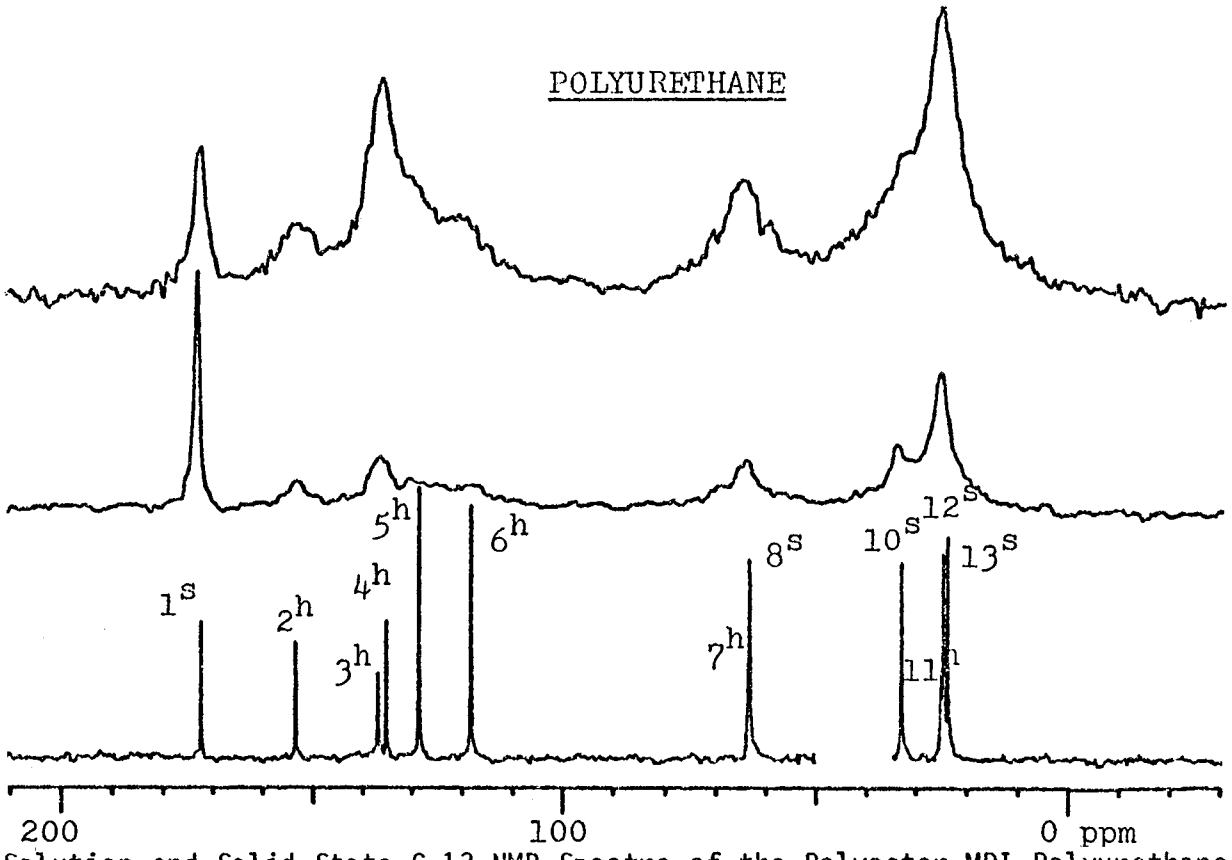

Figure 9. Solution and Solid State C-13 NMR Spectra of the Polyester-MDI Polyurethane with 31 wt% MDI. (a) and (b) are solid state spectra obtained with proton dipolar decoupling and magic angle spinning: spectrum (a) employed a cross polarization pulse sequence with a contact time of 1.0 ms and a pulse delay time of 4 s, spectrum (b) employed a single pulse sequence with a 90° pulse of 7.6 μs and a pulse delay time of 3.5 s. 7000 and 2000 scans were accumulated for spectra (a) and (b), respectively. (c) is a proton noise-decoupled 15.0 MH_Z C-13 spectrum from a hexadeteriodimethylsulfoxide (DMSO-d6) solution at the ambient condition. Spectrum (c) was carried out in different probe of the same spectrometer from which spectra (a) and (b) were obtained. The internal standard of spectrum (c) is the central peak of DMSO-d6, which occurs at 39.5 ppm with respect to TMS. Solvent peaks as well as the peak of MDI methylene carbon which occurs in the midst of them were deleted in the Figure.

obtained with both pulse sequences. The same figure also gives a proton noise-decoupled 15.0 MHz solution C-13 NMR spectrum in hexadeuteriodimethylsulfoxide (DMSO-d6). Peak assignments for the solution spectrum are listed in Table 9.

In Table 9 the following convention of identification was employed.

Hard Segment

MDI

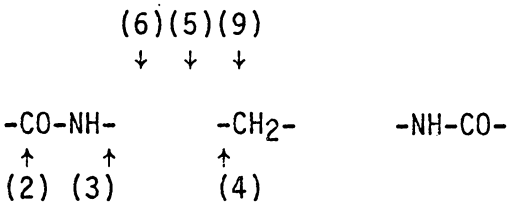

Butanediol

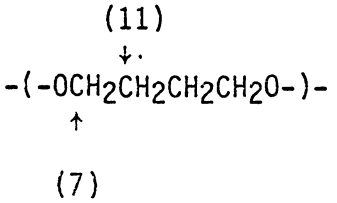

Soft Segment

Polyol

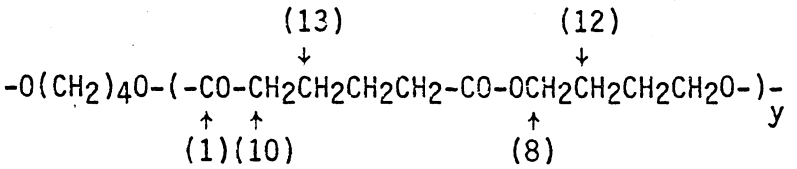

2. T_1 Measurements

The single pulse solid state C-13 spectrum with a pulse delay time of 3.5 s gives resonances from both the hard and soft segments as shown in Figure 9b. However, a comparison of single pulse spectral

Table 9

Assignment of Resonances in C-13 NMR Spectrum of the Polyester-MDI Polyurethane from DSMO-d6

Peak No.	ppm	Peak Assignments	
		Segments	Carbons
1.	172.9	soft	carbonyl
2.	153.8	hard	carbonyl
3.	137.3	hard	aromatic
4.	135.6	hard	aromatic
5.	129.0	hard	aromatic
6.	118.6	hard	aromatic
7.	63,9	hard	oxymethylene
8.	63.6	soft	oxymethylene
9.	41.1	hard	methylene (MDI)
10.	33.3	soft	methylene
11.	25.5	hard	methylene
12.	25.0	soft	methylene
13.	24.1	soft	methylene

intensities with the cross polarization spectrum, Figure 9a, and the solution spectrum, Figure 9c, shows that the relative intensities of the carbons in the hard segments are much weaker in the single pulse spectrum. This suggests that, in general, the T_1 values of the C-13 nuclei in the hard segments should be longer than those in the soft segments. From a progressive saturation experiment, T_1 values for the carbonyl and the non-protonated aromatic carbons of the hard segment were estimated to be ca. 5 sec.

T_1 values for the two most intense peaks of the single pulse spectrum were measured with the inversion-recovery method. The peak at 173 ppm came exclusively from the carbonyl carbon of the soft segment. The unresolved peak at 25 ppm came from the methylene carbons of both the hard and the soft segments. It should be noted that the contribution from the hard segment was expected to be small in view of the intensities of the solution spectrum and as a result of the longer T_1 of the carbons in the hard segment. Since T_1 values for the two peaks differ by more than an order of magnitude, two independent experiments with different τ values between the 180° and the 90° pulses and pulse delay times were carried out. These results, as well as the data analysis, are given in Table 10. The data analysis reveals characteristic one-component, first order spin-lattice relaxation behavior. Good correlation is especially noticed for the completely resolved carbonyl peak. The exponential spin-lattice relaxaion behavior for both peaks was plotted and is shown in Figure 10.

Table 10

^{13}C NMR T_1 Values for the Two Most Intense Peaks of the Polyester-MDI Polyurethane with 31 wt% MDI

Carbons (ppm)	T_1	Data Analysis		
		Y(x=0)	Variance	N
Carbonyl (173)	1.128s	-0.0160	0.0006	8
Methylene (25)	66.3 ms	-0.0635	0.0013	7

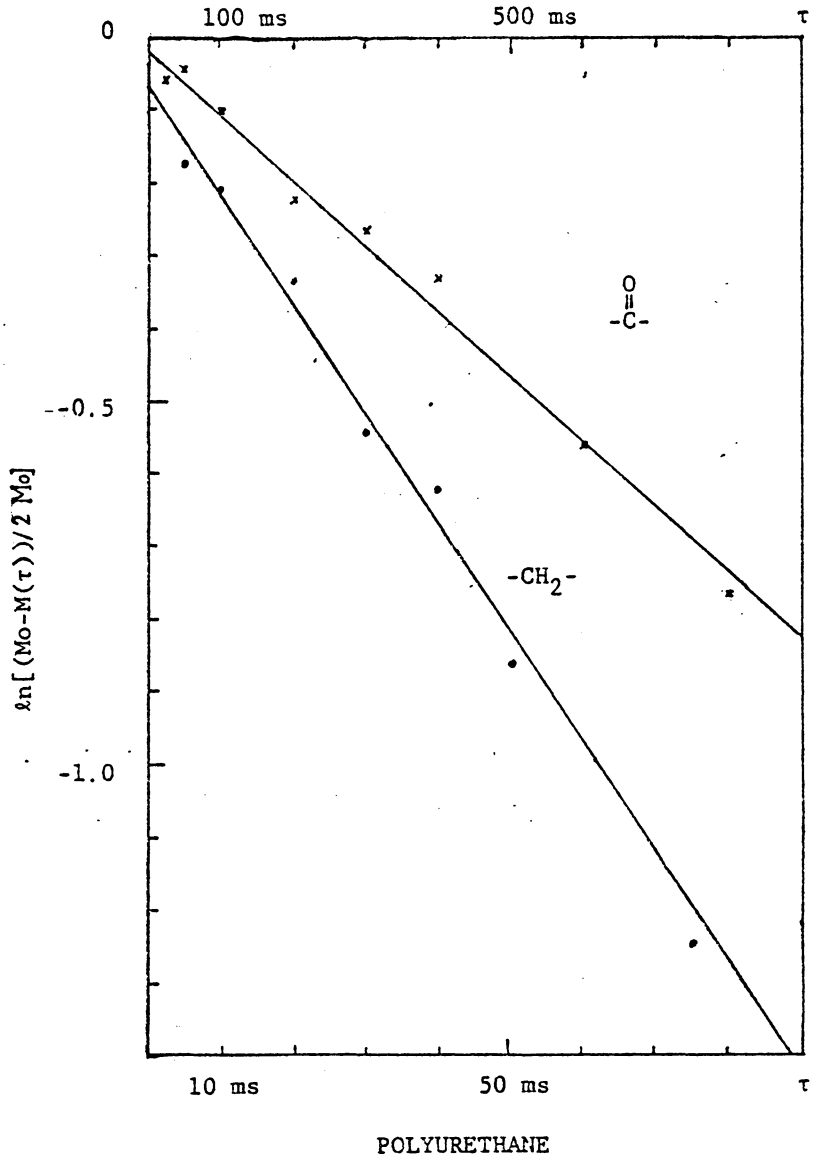

Figure 10. One Component, First Order Spin-Lattice Relaxation Behavior of the Polyurethane with 31 wt% MDI.

3. Cross Polarization Intensity as a Function of Contact Time

Two- or multi-component decays are often seen in the proton NMR of solid block or segmented copolymers and have been associated with the presence of phases with different mobilities as described in Chapter I. Shaefer et al. have pointed out that the decay of the C-13 cross polarization signal as a function of contact time (which reflects the proton's $T_{1\rho}$) can be used to characterize the polymer's homogeneity. In the absence of phase separation, the proton $T_{1\rho}$ values resolved from resonance signals of each carbon should be the same (135). Figure 11 contains the cross polarization spectra of the polyurethane obtained at four different contact times. The data are not sufficient for accurate quantitative proton $T_{1\rho}$ calculations. However, it can be seen from Figure 11 that all the carbons of the hard segments reveal about the same proton $T_{1\rho}$ value, as do all the carbons of the soft segments. Proton's $T_{1\rho}$ in the soft segments are obviously longer than the proton's $T_{1\rho}$ in the hard segments. For the spectrum with the longest contact time (5 ms), one can deduce that for practical purposes only the signals from the soft segments are detectable.

IV. DISCUSSION

A. SIS Copolymers

1. Phase Separation-Nature of Domain Boundaries

The fact that most block copolymers are not homogeneous materials in the solid state but rather undergo phase separation to produce a domain structure has been well established (4) as discussed in Chapter

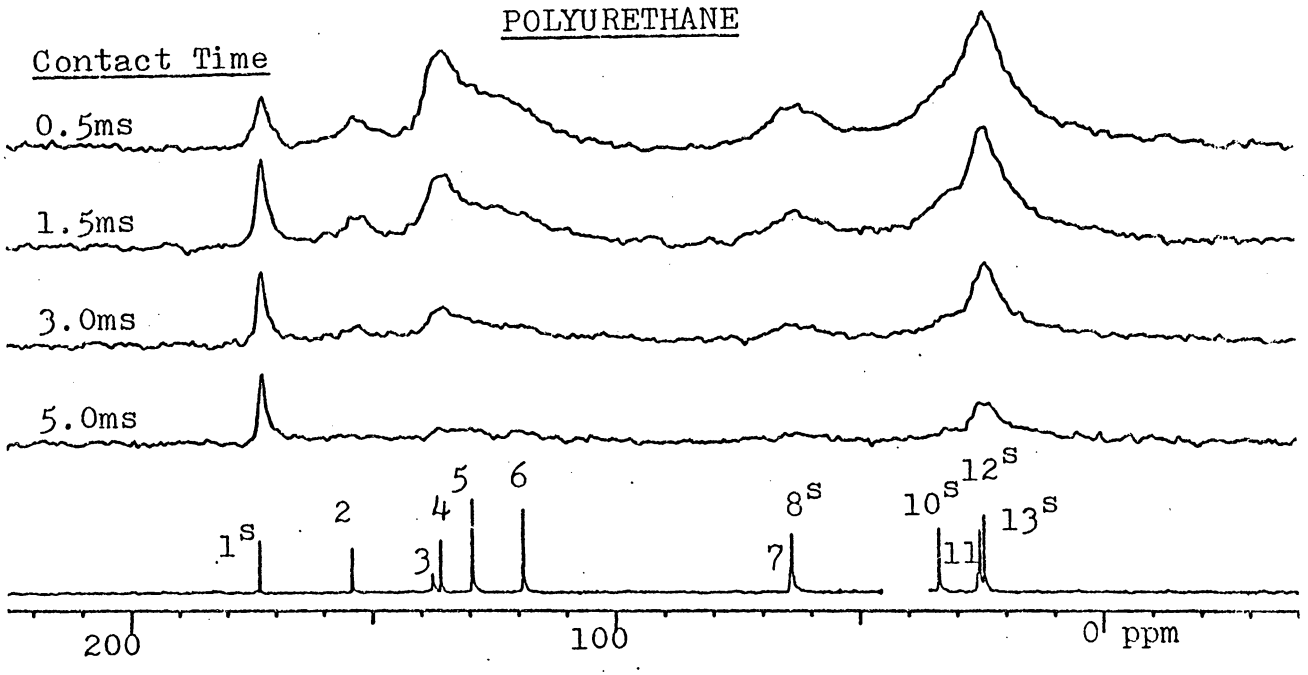

Figure 11. DD-MAS-CP 15.0 MHz C-13 NMR Spectra of the Polyester-MDI Polyurethane Obtained at Various Contact times. All the solid state spectra were obtained from 7,000 FID accumulations and a pulse delay time of 4 s. Solution spectrum of Figure 9(c) is shown on the bottom for peak assignments.

I. However, there has been considerable speculation and disagreement in the literature concerning the details of the domain interface in block copolymers, especially the AB and ABA block copolymers prepared from styrene and a diene monomer (isoprene or butadiene), viz, the "two-phase" vs. "three-phase" system, or a "thick" vs. "thin" interface also as discussed in Chapter I.

In this study, phase separation in the SIS copolymers is evident from the distinct dynamic properties of the carbons in the styrene segments and in the isoprene segments. As is shown in Figure 5, both segments can be observed selectively with different NMR experimental conditions.

The fact that no resonance signals from the isoprene segments were detectable in the cross polarization spectrum suggests that even though substantial mixed phases may exist, the styrene components in the mixed phases are not able to immobilize the isoprene segments to produce any substantial residual nuclear dipole-dipole interaction. This behavior which was observed can not be rationalized on the basis of a mixed phase system. Furthermore, the basically independent nature of the isoprene ^{13}C T_1 values on molecular weight and composition of the blocks together with the linearity of the exponential decay in the T_1 measurements also suggests that sharp boundaries exist between the styrene and isoprene domains for the samples we studied.

Theoretically, the isoprene segments in any "mixed phases" would be expected to have longer T_1 values than those in the pure isoprene domains due to the overall reduced mobility in the former case. The

mole fractions of the isoprene segments in the "mixed phases" can be calculated from the intercepts of the lines in $\ln\left(\frac{Mo-M(\tau)}{2Mo}\right)$ vs. τ plots such as in Figure 6. For example, intercepts of -0.02 and -0.05 in such plots indicate 4.0% and 9.8% respectively, of the isoprene segments was detected in the "mixed phases". Unfortunately, by comparing the intercepts (Y(X=0)) in Table 5 calculated for the five peaks in a sample and for the two samples which were studied by making two independent measurements, within the accuracy of our experiments, no definite conclusion could be reached regarding this matter. Possible experimental errors could arise from random noise and from other instrumental instability. They might also result from inaccuracy in the measurement of the duration of the 180° and the 90° pulses in the inversion-recovery experiments; e.g., either a positive or a negative 5% error in the length of the pulses would result in an intercept of -0.012 rather than zero. The T_1 values, nevertheless, would not be affected by this inaccuracy.

A "three-phase" statistical thermodynamic model has been proposed by Meier (114) which can predict the volume fractions of the mixed phases for the diblock A-B and triblock A-B-A copolymers from the molecular weights and the solubility parameters of the two components. According to this model, a S-I diblock copolymer with block molecular weight of 52,500-52,500 as well as a S-I-S triblock copolymer with block molecular weight of 52,500-105,000-52,500 would have an interfacial volume fraction of 0.20. (The model was based on the lamellar domain structure; however, the author indicated that the differences in

interfacial properties between the different possible domain structures were not large.) A S-I diblock copolymer of the same molecular weight (52,500-52,500) was investigated by Hasegawa, et al., (150). From small-angle x-ray scattering data, it was concluded that the interface constitutes a negligible fraction of the polymer, ca. 5-10%.

Our data, although inconclusive, tend to support the thin interface argument with two lines of evidence. First, from the data treatment of the peaks of the cis-α carbon (which has the highest intensity among the peaks and is completely resolved from the other chemically different carbons as well as from the α-carbon of the trans-isomer), the intercepts were negligible. They ranged from -0.0344 to +0.0275 for the six T_1 measurements. Very good data correlations were also observed for the T_1 measurements of the cis-α carbon peak, with the largest VARIANCE obtained to be 0.0003. Second, if a large amount of mixed phases were indeed present, as it was calculated by the Meier's model to be 20% by volume for the SIS triblock copolymers of block molecular weights of 52,500-105,000-52,500, then the SIS 20-60-20H sample having the closest composition and block molecular weights (48,000-142,000-48,000) among the samples would also be expected to have a substantial amount of mixed phases. That should have produced some detectable isoprene resonance signals in the cross polarization spectrum (Figure 5(a)).

2. Molecular Motion in the Mobile Domains

The fact that no isoprene carbons could be observed in the cross polarization spectra suggests that, in terms of frequencies, motion of these carbons is essentially "liquid-like" and is fast on the

time scale of dipolar interaction (ca. 10^5 Hz). The bandwidths observed in the static spectra can be narrowed further by magic angle spinning. This additionally indicates that the motions are anisotropic. However, the bandwidths of the sp^2 hybridized carbons in the static spectra are in the order of 100 Hz as compared to the typical values in the rigid anisotropic lattice which are found to be ca. 2000 Hz in a magnetic field of 1.4 Tesla (39). This reveals that motions average the chemical shift anisotropy to a large extent in the isoprene segments. Nevertheless, the residual chemical shift anisotropy is the primary source of line broadening observed in the static spectra.

The T_1 values (Table 4) and bandwidths with magic angle spinning (Table 6) indicate that the rates of these thermal motions is independent of the composition, molecular weight and morphology of the SIS samples in the ranges studied. This is consistent with the reports based on calorimetric (145,151), viscoelastic (142), broadline proton NMR (127) and esr spin-probe (143) studies which concluded that the diene's T_g of the SI and SIS (or SB and SBS) copolymers is not a strong function of composition and molecular weight.

Even though the T_1 values and the bandwidths obtained with magic angle spinning are independent of composition, molecular weight and morphology of the SIS copolymers studied, it appears that the bandwidths of the static spectra depends on the morphology of the samples (Table 7 and Figure 7). The morphology of the SIS copolymers actually depends on a variety of parameters, as discussed in Chapter I. For the long block samples, in general, the most important variable seems to be the volume

fraction of the phases. In the intermediate compositions (volume fractions between 0.25 and 0.75), selective casting solvent can also play an important role in determining the morphology of the two-phase systems. The component which has a solubility parameter similar to that of the solvent, tends to be the last to come out of solution and thus to form the continuous phase (152).

In the present experiments, there were two selective casting solvents; hexane has a solubility parameter (7.3) $((cal/cm^3)^{1/2})$, similar to the solubility parameter of poly(1,4-cis isoprene) (ca. 7.4), and MEK has a solubility parameter (9.3) close to the solubility parameter of polystyrene (ca. 9.8) (153). For the two samples of intermediate compositions (SIS 20-60-20H and SIS 30-40-30), the dramatic line broadening observed in the MEK cast films indicated that the motion of the isoprene segments in the SIS copolymers with intermediate compositions is more anisotropic in the samples cast from a solvent (MEK) which favors a morphology in which there was a styrene-continuous phase than those samples cast from a solvent (hexane) which promotes a morphology with an isoprene-continuous phase. The rate of motions is essentially the same in each case. This observation is consistent with a model proposed by Bovey et al. (136) for molecular motion of a series of segregated polyester thermoplastic elastomers. In this prior work the rate of motion of the mobile domain was found to be independent of the hard segment content of the polymer, in contrast to the angular range of molecular reorientation.

It has been reported that chain entanglements are main sources of

^{13}C NMR line broadening of the isoprene peaks in high molecular weight SI copolymers (145). This may also explain the results of the present bandwidth study of the static spectra. It suggests that the degree of chain entanglement among the isoprene segments of a SIS sample cast from a "poor" solvent of polyisoprene might be higher than that of the same sample cast from a "good" solvent of polyisoprene. This represents an area for future studies.

3. Molecular Motion in the Rigid Domains

Long T_1's of the styrene carbons in the SIS copolymers as evident from the disproportionate resonance intensities of the single pulse spectra with a short pulse delay time of 3 sec. (Figure 5) indicate that there was a low density of motions of the styrene components in the MHz region. This is consistent with the results for glassy polymers without methyl or other groups of substantially higher mobility (38).

The long T_1's of the styrene carbons make it infeasible to investigate their behavior with conventional inversion-recovery or progressive saturation methods. The rotating frame relaxation times ($T_{1\rho}$'s) which enable one to obtain information on molecular processes in a much lower frequency range than those encountered in ordinary T_1 studies (KHz instead of MHz) are usually much shorter than the T_1's in the case of rigid solid samples. This, together with the advantages of the cross polarization process, makes it feasible to do ^{13}C $T_{1\rho}$ experiments on the styrene components.

The glass transition depression of the styrene components in styrene-diene copolymers has been compared to that of the pure polymers of comparable molecular weight (127,142,143,151). In the same studies, the effect of composition and the molecular weight of the diene component on the styrene's T_g was found to be inconsequential. However, the effect of morphology on the molecules motions was not reported in these papers. The results of the ^{13}C $T_{1\rho}$ experiments of this current study for the two SIS 30-40-30 samples cast from different solvents indicated that selective casting solvents, or morphology, had no strong influence on the molecular motions of the rigid domains.

Data analysis of the styrene's ^{13}C $T_{1\rho}$ measurements revealed poorer correlations and larger intercepts than those obtained from the isoprene's ^{13}C T_1 measurements. However, besides the poor sensitivity and resolution of the $T_{1\rho}$ experiment, the inherent dynamic heterogenity of a polymer glass can result in ^{13}C $T_{1\rho}$ dispersion even for a homopolymer (38,154). Thus, it would be more difficult and complicated to estimate the interfacial regions of the SIS copolymers from the data analysis of the styrene's ^{13}C $T_{1\rho}$ measurements.

B. Polyurethane

1. Phase Separation

The morphology of urethane block copolymers is complicated not only by the two-phase structure as also found in the styrene-diene systems, but also by the possibilities of other physical phenomena, such as crystallization and hydrogen bonding in both segments (155). The time and temperature dependence of the morphology of the segregated

polyurethanes has been studied. It is believed that the domain interfaces of the polymers are diffusive and the degree of domain structure is a function of temperature and time (128-130,146,147).

In this C-13 NMR study, due to the limitation of sensitivity for the natural abundance sample, it was not possible to investigate the morphological kinetic behavior in the time scale of minutes and hours. However, conclusions regarding phase-separation and the sharpness of the interfacial boundary can be drawn from the present results for the polyurethane, given a specific composition and thermal history.

First, the fact that C-13 cross polarization spectra as a function of contact times revealed two sets of proton's $T_{1\rho}$, corresponding to those of the protons of the hard and soft segments, indicates phase separation between the hard and soft segments of the polyurethane.

Second, the fact that the C-13 resonance of the soft segments can be selectively observed with a long contact time (Figure 11) as well as an observed one-component first-order spin-lattice relaxation behavior of the soft segment carbons (Figure 10 and Table 10) indicated sharp domain boundaries for this specific polyurethane sample. This was especially true for the carbonyl carbon which has the highest peak intensity in the single pulse spectra and is completely resolved form the resonance of the other carbons.

2. Molecular Motions

The fact that C-13 NMR resonances of both segments of the polyurethane can be observed from both the single pulse and the cross polarization spectra (Figure 9) indicated that the molecular mobilities

in the soft and in the hard domains were not as dramatically different as was found in the case of the SIS copolymers. This is not unexpected, since, the T_g of the soft polytetramethylene adipate segment in the polyurethane is slightly above room temperature (37°C from a proton NMR study of a 35% MDI polyurethane sample of the same constituent monomers and prepared by the same company as the sample of this study (129)), while T_g of the polyisoprene is well below the room temperature (ca. -73°C).

Further studies comparing the resonance intensities of the two spectra of Figure 10 (a CP spectrum with a contact time of 1 ms which obtained approximately the maximum intensities as a function of contact time and 90° SP spectrum with a pulse delay time of 3.5 s) as well as a 90° SP spectrum with a pulse delay time of 20 sec. (Table 11) draw two lines of conclusions:

First, the resonance intensities of the soft segment carbons were not enhanced by the CP process. This is an indication that nuclear dipolar interactions in the mobile domains, although observable, are attenuated by the molecular motions to a large extent. Much weaker relative intensities for the carbonyl carbons (of both the soft and hard segments) in the CP spectrum are expected due to the long cross relaxation times of non-protonated carbons.

Second, the resonance intensities of the hard segment carbons (studied from the aromatic region) show a small enhancement by the CP process. The enhancement (1.2) is significantly smaller than the theoretical limit for a rigid lattice (4.0). This together with the

Table 11

Relative ^{13}C NMR Peak Intensities of the Polyurethane Obtained at Various Experimental Conditions

Pulse Sequence		90°-SP	90°-SP	CP (1ms)
Pulse Delay Time		3.5s	20s	4s
Relative Peak Intensities (per scan per mg)	172.9 ppm (S)	0.96	1.-	0.18
	153.8 ppm (H)	0.86	1.-	0.82
	137.3 ppm (H)	0.85	1.-	1.22
	63.6 ppm (S*)	1.10	1.-	0.86
	33.3 ppm (S*)	1.11	1.-	0.86
	25.0 ppm (S*)	1.01	1.-	0.67

* unresolvable from resonance signals of the hard segment nuclei

relative short T_1 values of the hard segment carbons of approximately 5 sec. according to the peak intensities at 153.8 and 137.3 ppm, indicates that for the rigid domains of the polyurethane at room temperature, high frequency motions (MHz), although more restricted relative to the mobile domains, are less restricted compared to most of the glassy polymers without fast relaxation sidechains.

Finally, although spin-lattice times of the hard segment carbons were observed, as expected, to be longer than those of the soft segment carbons. However, the proton's $T_{1\rho}$ was longer in the mobile domain than in the rigid domain. This is not what would be expected if the rotating frame relaxation is dominated by a spin-lattice process, as has been reported in the literature from the study of some glassy polymers (38, 154). Therefore, for the polyurethane, at least in the hard domain, the proton's rotating frame relaxation had a substantial contribution from the spin-spin process.

V. CONCLUSIONS

The principal conclusions of this chapter are summarized as follows:

SIS Copolymers

1. With dipolar decoupling and magic angle spinning, high resolution C-13 NMR spectra could be obtained at room temperature for the high molecular weight isoprene segments of the SIS copolymers. Using a conventional liquid probe, however, high resolution C-13 NMR spectra were obtained only for the low molecular weight diene samples or

for high molecular weight diene samples at an elevated temperature.

2. C-13 resonances of both segments of the SIS copolymers could be selectively observed with different experimental conditions and this is a strong indication of phase separation. Cross polarization pulse sequences (DD-MAS-CP) gave resonance signals almost exclusively from the carbons of the styrene segments. Single pulse sequence (SP-DD-MAS) with a short pulse delay time (3s) gave resonance signals predominantly due to the carbons of the isoprene components.

3. Sharp interfacial boundaries in the samples studied are indicated by two facts: First, the independence of the isoprene ^{13}C T_1 values on the molecular weights and compositions of the copolymers. Second, there was clearly a one component, first order spin-lattice relaxation behavior of the C-13 nuclei of the isoprene segments. In principle, the mole fraction of the isoprene segments in the interfacial regions can be estimated from the fraction of the isoprene carbons with longer T_1. This method did not give accurate results on the interfaces for the high molecular weight samples we studied. However, it might be possible to apply this method to the study of low molecular weight samples of a similar type which could have higher interfacial mixed composition fractions.

4. Non-cross-polarizability of the nuclei in the isoprene segments indicated high molecular mobility in the soft domains. The motions are essentially "liquid-like" in terms of frequencies.

5. Magic angle spinning narrowed the bandwidths of the isoprene C-13 resonances by factors of 5 to 10. This indicates that motion of

the isoprene segments is anisotropic due to the restictions imposed either by the rigid styrene domains and/or chain entanglements among the isoprene segments.

6. The effect of selective casting solvents on the bandwidth of the isoprene resonances in the static spectra indicated that the motion of the isoprene segments in the SIS copolymers was more anisotropic in the samples cast from a "poor" solvent of polyisoprene than in those cast from a "good" solvent. This could result from different morphology and/or a higher degree of isoprene chain entanglements.

7. Motion in the hard domains was not a strong function of the selective casting solvents or the morphology.

Polyurethane

1. Phase separation was indicated by two sets of proton's $T_{1\rho}$ (corresponding to those of the hard and soft segment protons) measured from the C-13 resonances as a function of the CP contact time.

2. Sharpness of domain boundaries in the sample studied is indicated by two facts: (i) resonance signals of the soft segments were selectively observed using a long CP contact time, (ii) one-component, first-order, spin-lattice relaxation behavior of the C-13 nuclei of the soft segments was found.

3. Although the resonances of the soft segments can be obtained with a cross polarization process, comparison of the resonance intensities of the CP and the SP spectra, however, indicated that the nuclear dipolar interactions in the mobile domains were attenuated by the molecular motions to a large extent.

4. Judging from the relatively small signal enhancement by the CP process as well as short ^{13}C T_1's, high frequency motions in the rigid domains of the polyurethane, although more resticted than those in the mobile domains, are less restricted when compared to those in most of the glassy polymers without fast relaxation sidechains.

5. The fact that proton's $T_{1\rho}$ in the mobile domains were longer than those in the rigid domains indicated that with the experimental conditions of a spin-locking field of 7.75 gauss, spin-spin process as well as spin-lattice process played an important role in the rotating frame relaxation of the polyurethane sample studied.

Chapter III

COMPATIBILITY STUDIES OF POLYMER BLENDS CONTAINING POLY(VINYLIDENE FLUORIDE)

I. INTRODUCTION

As a result of interest in polymer-polymer interactions in the solid state and the continued growth in commercial applications of polymer blends (1,2,5,6), a variety of experimental techniques have been employed to investigate polymer-polymer miscibility as was discussed in Chapter I. However, different methods reveal different facets of the nature of the mixing process; consequently, no single method has answered all the interesting questions at the molecular level (156,157). Hence, it was desirable to try to extend the range of the potential tools available for analysis in this important area and to compare the results to those obtained from the previous efforts.

High resolution solid state C-13 NMR has certain advantages over most of the other techniques due to its capability for probing the possible interactions at the molecular level. It has been used to study polymer-polymer miscibility through the measurement of T_1, T_2, $T_{1\rho}$ and other relaxation parameters (133-135). However, the studies reported in this chapter were undertaken to examine polymer blends of poly(vinylidene fluoride) from rather a unique point of view (158,159).

For most organic polymers in the solid state, use of MAS in combination with high power ^{13}C-^{1}H dipolar decoupling and cross polarization will result in a high resolution carbon-13 NMR spectra. One observes, though, that even with all three techniques applied,

complicated spectra result in the case of polymers which contain other NMR active nuclei (other than ^{13}C and ^{1}H) having high natural abundance and strong nuclear magnetic moments. Usually quite broad, or in some cases, completely featureless spectra are obtained due to dipolar coupling between the carbon-13 nuclei and the 'other nuclei'. Poly(vinylidene fluoride), (PVF_2), for instance, when analyzed without simultaneous decoupling of the fluorine-19 and the protons produces a ^{13}C frequency domain spectrum which is completely devoid of peaks. It is suggested, therefore, that a powerful method for investigating the miscibility of polymer blends containing PVF_2 might be through studying the intermolecular dipolar interactions between the ^{19}F nuclei in the PVF_2 and the ^{13}C nuclei in the second polymer. Strong dependance on internuclear distance would be expected for such interactions. The major advantage of this experiment over the previous ^{1}H-^{19}F work (124) would be the quantitative and specific identification of all of the sites of interaction. If a polymer was indeed immiscible with PVF_2, then its ^{13}C-NMR signal intensities in the mixture simply would be directly proportional to those shown by pure polymer alone, intensity reduction being accounted for by sample dilution. On the other hand, if a polymer was extensively and intimately intermixed with PVF_2, then its ^{13}C-NMR signal intensities in the blend would be additionally attenuated by the ^{19}F coupling, assuming an absence of ^{19}F decoupling.

Magic angle spinning is primarily a technique for overcoming the effect of ^{13}C chemical shift anisotropies in a solid which result from multiple orientations of the nuclear moment with respect to the applied

field. However, MAS can also decouple weak dipolar interactions, to a first approximation in those having strengths (in Hz) less than that of the frequency of the spinning (29,134). Since the spinning rates in the current experiments were about 2.0 kHz, a limit on the resolution of the estimated intimacy of mixing will be shown in later sections to be in the range of 3 to 4 angstroms, beyond which MAS decoupling will reduce any signal attenuation tendencies of ^{19}F on ^{13}C.

The major object of the work in this chapter was to demonstrate a new approach to the study of polymer-polymer miscibility at the molecular level. Toward this goal, a series of polymer blends containing PVF_2 which had been extensively explored by other techniques (118, 124, 160-171) was desirable. In particular, melting point depression of the PVF_2 crystalline region in the blends was compared with the NMR results.

II. EXPERIMENTAL

A. Sources and Characterization of Homopolymers

Poly(vinylidene fluoride), (PVF_2), was obtained from Polysciences, Inc. with a M_w = 100,000.

Poly(methyl methacrylate), (PMMA), also from Polysciences, Inc. had a M_w = 800,000. From our solution ^{13}C NMR spectrum it was found to be 75% syndiotactic. In pure form, it was compression molded for the solid state NMR studies.

Poly(vinyl acetate), (PVAc), Mw = 70,000 was obtained from Aldrich Chemicals. It was about 65% syndiotactic according to its

^{13}C NMR spectrum in solution. It was also compression molded for solid state NMR studies.

Poly(vinyl methyl ether), (PVME), Mw = 18,000 was obtained from Polysciences, Inc.. The tacticity was determined to be about 50% syndiotactic based on the solution ^{13}C NMR spectrum run in our labs. This material was packed neat into the NMR rotor.

B. Preparation of Blends

The PVF_2/PMMA blends were prepared in three ways; the first method was to use a melt extruder, in the other two methods, samples were prepared by using mutual solvents, methyl ethyl ketone (MEK) and dimethyl formamide (DMF), respectively. The PVF_2/PVAc blends were produced by using MEK and DMF as the common solvents. The PVF_2/PVME blends were produced by using DMF as the common solvent.

Extruded blends were prepared on a CSI-MAX mixing extruder at 190°C. Residence time at 190°C was relatively short (mins.). Blends using MEK as the common solvent were made by first dissolving the individual polymers at about a 2 g/100 ml concentration, then appropriately mixing these solutions. When mixed, all the solutions were clear in all proportions studied. These mixtures were poured into aluminum pans and subsequently dried in air for two days, followed by further drying in a vacuum oven for 24 hours at room temperature. Blends using DMF as a common solvent were made by the same procedures as those using MEK, except that the mixtures were first dried in air for at least one week, then further dried in a vacuum oven for 48 hours at room temperature.

Melted-and-quenched PVF_2/PMMA samples were prepared from solution blends by first heating the dried blends in a vacuum oven at 190°C until the PVF_2 crystals melted completely, then immediately immersing the materials into liquid nitrogen for 5 minutes.

Films from all the above preparations were punched to form circular discs which were weighed, and stacked into the MAS rotor.

C. NMR

The DD-MAS solid state carbon-13 experiments were carried out at room temperature at 15.0 MHz on the same JEOL-60Q spectrometer, using the same Kel-F 'bullet' type rotor and ca. 2.0 KHz spinning speeds, as described in Chapter II.

Adjustments of the Hartmann-Hahn condition and the magic angle, calibration of the spinning speeds as well as the chemical shift reference of the spectra were discussed in Chapter II. Experimental conditions including spectral width, data points, zero filling and acquisition time, were also the same as those described in Chapter II.

For pure PVME and the PVF_2/PVME blends, a single 90° pulse sequence was used (90° pulse = 7.6 μs). For pure PVAC and the PVF_2/PVAC blends and pure PMMA and the PVF_2/PMMA blends, matched spin-lock cross polarization transfers employed H_1's of 33 KHz with single contact times of 0.75 ms and 3 ms, respectively, as the standards for resonance intensity comparison. Appropriate pulse delay times were used to ensure full relaxation between scans. Contact times, pulse delays, and the number of scans per spectrum will be discussed in later sections.

Carbon-13 resolved proton's $T_{1\rho}$'s were calculated from the final slope of the CP intensity as a function of contact time, as discussed in Chapter I, (section II.D.4).

D. DSC

Thermal analysis of PVF_2 and its blends was carried out on a Perkin-Elmer DSC-2 differential scanning calorimeter at a heating rate of 20 degrees per minute. Melting points were taken as the temperature at which the last detectable trace of crystallinity disappeared (118).

III. RESULTS

A. General Description of NMR Spectra and DSC Curves

Figure 12 shows the high resolution solid state ^{13}C NMR spectra of pure PMMA, PVAc and PVME. Peak assignments were made according to the respective solution spectra available in the literature (172-174). Although not every carbon peak could be completely resolved, all of the other carbons were separable from one another at half peak height, except for the methylene carbon of PMMA.

Figure 13 gives one example of how pure PMMA signals were attenuated when placed in a blend with PVF_2. Spectra (A), (B) and (C) were obtained for PMMA, a 50:50 MEK blended PVF_2/PMMA and a 50:50 MEK, melted-and-quenched PVF_2/PMMA blend, respectively. The number of accumulations (scans) of (B) and (C) were selected in order to ensure that the three spectra would have equal sensitivity (signal to noise ratio) if there were no intermixing between the PVF_2 and PMMA.

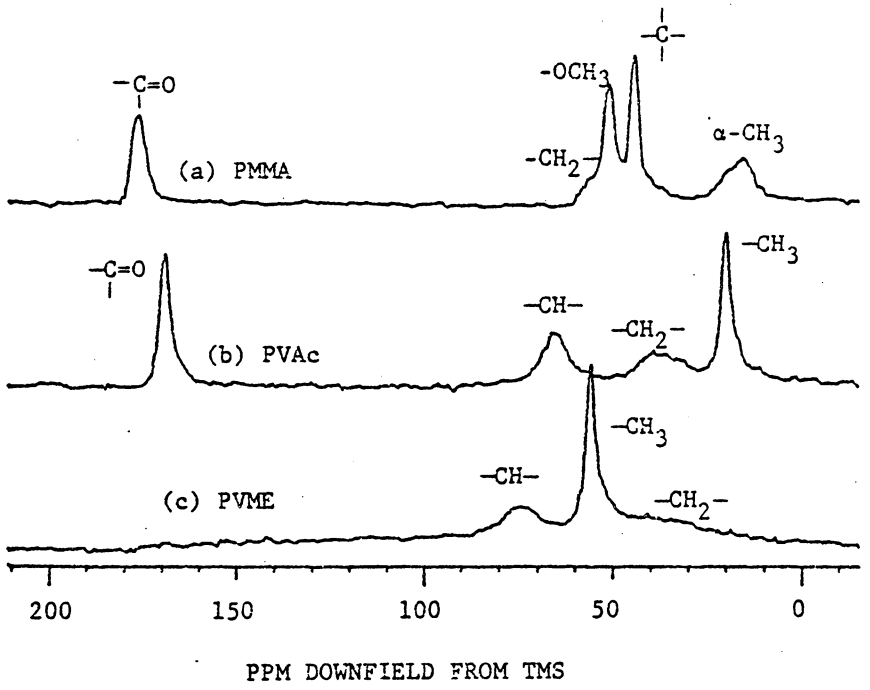

Figure 12. The 15.0 MHz DD-MAS Solid State C-13 NMR Spectra of Homopolymers.
(a) PMMA, obtained from 1,000 FID accumulations with a CP contact time of 3 ms and a pulse delay time of 3s.
(b) PVAC, obtained from 1,492 FID accumulations with a CP contact time of 0.75 ms and a pulse delay time of 3s.
(c) PVME, obtained from 4,800 FID accumulations with a single ^{13}C 90° pulse of 7.6 μs and a pulse delay time of 2s.
All the spectra were obtained from 1 K FT with zero-filling to a total of 4K points. Pulse delay times of all the three spectra were long enough to ensure relaxation between the scans. Peak assignments were referred to the respective solution spectra from literature (172,173,174).

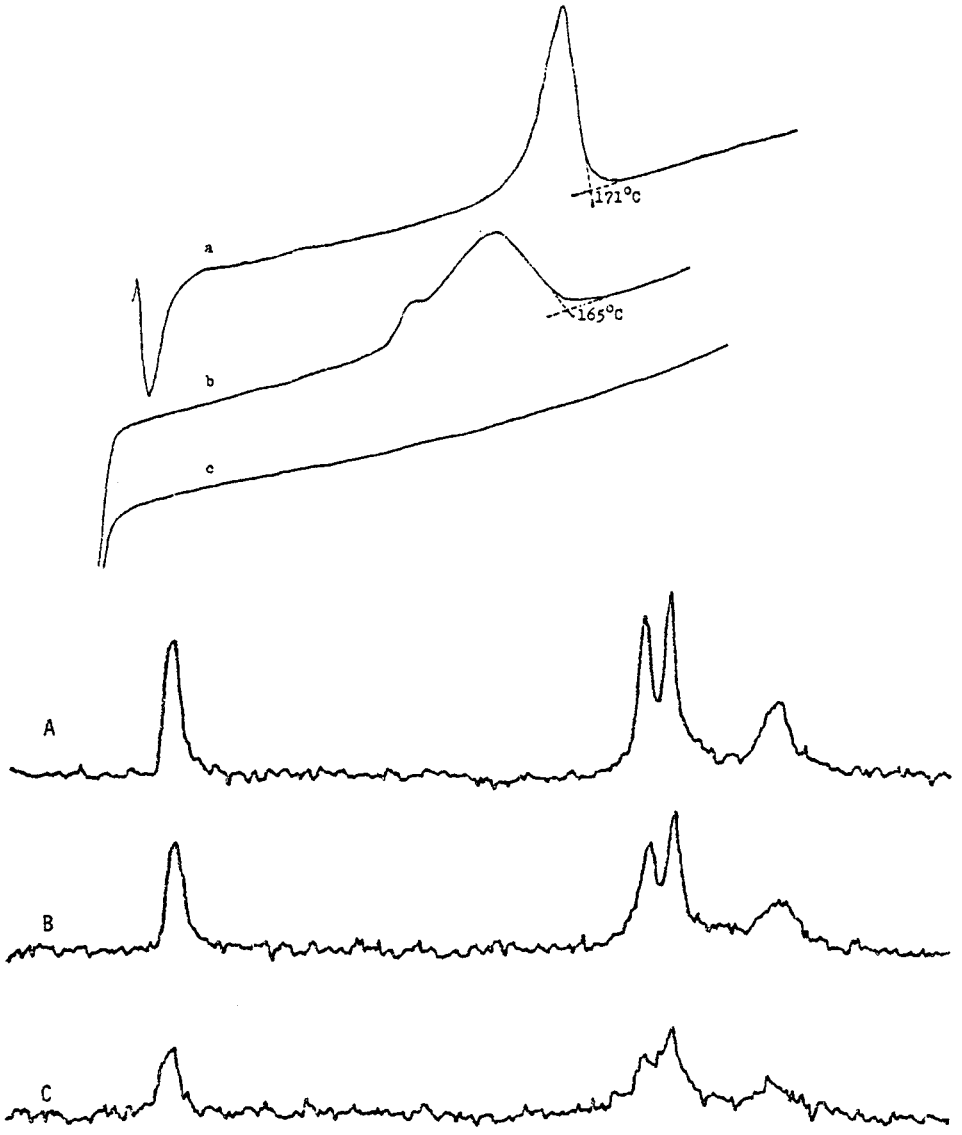

Figure 13. Melting Point Depressions of PVF_2 and NMR Signal Intensity Attenuations of PMMA in the PVF_2/PMMA Blends. Each of A,B and C is a 15.0 MHz DD-MAS-CP C-13 NMR spectrum. Each of a,b,and c is a DSC curve obtained at a heating rate of 20 degrees per minute.

(A) PMMA
(a) PVF_2
(B) and (b) 50:50 PVF_2/PMMA blend (MEK)
(C) and (c) 50:50 PVF_2/PMMA Blend (MEK, melted and quenched).

The three spectra A, B and C, are scanned to have equal signal to noise ratio if there is no intermixing between PVF_2 and PMMA. Calculations are shown in Table 12.

Table 12

Calculations of the Residual NMR Signal Intensities

Samples		PMMA	PVF_2/PMMA	PVF_2/PMMA (quenched)
Weight		463.2 mg	411.9 mg	390.6 mg
Weight fraction of PMMA		1.-	0.50	0.50
Number of accumulations		640	3238	3600
Relative sensitivity (calculated)		1.-	1.000	1.000
Relative signal intensities (calculated)		1.-	2.250	2.372
Signal intensities (experimental) (arbitrary unit)	carbonyl	3521	5935	3466
	methoxyl	4294	5770	3572
	quaternary	4844	7463	4948
	α-methyl	1937	2999	2660
Residual Signal intensities (%)	carbonyl	100	75	42
	methoxyl	100	60	35
	quaternary	100	69	43
	α-methyl	100	69	58

Sample calculations involving the chosen number of accumulations and the residual PMMA signal intensities in the blends are listed in Table 12. All are based on the following assumptions (52): (i) the absolute signal intensity was directly proportional to the number of nuclei (weight of PMMA) and to the number of accumulations, (ii) the sensitivity (S/N) was proportional to the number of nuclei and to the square root of the number of accumulations, and (iii) that the data handling capabilities of the NMR instrument's computer were not limiting as the number of scans increased. Thus, for any particular carbon in a blended polymer the ratio of expected signal intensity to the observed signal intensity directly provides the percentage of attenuation. This attenuation was ascribed to ^{19}F's in the immediate vicinity of a particular carbon, all other factors of data reduction being constant.

Examples of DSC curves are also given in Figure 13 for pure PVF_2 and the same two PVF_2/PMMA blends. Melting point depression or suppression of PVF_2 in the blends were observed.

B. Melting Point Depressions of PVF_2 and NMR Signal Attenuations of Non-PVF_2 Polymers

Tables 13, 14, and 15 present an analysis of the data in terms of the residual intensities of the various solid-state ^{13}C signals of PMMA, PVAc and PVME, respectively, when each was blended with PVF_2. All the calculations were based on peak heights. Comparisons of alternate approaches indicated that the use of peak areas instead of heights made little difference in the results. The melting points of PVF_2 in the blends was determined calorimetrically and are also listed in the

Table 13

Residual NMR Signal Intensities of PMMA in the PVF_2/PMMA Blends

Composition (wt.% of PVF_2)	Method of Blending	Residual ^{13}C Peak Intensities (%) carbonyl	methoxyl	quaternary	α-methyl	PVF_2 Tm(°C)
70	MEK	57	53	58	73	164
50	MEK	75	60	69	69	165
25	MEK	76	59	68	85	broad
70	MEK,quenched	43	31	38	57	161
50	MEK,quenched	42	35	43	58	none
25	MEK,quenched	69	59	72	68	none
70	DMF	109	118	116	94	173
50	DMF	113	111	116	94	174
25	DMF	114	101	104	112	174
70	DMF,quenched	44	29	35	41	163
50	DMF,quenched	62	40	59	69	163
25	DMF,quenched	73	60	68	84	none
70	extruded	41(44)*	30(30)*	43(42)*	50(58)*	159
50	extruded	35(42)*	28(26)*	37(30)*	51(49)*	148
25	extruded	52(50)*	45(46)*	47(52)*	66(71)*	no
100	--	--	--	--	--	171

* Results obtained at a higher MAS rate (2.3 KHz)

Table 14

Residual NMR Signal Intensities of PVAc in the PVF_2/PVAc Blends

Composition (wt.% of PVF_2)	Method of Blending	Residual ^{13}C Peak Intensities (%)				PVF_2 Tm(°C)
		carbonyl	methine	methylene	α-methyl	
69.8	DMF	72	100	122	73	175
49.9	DMF	32	51	58	29	157
24.8	DMF	19	18	28	15	153
13.7	DMF	16	--	--	18	152
8.5	DMF	17	--	--	15	--
4.1	DMF	62	49	58	59	--
100.0	--	--	--	--	--	171
69.8	DMF, molded	78	112	187	70	--
49.8	DMF, molded	73	88	110	66	--
24.8	DMF, molded	81	79	93	71	--
13.7	DMF, molded	65	61	80	57	--
8.5	DMF, molded	70	65	67	58	--
4.1	DMF, molded	53	53	39	43	--
45.5	MEK	14	--	--	14	159
45.5	MEK, molded	50	53	--	39	155

Table 15

Residual NMR Signal Intensities of PVME in the PVF_2/PVME Blends

Composition (wt.% of PVF_2)	Method of Blending	Residual ^{13}C Peak Intensities (%)			PVF_2 Tm(°C)
		methine	methyl	methylene	
75	DMF	110	119	109	177
50	DMF	123	110	124	175
100	--	--	--	--	171

tables. Various compositions, and thermal and solvent histories are and thermal and solvent histories are also indicated in the first two columns.

Values in these three tables which exceed 100% may do so for several reasons. Minor mass balance errors undoubtedly account for some scatter. Reproducibility in experiments on pure PMMA and its blends was found to be 5-10% (see Tables 16,17) for the peaks where S/N was in the range of 20-30. In other cases, weak or incompletely resolved peaks (e.g., the methylene carbon of PVAc) are estimated to have somewhat larger uncertainty in intensity. Some of the relevant instrument pulse sequence parameters which had to be considered and may be a factor in this regard and will be discussed in conjunction with Tables 18-20. The values greater than 100% were generally observed on all of the carbon peaks in the DMF cast films, regardless of blend; melting points of PVF_2 were also found to be higher in each case. This behavior was quite consistent and may be due to a modification of the crystal form of the PVF_2 (at least three are known) (175-177) that occurred on casting from DMF. Conceivably, a modification of relaxation times, particularly $T_{1\rho}^{H}$, might then result in larger initial ^{13}C magnetization in each recorded pulse, leading to enhanced peak intensities for the case materials at equal calculated S/N ratios.

C. Carbon-13 Resolved Proton's $T_{1\rho}$'s

Proton $T_{1\rho}$ values of PMMA and two melt extruded PVF_2/PMMA blends calculated from the PMMA ^{13}C CP intensity as a function of contact time (Figures 14-16) are given in Table 19. For any particular sample, the

Table 16

^{13}C NMR Signal Intensities of PMMA Obtained at Various Experimental Conditions

Run No.	CP Contact Time (ms)	Pulse Delay Time (s)	Peak Intensities (arbitrary unit)			
			carbonyl	methoxyl	quaternary	α-methyl
1	3	2	4833	6301	7190	2191
2	1	3	5227	7731	8853	2694
3	3	3	4941	6383	7383	2159
4	5	3	3734	4982	6124	1816
5	3	2	4788	6510	7617	2263

Table 17

^{13}C NMR Signal Intensities of the Melt-Extruded 25:75 PVF_2/PMMA Blend Obtained at Various Experimental Conditions

Run No.	CP Contact Time (ms)	Pulse Delay Time (s)	Peak Intensities (arbitrary unit)			
			carbonyl	methoxyl	quaternary	α-methyl
1	3	2	3882	4031	5121	2113
2	1	3	4939	6190	8370	2894
3	3	3	4296	4468	5588	2095
4	5	3	2703	2808	3829	1524
5	3	2	4068	4307	5676	2301

Table 18

Residual NMR Signal Intensities of PMMA in the 25:75 PVF_2/PMMA Melt-Extruded Blend, Calculated from the CP Spectra with Various Contact Times

CP Contact Time (ms)	Residual ^{13}C NMR Peak Intensities (%)			
	carbonyl	methoxyl	quaternary	α-methyl
1	68	59	68	77
3	63	50	54	70
5	52	60	45	60

Pulse delay time = 3 seconds

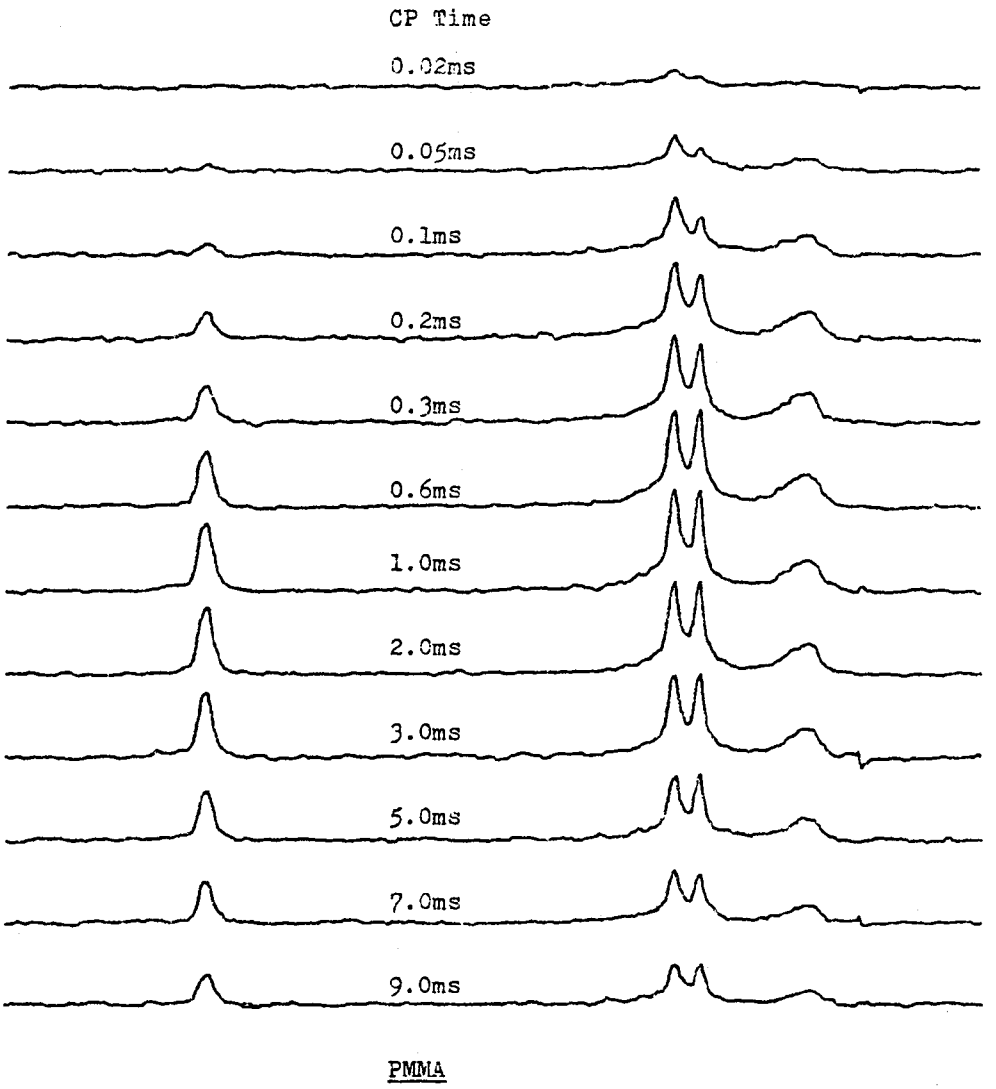

Figure 14. DD-MAS-CP 15.0 MHz C-13 NMR Spectra of PMMA Obtained at Various Contact Times.

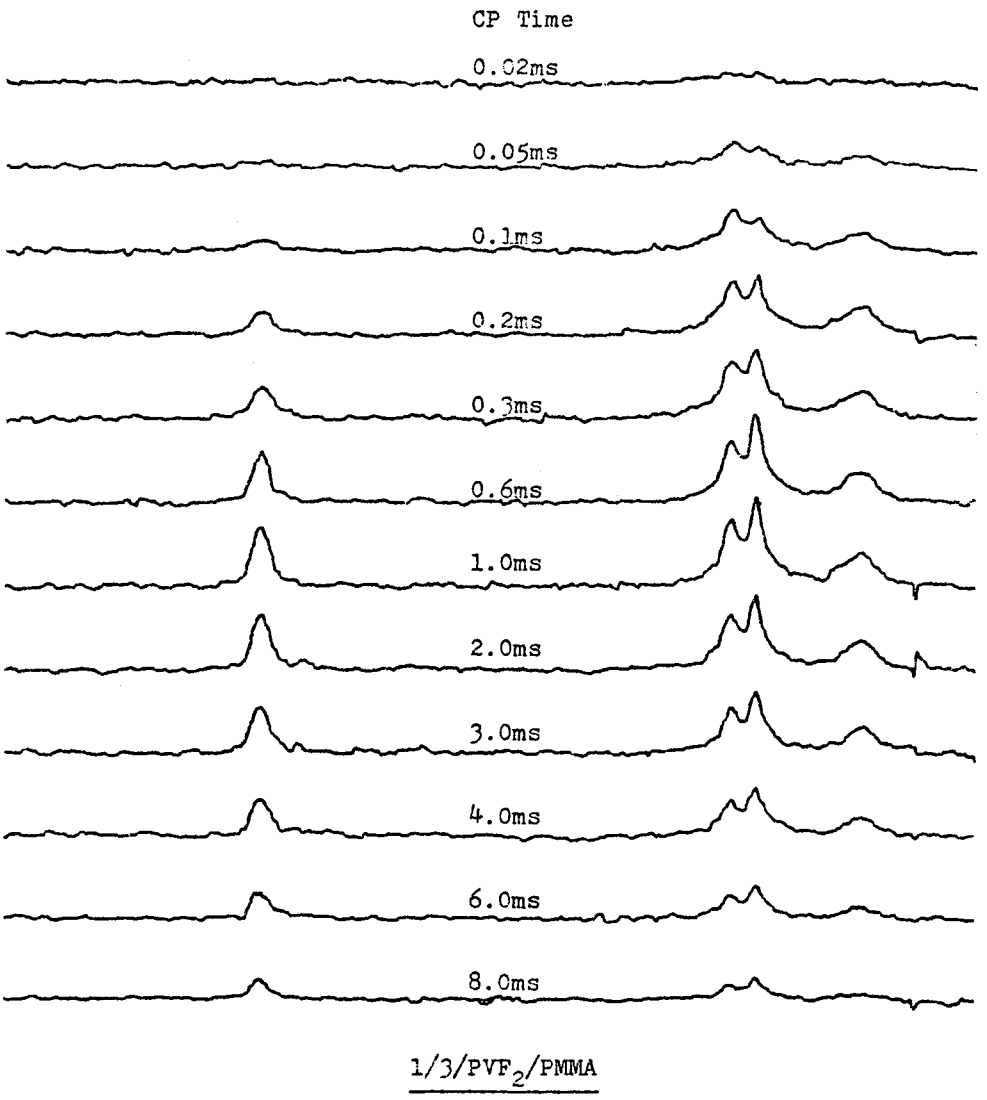

Figure 15. DD-MAS-CP 15.0 MHz C-13 NMR Spectra of the Melt-Extruded 25:75 PVF_2/PMMA Blend Obtained at Various Contact Times.

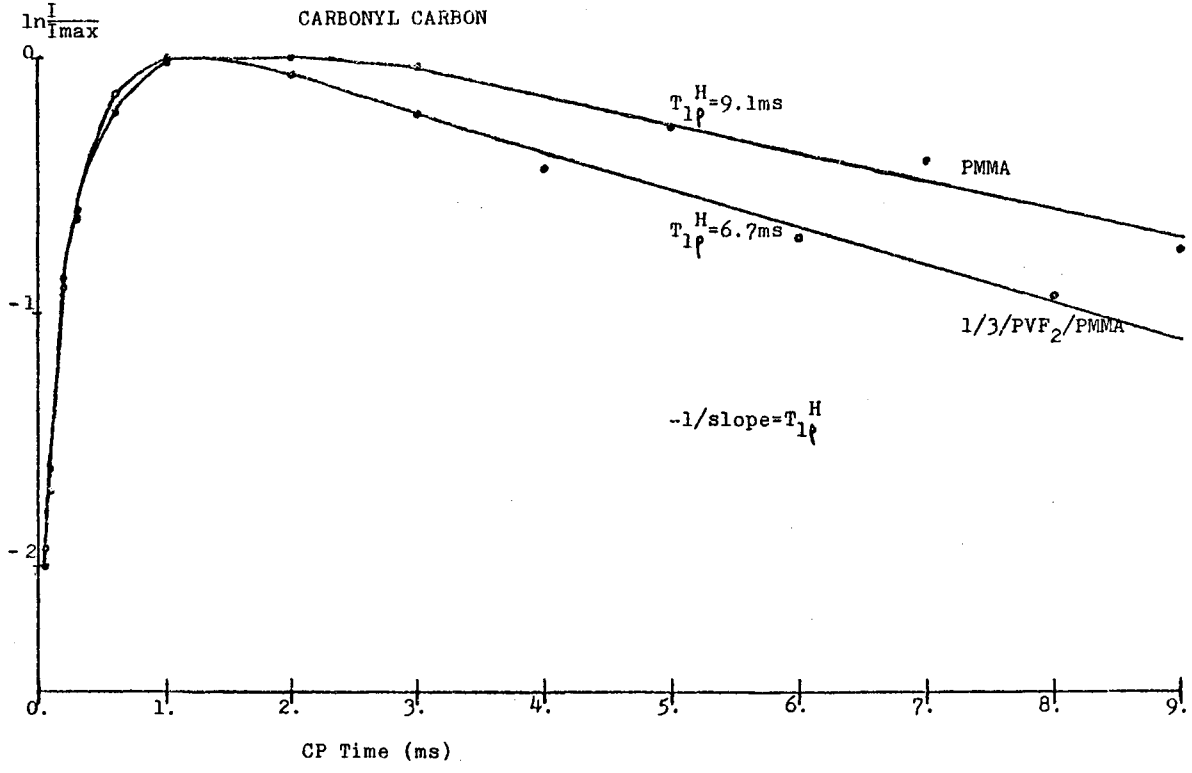

Figure 16. ^{13}C NMR Signal Intensity for the Carbonyl Carbon of PMMA in the Homopolymer and in the Melt-Extruded 25:75 PVF_2/PMMA Blend as a Function of Contact Time.

Table 19

PMMA C-13 Resolved Proton $T_{1\rho}$ Values of the Homopolymer and the PVF_2/PMMA Blends

Samples	Proton $T_{1\rho}$ Values (ms) Calculated From			
	carbonyl	methoxyl	quaternary	α-methyl
PMMA	9.1	9.4	8.6	8.3
25:75 extruded PVF_2/PMMA blend	6.7	5.4	5.8	5.9
50:50 extruded PVF_2/PMMA blend	3.8	3.9	3.7	3.4

Table 20

Residual NMR Signal Intensities of PMMA in Two Melt-Extruded PVF_2/PMMA Blends as an Effect of Sample Aging

Samples	CP Contact Time (ms)	Sample History (days after blending)	Residual ^{13}C NMR Peak Intensities (%) carbonyl	methoxyl	quaternary	α-methyl
25:75 Extruded PVF_2/PMMA Blend	3	1	52[a]	45[a]	47a	66[a]
	3	34	63[b]	50[b]	54[b]	70[b]
	3	118	56	47	61	75
	*	118	62*	58*	71*	85*
50:50 Extruded PVF_2/PMMA Blend	3	1	35[a]	28[a]	37[a]	51[a]
	3	218	47	32	46	64
	*	218	70*	50*	74*	111*

* calculated from Mo*, the theoretical maximum magnetization attainable, when $T_{1\rho}^{H} >> CP$ contact time$>> T_{CH}$

a. results of Table 13

b. results of Table 18

values obtained from four ^{13}C resonance peaks show some scatter (which should be the same) due to the limited number of spectra (data points) used in determining the $T_{1\rho}$'s and the limited sensitivity of the NMR instrument. However, it is obvious that proton's $T_{1\rho}$ values are different among the three samples.

The theoretical maximum magnetization of PMMA attainable in the CP process in the homopolymer and the two blends was calculated for the $T_{1\rho}^{H}$'s using Equation (91). Residual NMR signal intensitites of PMMA in the two blends calculated from the theoretical maximum magnetization are given in Table 20. The table also lists the results calculated from a CP contact time of 3 ms of the same experiments as well as results of the previous experiments on the same samples.

IV. DISCUSSION

A. Shifts of NMR Frequencies

As a result of the interactions between PVF_2 and the other polymers in the miscible blends, one might expect some shifting of various NMR peaks away from their initial frequencies similar to what is observed in FT-IR studies (165). However, due to the inherent resolution limitation of NMR instruments in addition to the decreased sensitivity obtained with the miscible blends (signal attenuations), no significant NMR chemical shifts were induced by blending. Mixed tacticities in the non-PVF_2 polymers also contributed to this lack of resolution.

B. NMR Signal Attenuations and Degrees of Intermixing

From Tables 13, 14,15, it is apparent that most of the data for the

magnitudes of ^{13}C signal attenuations of PMMA, PVAc and PVME in the blends with PVF_2 were in very good agreement with the melting point depressions of PVF_2 in the blends. The method of melting point depression has become widely accepted as an indicator of the degree of blend miscibility when semicrystalline polymers are involved. For example, this number can be directly related to the polymer-polymer free energy interaction parameter as discussed in Chapter I (section III.B.6). Clearly, a macroscopic, thermodynamic observation is all that may be obtained in this case. In comparison, NMR signal attenuations of any polymer blended with PVF_2 as observed in the present work indicate to some extent spatial proximity of that polymer with PVF_2. It will be shown below that intermolecular distances for ^{13}C-^{19}F dipolar coupling as observed by the present method was in the range of 3 to 4Å. Among the blends which were examined, except for the DMF cast PVF_2/PVAC blends with thermal treatment, both the methods of melting point depression and NMR signal attenuations indeed provided consistent indications of the extent of compatibility from very different experimental approaches. The data in Tables 13, 14 and 15 for the three series of blends are discussed individually in the next three sections.

1. PVF_2/PMMA Blends

Without any thermal treatment, MEK was a better common solvent for blending than was DMF; attenuation of ^{13}C resonances was nil in the latter case. Although the mixtures of PVF_2 and PMMA in DMF were clear, the dried samples of all compositions cast from DMF were totally immiscible as measured by both the NMR and DSC studies.

Melting-and-quenching the blends appeared to improve miscibility according to the NMR work; PVF_2 crystallinity was undetectable by DSC in some of these samples. The differences in NMR signal attenuations between the MEK-blended and the DMF-blended samples with the same composition became smaller after the melting and quenching process. However, the miscibility of both was indicated to remain poorer than that of the melt-extruded blends having the same composition.

For solvent-blended samples in the composition ranges studied, it was observed that the higher the PVF_2 content, the greater the amount of PMMA ^{13}C signal attenuation. For the melt-extruded blends, the one with medium PVF_2 content (50% by weight) showed the highest degree of ^{13}C signal loss.

The significant disparity in miscibility between the DMF and MEK cast films could result from the difference in rates of solvent evaporation. For the 2% solutions, it was observed that DMF evaporated about ten times more slowly than MEK. This is consistent with a better and more complete crystalliaztion as well as a poorer miscibility of the DMF cast films.

The polymorphic nature of the PVF_2 crystallinity may also in part explain the results. The morphology of PVF_2 homopolymers has been extensively investigated (177). The effect of sample history on the morphology of PVF_2 is summarized in Figure 17 (178). It was reported that crystallization from DMF resulted in a γ-phase, while crystallization from melt and from cyclohexane (which, like MEK, is a saturated aliphatic ketone) usually resulted in an α-phase. Therefore,

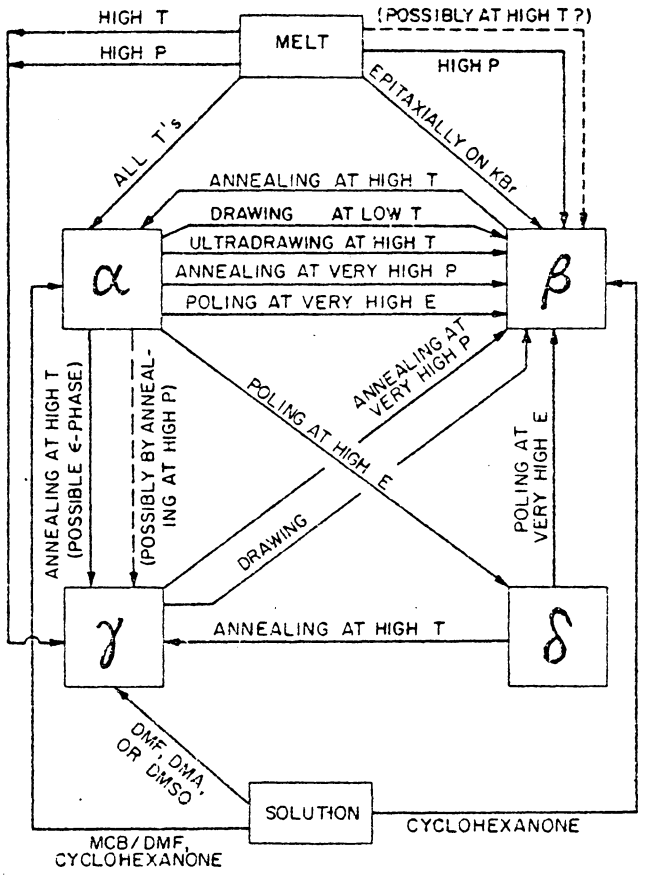

Figure 17. Schematic Summary of Crystallization and Interconversions of the Polymorphic Phases of PVF_2 (178). (T = temperature; P = pressure; E = electric field).

the MEK cast films are expected to have closer miscibility to the melt-extruded blends than the DMF cast films.

Melting-and-quenching the solution cast films are likely to result in the same crystal form as the melt-extrusion process. However, in the former case, the driving force of miscibility would be solely from diffusion. In contrast, in the latter case, molecular diffusion in addition to mechanical force could result in better homogeneity or miscibility of the blends. The difference in dependence of PMMA ^{13}C signal attenuation on the composition for the blends prepared from the two methods may also result from the complicated crystallization process of PVF_2.

2. PVF_2/PVAc Blends

For PVF_2/PVAc blends, as for PVF_2/PMMA blends,without any thermal treatment, MEK appeared to be a better common solvent for blending than DMF, although miscibility for the DMF cast PVF_2/PVAc samples was observed over a wide range of compositions. Compared to the PFV_2/PMMA blends made with the same common solvent, the PVF_2/PVAc blends made from both DMF and MEK solutions were found to have much better miscibility as indicated by both the NMR and DSC results shown in Table 14. This better miscibility could be due to the slightly greater interaction between PVF_2 and PVAc than that between PVF_2 and PMMA, as has been reported from melting point depression studies (171). It may also result from the glass transition temperature of the PVF_2/PVAc blends (about or below room temperature) which is lower than that of PVF_2/PMMA blends (above room temperature) (171). For the DMF cast

samples, carbon-13 NMR signal attenuations of PVAc were found to pass through a minimum as the PVF_2 content was increased. The loss of miscibility at the higher PVF_2 content probably was due to the higher degrees of PVF_2 crystallinity in those blends.

For the solvent (DMF and MEK) blended PVF_2/PMMA samples, the degree of intermixing was found to be enhanced after a melting-and-quenching process, as evident from both the NMR and DSC studies. On the contrary, the NMR studies of the solvent blended PVF_2/PVAc samples revealed that a process of high temperature (ca. 200°C) compression molding and subsequent cooling to ambient temperature reversed the intimacy of the mixing between the two polymers even though the melting point of PVF_2 was practically unchanged with the process.

Although thermally induced phase separation, or the lower critical solution temperature behavior (LCST) (Figure 4 shows an upper critical solution temperature behavior (UCST)) has been observed in many blends of PVF_2, a cloud point due to reaching the LCST for the PVF_2/PVAc blends was not observed up to 350°C (169,171). The reasons for the absence of LCST behavior were reported to be either from the enhanced phase stability caused by the intense interaction between PVF_2 and PVAc or due to a close similarity of refractive indices of the two polymers (169).

The inconsistency between the NMR and DSC results for the molded PVF_2/PVAc samples can be partially understood by knowing that the experimental probe size in this NMR studies was about two orders samller than those associated with the glass transition or light transparency methods. It can be concluded that molding-and-cooling process is likely

to result in small scale modification of the crystals of PVF_2 in the PVF_2/PVAc blends.

3. PVF_2/PVME Blends

In Table 15, a summary of observations on the PVF_2/PVME blends is presented. Although both pure materials dissolve readily in DMF the cast films were concluded to be totally immiscible by both the NMR and DSC results, confirming previously observed data of other researchers (171). The coincidence of signal intensities which are enhanced rather than diminished by the DMF casting sequence and elevated PVF_2 melting point is especially noticeable in Table 15.

4. NMR Signal Attenuations of Individual Carbons

The nature of the miscibility of both the PVF_2/PMMA and the PVF_2/PVAc blends previously has been attributed to a weak intermolecular 'acid-base' association. In particular, an interaction was postulated between the acidic protons of PVF_2 and the basic carbonyl groups in the case of both PMMA and PVAc (165,171). Knowing that the definition of miscibility in these NMR experiments has to be confined to approaches of dissimilar nuclei to within about 4Å, it was expected that it might be possible to observe differing extents of NMR peak attenuations for each carbon. Depending on how much less than 4Å the contact actually was on the average, an estimate of the specificity of interatomic mixing could be made.

From Table 13, for the PVF_2/PMMA blends, there were four resolvable NMR peaks in the spectra of PMMA; the methoxyl carbon which

is adjacent to the carbonyl groups was the most attenuated, while the α-methyl carbon was the least attenuated. This difference became more pronounced in the melt-and-quenched and the melt-extruded blends. Although sample history resulted in different degrees of C-13 resonance signal attenuations for the miscible PVF_2/PMMA blends, the order of the attenuations among the four resolvable PMMA peaks remained essentially the same regardless of the sample history (Figures 18-21).

For the PVF_2/PVAc blends without thermal treatment, it seems that the signal intensities of the two main chain carbons of PVAc were less attenuated than those of the two side chain carbons of PVAc, especially for the samples with higher PVF_2 contents (Figure 22). However, the initial peak intensities of the two main chain carbons were much weaker than those of the two side chain carbons (see Figure 12), partially due to the effects of tacticity. Thus, in view of the inherent accuracy of the measurements, it should be kept in mind that the uncertainty of any conclusion concerning the two main chain carbons is higher than that of the two side chain carbons.

C. NMR Signal Attenuations and Magic Angle Spinning Rates

From Equation (50), the direct nuclear dipolar coupling between a ^{19}F nucleus and a ^{13}C nucleus in a rigid lattice can be calculated. If r is considered in angstroms, then

$$2\,D(^{13}C - ^{19}F) = \frac{56815.2}{r^3}\left|\frac{3\cos^2\theta - 1}{2}\right| \text{ Hz} \qquad (115)$$

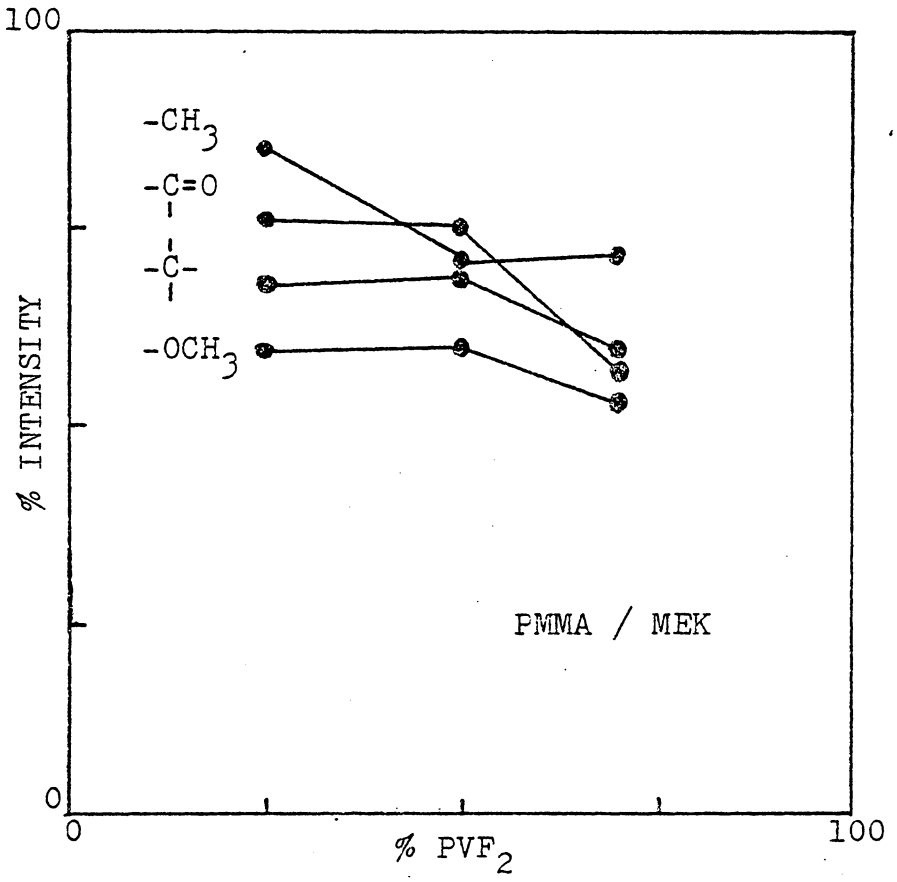

Figure 18. % Residual C-13 Resonance Intensities of PMMA in the MEK-Cast PVF_2/PMMA Blends.

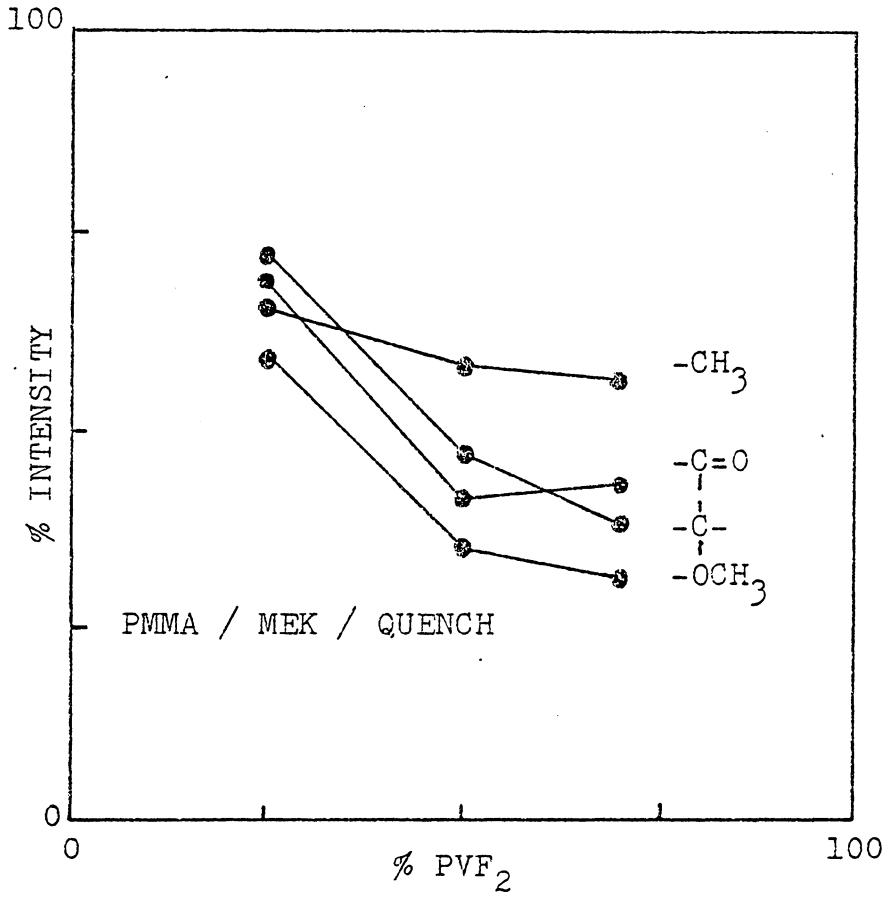

Figure 19. % Residual C-13 Resonance Intensities of PMMA in the MEK-Cast, Melted-and-Quenched PVF_2/PMMA Blends.

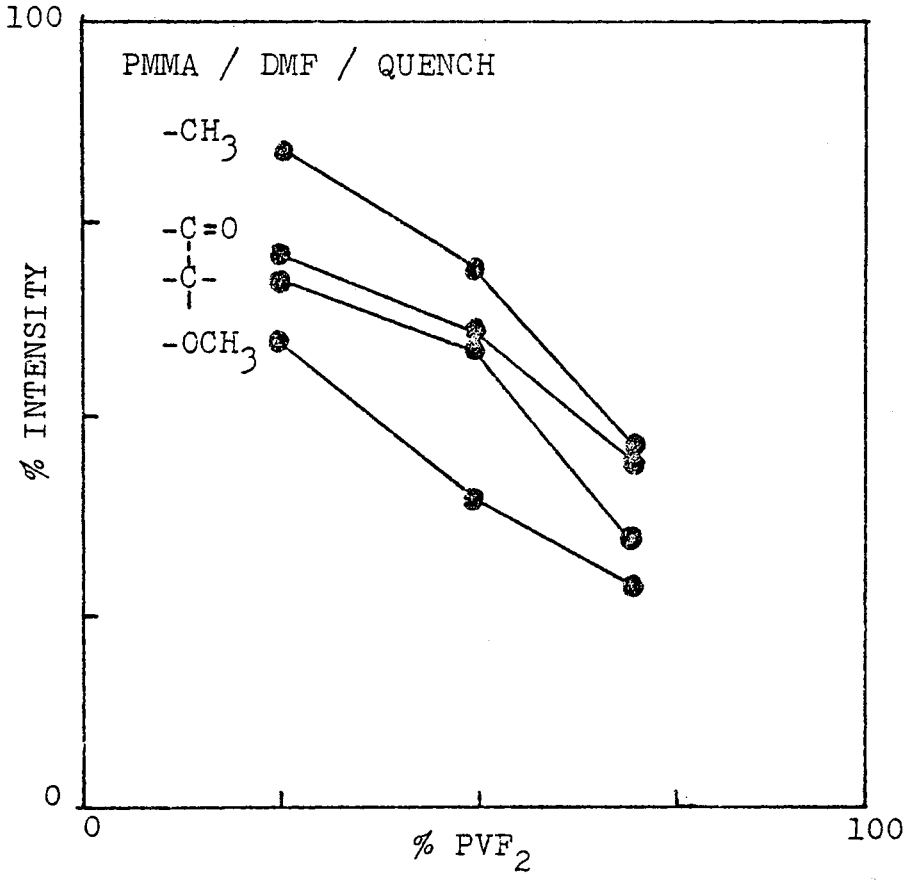

Figure 20. % Residual C-13 Resonance Intensities of PMMA in the DMF-Cast, Melted-and-Quenched PVF_2/PMMA Blends.

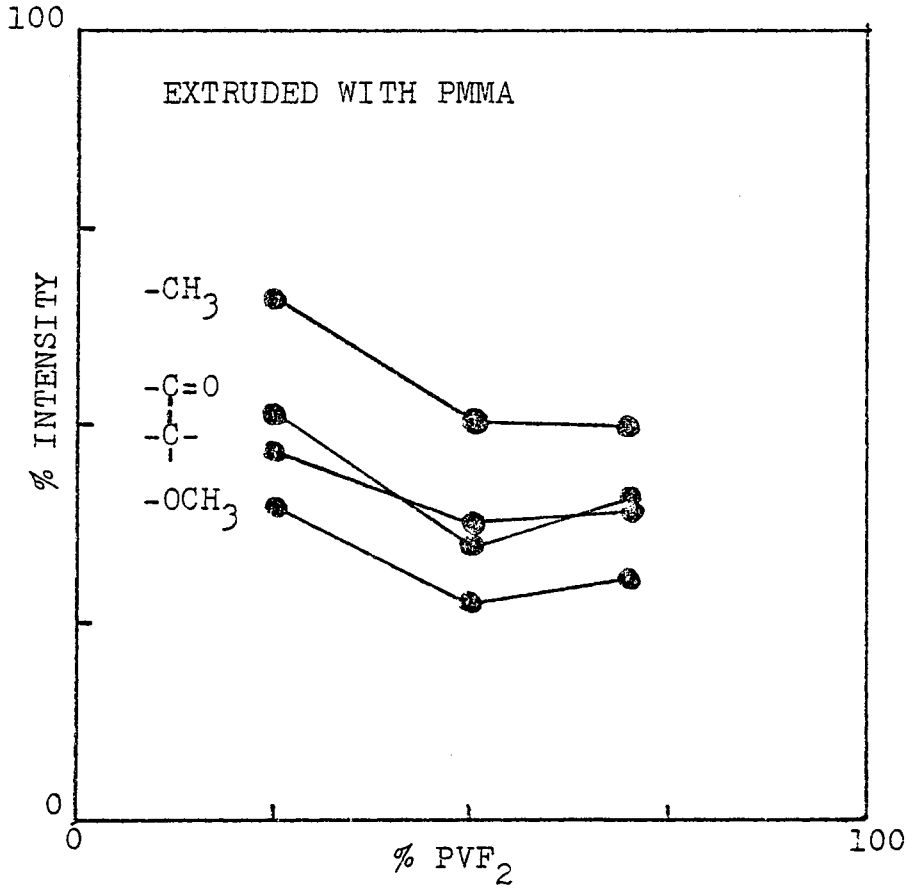

Figure 21. % Residual C-13 Resonance Intensities of PMMA in the Melt-Extruded PVF_2/PMMA Blends.

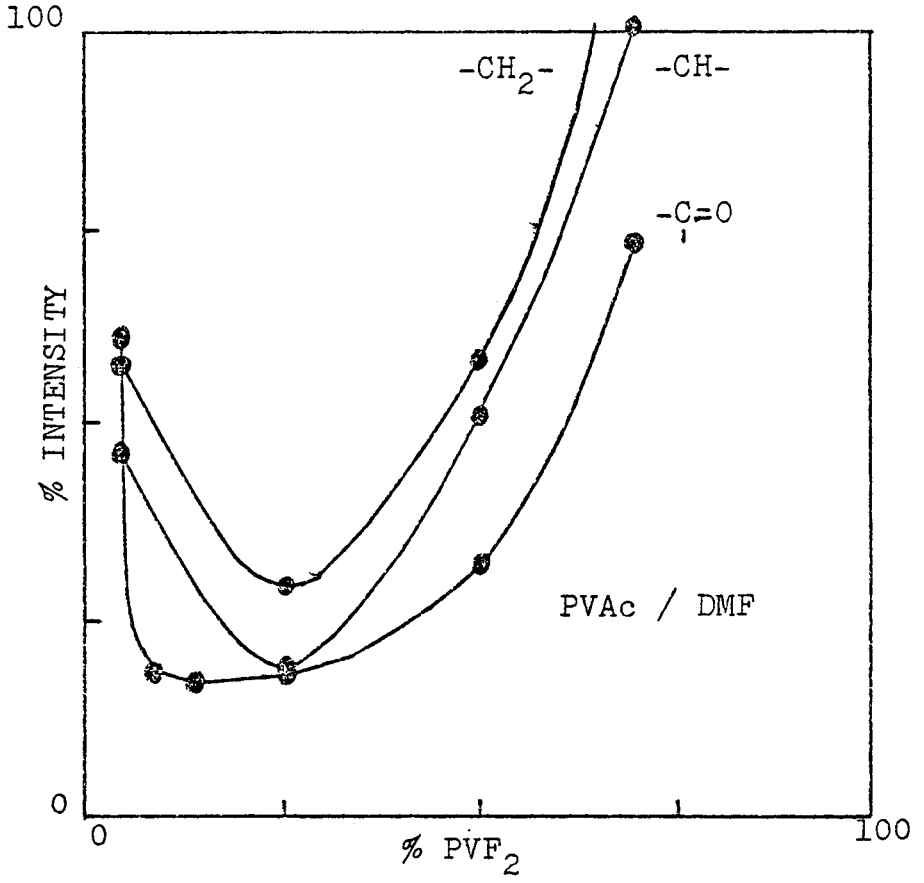

Figure 22. % Residual C-13 Resonance Intensities of PVAc in the DMF-Cast PVF_2/PVAc Blends.

$$\text{i. e.} \quad 2D = 56815.2 \left| \frac{3\cos^2\theta - 1}{2} \right| \text{Hz., if } r = 1\text{Å}$$

$$2D = 7101.9 \left| \frac{3\cos^2\theta - 1}{2} \right| \text{Hz., if } r = 2\text{Å}$$

$$2D = 2104.2 \left| \frac{3\cos^2\theta - 1}{2} \right| \text{Hz., if } r = 3\text{Å}$$

$$2D = 887.7 \left| \frac{3\cos^2\theta - 1}{2} \right| \text{Hz., if } r = 4\text{Å}$$

The maximum value of D would be realized when the angular term within the brackets is unity.

In looking at the influence of distance on dipolar coupling the salient fact is that the MAS itself can decouple long range weak dipolar interactions, with faster MAS decoupling only those of shorter range; i.e., estimation of miscibility in this study is limited by the chosen MAS rate. On the other hand, an investigation of NMR signal attenuations of polymer blends containing PVF_2 over a wide range of MAS rates would generate an average concentration profile of the spatial distribution of those ^{19}F nuclei in the vicinity of any resolvable ^{13}C nucleus. Unfortunately, due to the limitations of our equipment, the only comparison that could be made was at the spinning rates of 2.0 and 2.3 KHz. Some results for the melt-extruded PVF_2/PMMA blends are shown in Table 13. No significant spectral differences were seen at these two spinning rates. Considering the inverse third power dependence of the dipolar coupling on the internuclear distance, the expected effect is only $(2.3/2.0)1/3 = 1.048$ in magnitude. Consequently, the results are

not surprising given the limited frequency range. MAS rates as high as 15 KHz have been achieved using helium as the driving gas (63) which suggests that if the NMR signal attenuations were compared at, e.g. the MAS rates of 16 and 2 KHz, then a factor of 2 in the decoupling-distance relationship might be achieved with an added gain in insight to the understanding of the internuclear distance questions.

D. NMR Signal Attenuations and Relaxation Times

As discussed in Chapter I (section II.D.4), the technique of (^{13}C-^{1}H) cross polarization is used not only to rapidly polarize carbon magnetization (by $\sim T_{1H}/T_{1C}$) but also to achieve greater total nuclear magnetic alignment with the applied field than would otherwise be possible. The cross polarization enhancement of ^{13}C polarization at the end of the CP contact is by a factor of $M_0^{*C} = \gamma_H/\gamma_C \approx 4\ M_0^C$, where M_0^C is the polarization which would be generated in H_0 after waiting several relaxation times, T_{1C}. However, this optimal enhancement of M_0^C can be achieved only if $T_{1\rho}^H >>$ CP contact time $>> T_{CH}$. If ^{13}C nuclear spin alignment varied with the composition of PVF_2 polymer system, then unfair comparisons of attenuation might result. An equivalent statement would be that the ^{13}C relaxations might begin at different spin temperatures and attenuation calculations thus might be erroneous.

Both the $T_{1\rho}^H$ and the T_{CH} are modulated by molecular motion. It follows that average molecular mobility for a component in a pure polymer and in a polymer blend (especially highly miscible ones) might conceivably be different. Thus, while comparing the NMR signal intensities from the CP spectra of a polymer and of its blends, these

relaxation parameters have to be considered for reasons given above. In fact, any change of these relaxation times in itself is an indication of the miscibility. The choice of CP time is especially important; comparing NMR intensities of a polymer and those of its blends from CP spectra in which the same contact time was specified could be misleading depending on $T_{1\rho}^{H}$ and T_{CH}. Further investigation of this point was required in order to have confidence in the results.

Tables 16 and 17 list the ^{13}C NMR peak intensities of the PMMA and the melt-extruded 25:75 PVF_2/PMMA blend, respectively, obtained from spectra in which three CP contact times and different pulse delays were employed. Runs 1 and 5 were carried out at exactly the same conditions to show the reproducibility of the experiments. Run 3 used the same CP contact time as runs 1 and 5 but employed a longer pulse delay time. The results show that for both the PMMA neat and the blends, 3 seconds of pulse delay time was certainly long enough to assure the full repolarization of the protons between the scans.

From Tables 16 and 17, it is apparent that the spin-locked magnetization relaxed faster in the blends than in the PMMA homopolymer (i.e. $T_{1\rho}^{H}$ is shorter in the blend than in the homopolymer). The CP contact time used in all the examples in this study for the PMMA and its blends was 3ms, which is obviously not the optimum for all systems investigated. The residual NMR signal intensities of PMMA in the 25:75 melt- extruded PVF_2/PMMA blend were calculated from Tables 16 and 17 for the CP spectra obtained at various CP contact times; the results are shown in Table 18.

Further investigation was done by studying PMMA as well as the melt-extruded 25:75 and 50:50 PVF_2/PMMA blends at twelve different contact times for each (Figures 14 and 15). Averaged proton $T_{1\rho}$ values of the three samples resolved from carbon-13 CP spectra showed a decrease from 8.9 ms to 6.0 ms to 3.7 ms as the PVF_2 content was increased from 0 to 50 wt. % (Table 19). This is consistent with the results of NMR signal attenuations (Tables 13 and 20) as well as the glass transition behavior of the PVF_2/PMMA blends reported in the literature (171).

The contributions of the NMR signal attenuations of PMMA in the two blends due to the modifications of proton $T_{1\rho}$ values were estimated by comparing the theoretical maximum CP peak intensities of pure PMMA and the two blends (Table 20). This exploration showed that among the three resolvable peaks of the highest intensities, with a contact time of 3 ms, 14-26% and 26-52% of the attenuations resulted from the shorter proton's $T_{1\rho}$'s in the 25:75 and 50:50 PVF_2/PMMA blends, respectively. The results of NMR signal attenuations calculated from the theoretical CP magnetization showed insignificant differences between the two blends. This indicated that the degrees of intermixing were about the same between PMMA and PVF_2 in the two blends. Nonetheless, proton $T_{1\rho}$ values indicated that there was a stronger dynamic interaction between the two polymers in the amorphous region of the 50:50 PVF_2/PMMA blend than in the 25:75 PVF_2/PMMA blend.

It is clear that the severity of attenuation of the C-13 resonance intensities of PMMA in the blend as calculated from CP spectra can be

different for different contact times. However, among the four resolvable peaks of the PMMA in the two melt-extruded blends, the methoxyl carbon remains the most attenuated and the α-methyl carbon the least attenuated regardless of the contact time. This point can be elaborated by referring to Figures 14 and 15. In Figure 14, for the pure PMMA, the peak intensity of the methoxyl carbon is greater than that of the quaternary carbon regardless of the contact times. The opposite trend between the peak intensities of these two carbons in the blends can be seen in Figure 15.

E. NMR Signal Attenuations and Effect of Aging

When compared to the results on the freshly prepared samples (Table 13) a loss in magnitude of the attenuations of the C-13 resonance intensities was observed over time. For the same melt-extruded 25:75 and 50:50 PVF_2/PMMA blends discussed above in the variable contact time studies (Tables 16-18) and in the $T_{1\rho}{}^H$ studies, a significant drift toward the homopolymer signal intensities was observed. The discrepancy of NMR signal attenuations for the two blends obtained at from various experiments is summarized in Table 20. This descrepancy might conceivably be due to unknown experimental errors involving changes in instrument response. However, perhaps the aging process of the blends is more likely in the cause.

F. NMR Signal Intensities and Number of Accumulations

One of the assumptions in this study is that the NMR signal intensities are directly proportional to the number of total

accumulations for each sample. However, when a large number of scans are stored using only time domain accumulations, considerable deterioration of the accumulation efficiency may take place because of the limited computer bit number. The JEOL-60Q instrument employed a technique of progressive decrement of the A to D converter bit number in order to avoid data overflow. This means that the dynamic range of the spectra was thereby reduced, which would make the assumption of S/N less reliable, especially for the weak peaks. Thus, to avoid this problem, all the spectra of this study were carried out at conditions such that the final A to D converter bit number remained at 5 bits or more. Table 21 gives ^{13}C NMR signal intensities of PMMA obtained at various number of accumulations. The table shows that with our experimental conditons, the assumptions concerning S/N remained effective.

V. CONCLUSIONS

From the results of this chapter, the following conclusions have been reached.

1. Solid state ^{13}C NMR is able to probe the miscibility of the polymer blends of PVF_2. Degrees of molecular intermixing in the blends were reflected through the ^{13}C NMR signal attenuations. These attenuations are mainly due to ^{13}C-^{19}F intermolecular dipolar interactions, which were not decoupled.

2. Molecular level indications of the proximity in the blends were observed in this NMR study. The experimental probe size, or the resolution of the intimacy of mixing between the two constituent

Table 21

^{13}C NMR Signal Intensities of PMMA Obtained at Various Number of Accumulations

Number of Accumulations	Word Length (bits)	Final AD Converter (bits)	^{13}C Peak Intensities (arbitrary unit)			
			carbonyl	methoxyl	quaternary	α-methyl
800	16	8	3565x28	4761x28	5844x28	1882x28
1600	16	7	3488x29	5095x29	5323x29	1730x29
3200	16	6	3468x210	4805x210	5592x210	1731x210
6400	16	5	3446x211	4732x211	5787x211	1852x211

polymers in the blends, was estimated to be in the range of 3 to 4 angstroms. Beyond this range, a MAS rate of 2 KHz reduced any signal attenuation of ^{19}F on ^{13}C nuclei. Various degrees of NMR signal attenuations among the individual chemically different carbons of a polymer support a postulation of weak intermolecular 'acid-base' association between the acidic protons of PVF_2 and the basic carbonyl groups in the case of both the PMMA and the PVAc blends. For the miscible blends, the order of the attenuations among individual carbons of either the PVF_2/PMMA or the PVF_2/PVAc system remained essentially unchanged regardless of their compositions and sample histroy as well as the NMR experimental parameters.

3. Results of ^{13}C NMR signal attenuations revealed that with the same sample history, PVAc is more miscible with PVF_2 than is PMMA, while PVME is immiscible with PVF_2. This order is consistent with the conclusions of thermodynamic studies reported in the literature. In this study, the results of ^{13}C NMR signal attenuations were, in general, in good agreement with the melting point depression of PVF_2 in the blends. Exceptions were observed for the DMF-cast PVF_2/PVAc blends having thermal treatment. This disparity is likely to be due to the significantly different experimental probe sizes of the two techniques.

4. It has been well recognized that PVF_2 forms miscible blends with both PMMA and PVAc. However, from this solid state ^{13}C NMR studies, the methods of sample preparation and thermal treatment were found to play a significant role in determining the miscibility. The crystallization and interconversions of the polymorphic phases of PVF_2

are likely to be an important factors and reflect the effect of sample history.

5. Although the ^{13}C-^{19}F intermolecular dipolar interactions were concluded to be the main source of the ^{13}C signal attenuations of the blends, relaxation times (proton's $T_{1\rho}$'s in particular) could also contribute to the attenuations. The modifications of proton $T_{1\rho}$'s are more obvious in the highly miscible blends. The changes in themselves are indications of miscibility.

6. With the experimental conditions of this study, deterioration in the accumulation efficiency due to the progressive decrement of the dynamic range was not a factor for the ^{13}C NMR signal attenuations of the blend.

7. The aged melt-extruded PVF_2/PMMA blends showed less degrees of ^{13}C NMR signal attenuations than the freshly prepared samples. This discrepancy is probably due to the aging process of the blends.

8. No significant shifts of NMR frequencies induced by blending were observed. This may be due to the inherent limitation in resolution in solid state ^{13}C NMR.

VI. FUTURE WORK

All the NMR experiments of this study were carried out at room temperature in an instrument whose dipolar decoupling capability is limited only to the protons. Some questions, though further investigation on them were desired, could not be answered. Moreover, the extension of this method of compatibility studies beyond ^{19}F might

not be possible with the present instrumental capability.

In view of the upgrading of the present instrument, namely, the variable temperature capability (VT-MAS (179,180)), in the very near future, two aspects are recommended for future work as discussed below. Another aspect which requires the capability of simultaneous dipolar decouplings of both protons and fluorine-19 nuclei is also recommended below.

A. Variable Temperature Studies

In this NMR study of polymer blends, sample history was found to be very important in determining the compatibility. Although the effects of thermal treatments on the polymer blend compatibility have been studied, all the spectra were obtained at room temperature. With the variable temperature capability, questions left unanswered in this study can be further investigated. One example is the possible small scale phase separation due to the LCST behavior of the PVF_2/PVAc blends.

B. Compatibility Studies Through Heteronuclei Other Than Fluorine-19

This compatibility study of polymer blends through intermolecular heteronuclear dipolar interactions should be extensible to nuclei other than fluorine-19. In terms of commercial organic polymers, chlorine is a possible candidate. However, dipolar interactions due to chlorine nuclei are usually negligible for solid polymers above their glass transition temperature (84). This is due to the self-decoupling induced by effective quadrupolar relaxations in these systems. With the VT-MAS capability, compatibility studies through intermolecular ^{13}C-^{35}Cl and

^{13}C-^{37}Cl dipolar interactions at a temperature well below the glass transition of a polymer blend might be possible.

C. Compatibility Studies by Varying Heteronuclear Dipolar Decoupling Power

In the previous section, it was suggested that an ivestigation of ^{13}C NMR signal attenuations of polymer blends containing PVF_2 over a wide range of MAS rates would generate an average concentration profile of the spatial distribution of ^{19}F nuclei that are in the vicinity of the resolvable ^{13}C nucleus. Besides the experimental difficulty in achieving high MAS rates, low MAS rates could generate complex spinning sidebands. The sidebands would make the quantitative treatment of the spectra more complicated. An alternative approach to the variable MAS rates could be achieved by simultaneously decoupling fluorine-19 nucleus in addition to the protons. With a fixed rate of ca. 2 KHz, varying the ^{19}F decoupling power might reveal the spatial distribution of ^{19}F nuclei within 3 to 4 angstroms of any resolvable ^{13}C nucleus of a polymer in a blend with PVF_2.

Literature Cited

1. N.A.J. Platzer, Ed., "Multicomponent Polymer Systems", Adv. Chem. Ser., 99, ACS, Washington, D.C., 1971.

2. N.A.J. Platzer, Ed., "Copolymers, Polyblends, and Composites", Adv. Chem. Ser., 142, ACS, Washington, D.C., 1975.

3. S. L. Aggarwal, Ed., "Block Copolymers", Plenum Press, New York, 1970.

4. A. Noshay and J. E. McGrath, "Block Copolymers: Overview and Critical Survey", Academic Press, New York, 1977.

5. O. Olagoke, L. M. Robeson and M. T. Shaw, "Polymer-Polymer Miscibility", Academic Press, New York, 1977.

6. D. R. Paul and S. Newman, Ed., "Polymer Blends", Academic Press, New York, 1978.

7. F. A. Bovey, "Encyclopedia of Polymer Science and Technology", N. M. Bikales, Ed., Wiley-Interscience, New York, 1968, Vol. 9, pp. 356-396.

8. I. Ya Slonim and A. N. Lyubimov, "The NMR of Polymers", Plenum Press, New York, 1970.

9. P. Diehl, E. Fluck and R. Kosfeld, Ed., "NMR Basic Principles and Progress", Vol. 4: Nature and Synthetic High Polymers, Springer-Verlag, Berlin, 1971.

10. F. A. Bovey, "High Resolution NMR of Macromolecules", Academic Press, New York, 1972.

11. E. M. Purcell, H. C. Torrey and R. V. Pounds, Phys. Rev., 69, 37, 1946.

12. F. Block, W. M. Hansen and M. E. Packard, Phys. Rev., 69, 127, 1946.

13. T. C. Farrar and E. D. Becker, "Pulse and Fourier Transform NMR: Introduction to Theory and Methods", Academic Press, New York, 1971.

14. K. Mullen and P. S. Pregosin, "Fourier Transform NMR Techniques - A Practical Approach", Academic Press, New York, 1976.

15. D. Shaw, "Fourier Transform NMR Spectroscopy", Elsevier, Amsterdam, 1976.

16. C. Brevard and P. Granger, "Handbook of High Resolution Multinuclear NMR", Wiley-Interscience, New York, 1981.

17. J. B. Stothers, "Carbon-13 NMR Spectroscopy", Academic Press, New York, 1972.

18. F. W. Wehrli and T. Wirthlin, "Interpretation of Carbon-13 NMR Spectra", Heyden, London, 1976.

19. E. Breitmaier and W. Voelter, "13C NMR Spectroscopy: Methods and Applications in Organic Chemistry", 2nd. Ed., Verlag Chemie, Weinheim, 1978.

20. R. J. Abraham and P. Loftus, "Proton and Carbon-13 NMR Spectroscopy: An Integrated Approach", Heyden, London, 1979.

21. G. C. Levy, R. L. Lichter and G. L. Nelson, "Carbon-13 Nuclear Magnetic Resonance Spectroscopy", 2nd Ed., Wiley-Interscience, New York, 1980.

22. J. Schaefer, "Topics in Carbon-13 NMR Spectroscopy", Vol. 1, G. C. Levy, Ed., Wiley-Interscience, New York, 1974, pp. 150-208.

23. W. M. Pasika, Ed., "Carbon-13 NMR in Polymer Science", ACS Symposium Series 103, ACS, Washington, D.C., 1979.

24. J. C. Randall, "Polymer Sequence Determination: Carbon-13 NMR Method", Academic Press, New York, 1977.

25. J. R. Lyerla, Jr., T. T. Horikawa and D. E. Johnson, J. Am. Chem. Soc., 99, 2463, 1977.

26. G. C. Levy, P. L. Rinaldi, J. J. Dechter, D. E. Axelson and L. Mandelkern, "Polymer Characterization by ESR and NMR", ACS Symposium Series, 142, A. E. Woodward and F. A. Bovay, Ed., ACS, Washington, D.C., 1980, pp. 119-146.

27. W. P. Slichter, in Reference 9, pp. 209-231.

28. T. M. Connor, in Reference 9, pp. 247-270.

29. V. T. McBriety, Polymer, 15, 503, 1974.

30. V. T. McBriety and D. C. Douglass, J. of Polym. Sci.: Macromolecular Reviews, 16, 295, 1981.

31. I. Ya Slonim, "The Ageing and Stabilization of Polymers", A. S. Kuz'minskii, Ed., Elsevier, Amsterdam, 1971, pp. 244-262.

32. M. Mehring, "High Resolution NMR Spectroscopy in Solids", Springer-Verlag, Berlin, 1976.

33. "Pulse Nuclear Magnetic Resonance in Solids", Faraday Symposia of the Chemical Society, No. 13, The Chemical Society, London, 1978.

34. "Nuclear Magnetic Resonance Spectroscopy in Solids", The Royal Society, London, 1981; also published as Phil. Trans. Roy. Soc. London, A299, pp. 475-686, 1981.

35. G. Scheler, U. Haubenreisser and H. Rosenberger, J. Magn. Reson., 44, 134, 1981.

36. C. S. Yannoni, Acc. Chem. Res., 15, 201, 1982.

37. Chem. Eng. News, October 16, 1978, p. 23.

38. J. Schaefer, E. O. Stejskal and R. Buchdahl, Macromolecules, 10, 384, 1977.

39. J. R. Lyerla, "Contemporary Topics in Polymer Science", Vol. 3, M. Shen, Ed., Plenum Press, New York, 1979, pp. 143-213.

40. R. K. Harris, K. J. Packer and B. J. Say, Makromol. Chem., Suppl. 4, 117, 1981.

41. H. A. Resing, A. N. Garroway, D. C. Weber, J. Ferraris and D. Slotfeldt-Ellingsen, Pure & Appl. Chem., 54, 595, 1982.

42. J. A. Pople, W. G. Schneider and H. J. Berstein, "High-Resolution Nuclear Magnetic Resonance", McGraw-Hill, New York, 1959.

43. A. Abragam, "The Principles of Nuclear Magnetism", Clarendon Press, Oxford, 1961.

44. C. P. Slichter, "Principles of Magnetic Resonance", 2nd. Ed., Springer-Verlag, Berlin, 1978.

45. M. L. Martin, G. J. Martin and J. -J. Delpuech, "Practical NMR Spectroscopy", Heyden, London, 1980.

46. E. Fukushima and S.B.W. Roeder, "Experimental Pulse NMR: A Nuts and Bolts Approach", Addison-Wesley, London, 1981.

47. Reference 45, pp. 411-413.

48. Reference 13, pp. 8-15.

49. F. Bloch, Phys. Rev., 70, 460, 1946.

50. F. Bloch, W. W. Hanson and M. Packard, Phys. Rev., 70, 474, 1946.

51. E. L. Hahn, Phys. Rev., 80, 580, 1950.

52. J. W. Cooper, Comput. Chem., 1, 55, 1976.

53. Reference 43, Chapter 4.

54. J. Schaefer, Macromolecules, 6, 882, 1973.

55. K. Yokota, A. Abe, S. Hosaka, I. Sakai and H. Saito, Macromolecules, 11, 95, 1978.

56. A. A. Jones, G. L. Robinson and F. E. Gerr, in Reference 23, pp. 271-290.

57. Reference 45, p. 17.

58. J. W. Emsley and J. C. Lindon, "NMR Spectroscopy Using Liquid Crystal Solvents", Pergamon Press, Oxford, 1975.

59. J. H. Noggle and R. E. Schirmer, "The Nuclear Overhauser Effects - Chemical Applications", Academic Press, New York, 1971.

60. B. C. Gerstein, Anal. Chem., 55, 781A, 1983.

61. E. R. Andrew, "Progress in Nuclear Magnetic Resonance Spectroscopy", Vol. 8, J. W. Emsley, J. Feeney and L. H. Sutcliffe, Ed., Pergamon Press, New York, 1972, pp. 1-39.

62. E. R. Andrew, in Reference 34, pp. 505-520.

63. K. W. Zilm, D. W. Alderman and D. M. Grant, J. Magn. Reson., 30, 563, 1978.

64. I. J. Lowe, Phys. Rev. Lett., 2, 285, 1959.

65. E. R. Andrew, L. F. Farnell and T. D. Gledhill, Phys. Rev. Lett., 19, 6, 1967.

66. E. R. Andrew and L. F. Farnell, Molec. Phys., 15, 157, 1968.

67. A. C. Cunningham and S. M. Day, Phys. Rev., 152, 287, 1966.

68. U. Haeberlen, "High Resolution NMR in Solids: Selective Averaging", Adv. Magn. Reson., Suppl. 1, Academic Press, New York, 1976.

69. J. Herzfeld and A. E. Berger, J. Chem. Phys., 73, 6021, 1980.

70. L. W. Jelinski, Macromolecules, 14, 1341, 1981.

71. S. R. Hartmann and E. L. Hahn, Phys. Rev., 128, 2042, 1962.

72. J. P. Jesson, P. Meakin and G. Kneissel, J. Am. Chem. Soc., 95, 618, 1973.

73. J. S. Waugh, L. M. Huber and U. Haeberlen, Phys. Rev. Lett., 20, 180, 1968.

74. P. Mansfield, J. Phys. C: Solid St. Phys., 4, 1444, 1971.

75. W. -K. Rhim, D. D. Elleman and R. W. Vaughan, J. Chem. Phys., 58, 1772, 1973.

76. D. P. Burum and W. -K. Rhim, J. Chem. Phys., 71, 944, 1979.

77. U. Haeberlen and J. S. Waugh, Phys. Rev., 175, 453, 1968.

78. Reference 44, Chapter 3.

79. H. Kessemeier and R. E. Norberg, Phys. Rev., 155, 321, 1967.

80. D. L. VanderHart, W. L. Earl and G. N. Garroway, J. Magn. Reson., 44, 361, 1981.

81. W. P. Aue, D. J. Ruben and R. G. Griffin, J. Magn. Reson., 43, 472, 1981.

82. W. T. Dixon, J. Magn. Reson., 44, 220, 1981.

83. W. P. Rothwell and J. S. Waugh, J. Chem. Phys., 74, 2721, 1981.

84. W. W. Fleming, C. A. Fyfe, J. R. Lyerla, H. Vanni, and C. S. Yannoni, Macromolecules, 13, 460, 1980.

85. A. Pines, M. G. Gibby and J. S. Waugh, J. Chem. Phys., 59, 569, 1973.

86. S. R. Hartmann and E. L. Hahn, Phys. Rev., 128, 2042, 1962.

87. E. O. Stejskal and J. Schaefer, J. Magn. Reson., 18, 560, 1975.

88. E. O. Stejskal, J. Schaefer and T. R. Steger, in Reference 33, pp. 56-62.

89. S. J. Opella and M. H. Frey, J. Am. Chem. Soc., 101, 5854, 1979.

90. D. A. Torchia, J. Magn. Reson., 30, 613, 1978.

91. Reference 2. Preface

92. M. Steinberg, L. E. LuKacka, P. Colombo and B. Manowitz, in Reference 1, pp. 547-561.

93. P. J. Flory, "Principles of Polymer Chemistry", Cornell University Press, Cornell, 1953.

94. O. Olabishi, J. Chem. Ed., 58, 944, 1981.

95. R. Koningsveld, L. A. Kleintjens and H. M. Schoffeleers, Pure Appl. Chem., 39, 1, 1974.

96. A. J. Yu, in Reference 1, pp. 2-14.

97. P. Glansdorff and I. Prigogine, "Thermodynamic Theory of Structure, Stability and Fluctuations", Wiley-Interscience, London, 1971.

98. J. H. Hildebrand and R. L. Scott, "The Solubility of Non-Electrolytes", Reinhold, 1950.

99. L. Bohn, Rubber Chem. Technol., 41, 495, 1968.

100. T. L. Hill, "An Introduction to Stastical Thermodynamics", Addison-Wesley, Reading, 1960.

101. P. J. Flory, J. Chem. Phys., 9, 660, 1941.

102. P. J. Flory, J. Chem. Phys., 10, 51, 1942.

103. M. L. Huggins, J. Chem. Phys., 9, 440, 1941.

104. M. L. Huggins, J. Phys. Chem., 46, 151, 1942.

105. P. J. Flory, J. Am. Chem. Soc., 87, 1833, 1965.

106. D. Patterson, Macromolecules, 2, 672, 1969.

107. D. J. Meier, J. Polym. Sci., Part C, 26, 81, 1969.

108. D. J. Meier, Polym. Prepr., Am. Chem. Soc., Div. Polym. Chem., 11, 400, 1970.

109. S. Krause, J. Polym. Sci., Part A-2, 7, 249, 1969.

110. S. Krause, Macromolecules, 3, 84, 1970.

111. D. F. Leary and M. C. Williams, J. Polym. sci., Part B, 8, 335, 1970.

112. D. F. Leary and M. C. Williams, J. Polym. Sci., Polym. Phys. Ed., 11, 345, 1973.

113. D. F. Leary and M. C. Williams, J. Polym. Sci., Polym. Phys. Ed., 12, 265, 1974.

114. D. J. Meier, Polym. Prepr., Am. Chem. Soc., Div. Polym. Chem., 15, 171, 1974.

115. D. S. Kaplan, J. Appl. Polym. Sci., 20, 2615, 1976.

116. R. W. Smith and J. C. Andries, Rubb. Chem. Tech., 47, 64, 1974.

117. M. Matsuo, C. Nozaki and Y. Jyo, Polym. Eng. Sci., 9, 197, 1969.

118. T. Nishi and T. T. Wang, Macromolecules, 8, 909, 1975.

119. T. K. Kwei, G. D. Patterson and T. T. Wang, Macromolecules, 9, 780, 1976.

120. V. J. McBrierty, D. C. Douglass and T. K. Kwei, Macromolecules, 11, 1265, 1978.

121. T. K. Kwei, T. Nishi and R. F. Roberts, Macromolecules, 7, 667, 1974.

122. T. Nishi, T. T. Wang and T. K. Kwei, Macromolecules, 8, 227, 1975.

123. T. Nishi, T. K. Kwei and T. T. Wang, J. Appl. Phys., 46, 4157, 1975.

124. D. C. Douglass and V. T. McBriety, Macromolecules, 11, 766, 1978.

125. D. C. Douglass, Polym. Prepr. Am. Chem. Soc., Div. Polym. Chem., 20, 251, 1979.

126. J. E. Anderson and K. J. Liu, Macromolecules, 4, 260, 1971.

127. G. E. Wardell, V. J. McBriety and D. C. Douglass, J. Appl. Phys., 45, 3441, 1974.

128. R. A. Assink and G. L. Wilkes, Polym. Eng. Sci., 17, 606, 1976.

129. M. F. Froix and J. M. Pochan, J. Polym. Sci., Polym. Phys. Ed., 14, 1047, 1076.

130. R. A. Assink, J. Polym. Sci., Polym. Phys. Ed., 15, 59, 1977.

131. R. A. Assink, Macromolecules, 11, 1233, 1978.

132. D. J. Goldwasser, J. Polym. Sci., Polym. Phys. Ed., 17, 1464, 1979.

133. J. Schaefer, M. D. Sefcik, E. O. Stejskal, and R. A. McKay, Polym. Prepr., Am. Chem. Soc., Div. Polym. Chem., 20, 247, 1979.

134. J. Schaefer, M. D. Sefcik, E. O. Stejskal, and R. A. McKay, Macromolecules, 14, 188, 1981.

135. E. O. Stejskal, J. Schaefer, M. D. Sefcik, and R. A. McKay, Macromolecules, 14, 275, 1981.

136. L. W. Jelinski, F. C. Schilling and F. A. Bovay, Macromolecules, 14, 581, 1981.

137. M. Morton, Ed., "Rubber Technology", 2nd Ed., Van Nostrand Reinhold, New York, 1973.

138. D. A. Meyer, in Reference 137, pp. 440-458.

139. W. R. Hendricks and R. J. Enders, in Reference 137, pp. 515-533.

140. M. Shen and D. H. Kaelble, J. Polym. Sci., Polym. Lett. Ed., 8, 149, 1970.

141. E. Helfand, Macromolecules, 8, 552, 1975.

142. G. Kraus and K. W. Rollmann, J. Polym. Sci., Polym. Phys. Ed., 14, 1133, 1976.

143. P. L. Kumler and S. E. Keinath, Polym. Eng. Sci., 17, 613, 1977.

144. U. Bianchi, E. Pedemonte and A. Turturro, Polymer, 11, 268, 1970.

145. B. Morēse-Sēguēla, M. St-Jacques, J. M. Renaud and J. Prud'homme, Macromolecules, 13, 100, 1980.

146. G. L. Wilkes and R. Wildnauer, J. Appl. Phys., 46, 4148, 1975.

147. G. L. Wilkes and J. A. Emerson, J. Appl. Phys., 47, 4261, 1976.

148. Reference 10, pp. 125-126 and pp. 226-229.

149. FAFT 70 Floppy Disk FG/BG Program, Intruction Manual, JEOL. LTD.

150. T. Hashimoto, K. Nagatoshi, A. Todo, H. Hasegawa and H. Kawai, Macromolecules, 7, 364, 1974.

151. P. M. Toporowski and J. E. L. Rooves, J. Polym. Sci., Polym. Chem. Ed., 14, 2233, 1976.

152. Reference 4, pp. 198-203.

153. J. Brandrup and E. H. Immergnt, Ed., "Polymer Handbook", 2nd Ed., Wiley-Interscience, New York, 1975.

154. J. Schaeffer, E. O. Stejskal and R. Buchdahl, J. Macromol. Sci., Phys., B 13, 665, 1977.

155. Reference 4, pp. 371-379.

156. H. Morawetz, F. Amrani, Macromolecules, 11, 281, 1978.

157. C. W. Frank, M. A. Gashgari, Macromolecules, 12, 163, 1979.

158. T. C. Ward and T. S. Lin, AIChE Meeting, Nov. 1982, and ACS Adv. Chem. Ser., in press.

159. T. S. Lin and T. C. Ward, Polym. Prep., Am. Chem. Soc., Div. Polym. Chem., 24, Sept. 1983, in press.

160. F. F. Koblitz, R. G. Petrella, A. A. Dukert and A. Christofas, U. S. Patent, 3,253,060, 1966.

161. C. H. Miller, Jr., U. S. Patent, 3,458,391, 1969.

162. J. M. Schmitt, U. S. Patent, 3,459,834, 1969.

163. J. S. Noland, N. N.-C. Hsu, R. Saxon and J. M. Schmitt, in Reference 1, pp. 15-28.

164. D. R. Paul and J. O. Altamirano, in Reference 2, pp. 371-385.

165. M. M. Colemann, J. Zarian, D. F. Varnell and P. C. Painter, J. Polym. Sci., Polym. Lett. Ed., 15, 745, 1977.

166. T. K. Kwei, H. L. Frisch, W. Radigan and S. Vogel, Macromolecules, 10, 157, 1977.

167. F. A. Bovey, F. C. Schilling, T. K. Kwei and H. L. Frisch, Macromolecules, 10, 559, 1977.

168. D. C. Wahrmund, R. E. Bernstein, J. W. Barlow and D. R. Paul, Polym. Eng. Sci., 18, 677, 1978.

169. R. E. Bernstein, D. R. Paul and J. W. Barlow, Polym. Eng. Sci., 18, 683, 1978.

170. R. E. Bernstein, D. C. Wahrmund, J. W. Barlow and D. R. Paul., Polym. Eng. Sci., 18, 1220, 1978.

171. D. R. Paul, J. W. Barlow, R. E. Bernstein and D. C. Wahrmund, Polym. Eng. Sci., 18, 1225, 1978.

172. I. R. Peat and W. F. Reynolds, Tetrahedron Lett., 14, 1359, 1972.

173. T. K. Wu and D. W. Ovenall, Macromolecules, 7, 776, 1974.

174. L. F. Johnson, F. Heatly and F. A. Bovey, Macromolecules, 3, 175, 1970.

175. J. B. Lando, H. G. Olf and A. Peterlin, J. Polym. Sci., Part A-1, 4, 941, 1966.

176. R. Hasegawa, Y. Takahashi, Y. Chatani and H. Tadokoro, Polym. J., 3, 600, 1972.

177. A. J. Lovinger, "Developments in Crystalline Polymers-1", D. C. Bassett, Ed., Applied Science, London, 1982, pp. 195-273.

178. Reference 177, p. 216.

179. W. W. Fleming, C. A. Fyfe, R. D. Kendrick, J. R. Lyerla, H. Vanni and C. S. Yannoni, "Polymer Characterization by ESR and NMR", ACS Symposium Series, 142, A. E. Woodward and F. A. Bovay, Ed., ACS, Washington, D.C., 1980, pp. 193-217.

180. J. R. Lyerla and C. S. Yannoni, Acc. Chem. Res., 15, 208, 1982.

The vita has been removed from the scanned document

Applications of High Resolution Solid State Carbon-13 NMR to the Study of Multicomponent Polymer Systems

by

Tso-Shen Lin

(ABSTRACT)

The technique of high resolution solid state carbon-13 NMR, achieved with magic angle spinning (MAS) and high power ^{13}C-^{1}H dipolar decoupling and cross polarization, was applied to a number of multicomponent polymer systems. Specific problems which were addressed are: (1) the nature of domain structure and molecular motion of two thermoplastic elastomer systems, including a series of styrene-isoprene-styrene linear triblock copolymers (SIS's) of various compositions, molecular weights and sample histories, and a poly(ester)-urethane based on poly(1,4-butylene adipate) and 4,4'-diphenylmethane diisocyanate, (2) the compatibility at the molecular level of polymer blends containing poly(vinylidene fluoride) (PVF_2), including its solution and mechanical blends with poly(methyl methacrylate) (PMMA), poly(vinyl acetate) (PVAc) and poly(vinyl methyl ether) (PVME).

For the thermoplastic copolymers, higher degree of phase separation between the hard and soft domains was indicated by two facts: First, ^{13}C resonances of either domain could be selectively observed with different experimental conditions. Second, there was a one-component, first-order, spin-lattice relaxation behavior of the ^{13}C nuclei in the soft domains. For the SIS copolymers, results of T_1 and T_2^* determinations (both with MAS) suggest that molecular motion,

in terms of frequency, was independent of composition, molecular weight and selective casting solvents. However, from static spectra, molecular motion of the isoprene blocks was found to be more anisotropic for the samples cast from a poor solvent for polyisoprene (MEK) in contrast to samples cast from a good solvent of polyisoprene (hexane).

For the polymer blends of poly(vinylidene fluoride), the level of molecular intermixing were reflected through the degree of ^{13}C NMR signal attenuations of the non-PVF_2 polymers. These attenuations are mainly due to undecoupled intermolecular ^{13}C-^{19}F dipolar interactions. With a MAS rate of 2KHz, resolution of the intimacy of mixing between the two constituent polymers in the blends was estimated to be in the range of 3 to 4 angstroms. Varying degrees of NMR signal attenuations among the individual chemically different carbons of a polymer support a postulation of weak intermolecular 'acid-base' association between the acidic protons of PVF_2 and basic carbonyl groups in the case of both the PMMA and PVAc.